


Spring 1-1-2013

Using Small Scale Physical Experiments to Improve Enthalpy Based Models of Ice Sheets

Austin Nossokoff

University of Colorado at Boulder, aus424@msn.com

Follow this and additional works at: https://scholar.colorado.edu/cven_gradetds

 Part of the [Civil Engineering Commons](#), [Hydrology Commons](#), and the [Physical and Environmental Geography Commons](#)

Recommended Citation

Nossokoff, Austin, "Using Small Scale Physical Experiments to Improve Enthalpy Based Models of Ice Sheets" (2013). *Civil Engineering Graduate Theses & Dissertations*. 316.
https://scholar.colorado.edu/cven_gradetds/316

This Thesis is brought to you for free and open access by Civil, Environmental, and Architectural Engineering at CU Scholar. It has been accepted for inclusion in Civil Engineering Graduate Theses & Dissertations by an authorized administrator of CU Scholar. For more information, please contact cuscholaradmin@colorado.edu.

Using Small Scale Physical Experiments to Improve
Enthalpy Based Models of Ice Sheets

By

Austin Nossokoff

B.S., University of Colorado, 2013

A thesis submitted to the Faculty of the Graduate
School of the University of Colorado in partial fulfillment
of the requirement for the degree of Master of Science
Department of Civil Engineering

2013

This thesis entitled:
Using Small Scale Physical Experiments to Improve Enthalpy Based Models of Ice
Sheets

Written by Austin Nossokoff

Has been approved for the
Department of Civil, Environmental and Architectural Engineering

Dr. Harihar Rajaram

Dr. John McCartney

Dr. William Tad Pfeffer

Date _____

The final copy of this thesis has been examined by the signatories, and we find that both the content and the form meet acceptable presentation and standards of scholarly work in the above mentioned discipline.

Abstract

Nossokoff, Austin (MS, Civil Engineering)

Using Small-Scale Experiments to Improve Enthalpy Based Models of Ice Sheets

Directed by Professor Dr. Harihar Rajaram

Recent work has demonstrated the potential warming influence of meltwater and englacial water bodies on the Greenland Ice Sheet. The equilibrium line has been ascending in altitude, resulting in inland propagation of areas receiving melt. The physical processes involved in the interaction between the liquid and solid phases of water within cold ice bodies is not completely understood. This work is meant to improve the understanding of the thermodynamic interactions between englacial water bodies and surrounding ice in polythermal glaciers and ice sheets. The growth of conduits that carry water through the englacial system due to frictional heating along the conduit walls and refreezing when frictional heating is insufficient is studied based on experimental measurements of heat transfer from water filled conduits in cold ice. The important heat exchange processes involved are conductive loss of energy from the conduit and supply of energy by viscous/turbulent dissipation in water flowing through the conduit.

Three sets of experiments were designed based on a theoretical analysis which established the threshold water discharge rate in a conduit above which conduit growth can occur. One set focused on a conduit filled with stagnant water, another with a low water flow rate, and a third with a high water flow rate. Refreezing occurred in the first two sets, while conduit growth occurred beyond a critical discharge value. Scalloping of conduit walls occurred in the conduit growth regime, leading to a large roughness of conduit walls. Even in the case where

refreezing occurs, the ice temperature surrounding the conduit will increase due to the release of latent heat by refreezing water. Using the assumption of radial symmetry, a numerical model was developed to quantify the temperature distribution in the ice. This model represents the conduction and energy supply at the conduit walls by turbulent dissipation and includes movement of the ice-water interface by either refreezing or conduit growth. The scalloping effects under high flow rates produced relatively high friction factors. The model and experiments agree well in all three experimental cases.

Acknowledgements

I would like to thank my advisor, Dr. Harihar Rajaram, for the support, patience, and inspiration to write a successful thesis in the Civil, Environmental and Architectural Engineering Department at the University of Colorado. I would not have been able to complete this thesis without the support of him, or everyone else that has helped me along the way.

I would also like to thank Dr. Tom Neumann for the opportunity to perform research experiments at his cryospheric laboratory at the NASA Goddard Space Flight Center in Greenbelt, Maryland. Dr. Richard Regueiro and graduate students Jose Solis and Yevgeniy Kaufman for their help and mentorship throughout my initial academic research experiences. Dr. John McCartney for serving on my thesis committee and introducing me to geotechnical engineering. Dr. Tad Pfeffer for serving on my thesis committee and inspiring me further in the studies of glaciology through classroom experiences and in the field.

I would like to thank my office mates at CU and NASA for providing enjoyable times in the office and in the lab. My roommates, both past and present, for the distractions and adventures during my time at the University of Colorado. Lastly, I would like to thank my family, my father, mother and sister, for giving me the opportunity to pursue my education and for their encouragement through the years.

Table of Contents

Abstract	iii
Acknowledgements	v
1 Introduction and Motivation.....	1
1.1 Glacial Network	11
1.1.1 The Supraglacial Network (On the Surface)	16
1.1.2 The Englacial Network (Contained Within the Ice)	17
1.1.3 The Subglacial Network (Beneath the Ice).....	20
1.2 Research Motivation.....	21
2 Experimental Overview	22
3 Experimental Rationale	26
4 Experimental Setups	32
4.1 Preliminary Trials.....	32
4.2 Stagnant Water Tests	35
4.3 Low Water Flow Rate Tests	38
4.4 High Water Flow Rate Tests.....	43
4.5 Results (Stagnant Experiments)	54
4.6 Discussion (Stagnant Experiments).....	59
4.7 Results (Low Flow).....	60
4.8 Discussion (Low Flow).....	65
4.9 Results (High Flow)	66

4.10	Discussion (High Flow)	75
5	Numerical Model	77
5.1	Critical Flow Rate	90
6	Experimental and Numerical Comparison	105
6.1	Comparison (Stagnant water cases).....	105
6.2	Discussion (Stagnant water comparison)	108
6.3	Comparison (Low water flow cases)	109
6.4	Discussion (Low water flow comparison).....	115
6.5	Comparison (High water flow cases).....	117
6.6	Discussion (High water flow comparison)	123
7	Conclusion	125
8	Appendix: The Bessel Function.....	126
9	Bibliography	130

1 Introduction and Motivation

The world's climate is changing, and we must adapt to it. Earth has been steadily warming up since the turn of the century, and the majority of the world's glaciers and ice sheets have been on a steady rate of decline (Alexander et al., 2013; Thomas et al., 2008). These large masses of ice and snow are losing their mass in record numbers, and Figure 1-1 shows all of the glaciers and ice sheets currently frozen on the planet.

It is estimated that approximately 56 million cubic kilometers of ice remain frozen upon the earth, with the majority located in the Greenland and Antarctic ice sheets (Lemke, P. et al., 2007). There are glaciers, however, located in every continent on the planet, and the figure below chronicles the land areas of these per region of the globe.

The introduction will provide a broad based overview of the cryosphere, progressively narrowing the focus to the motivation for this research in Section 1.2.

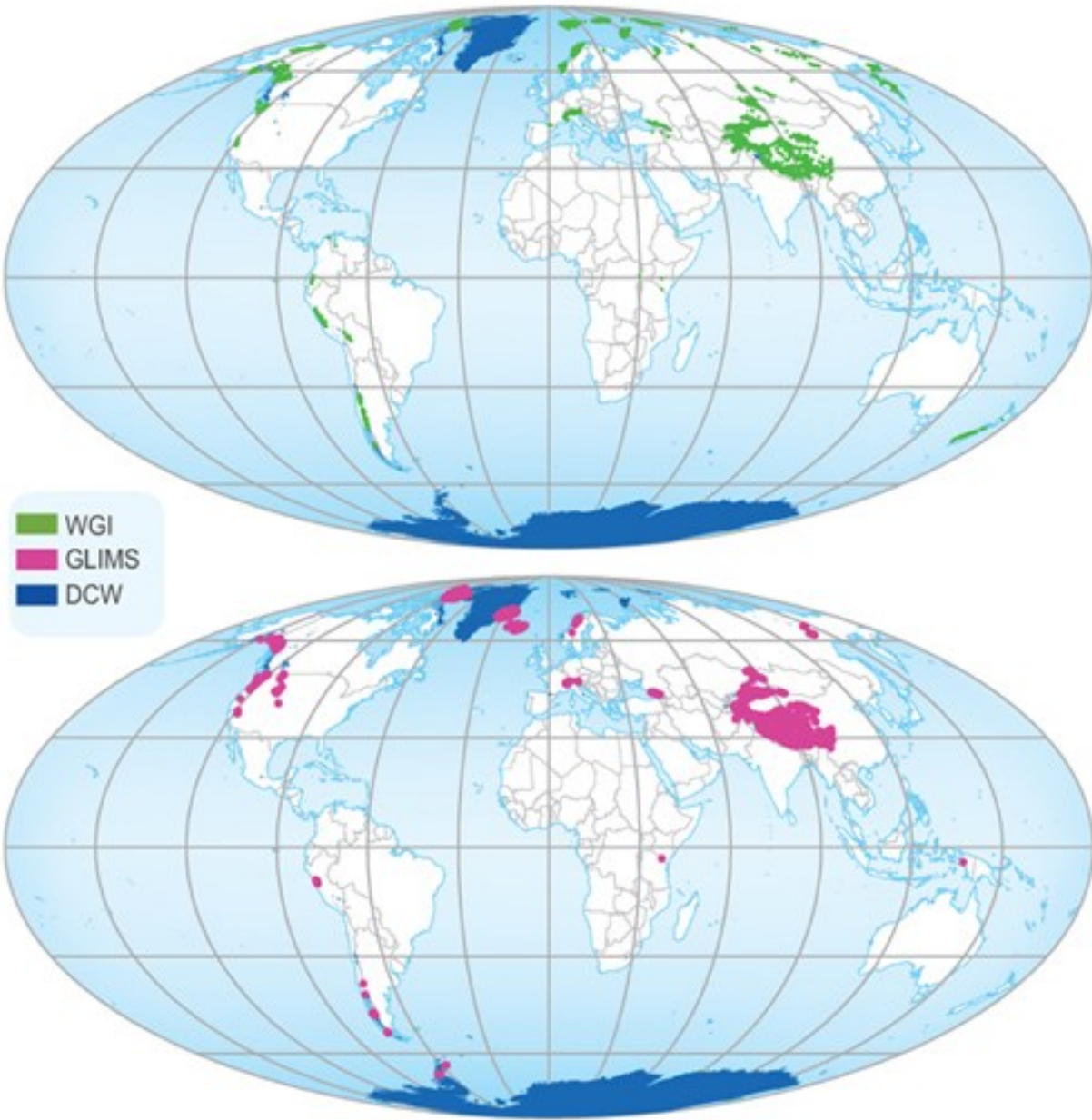


Figure 1-1: From the United Nations Environment Program (UNEP) Global Glacier Changes, facts and figures. Worldwide distribution of ice sheets and glaciers, approximately, from ESRI's Digital Chart of the World (DCW), the World Glacier Inventory (WGI), and Global Land Measurements from Space (GLIMS).

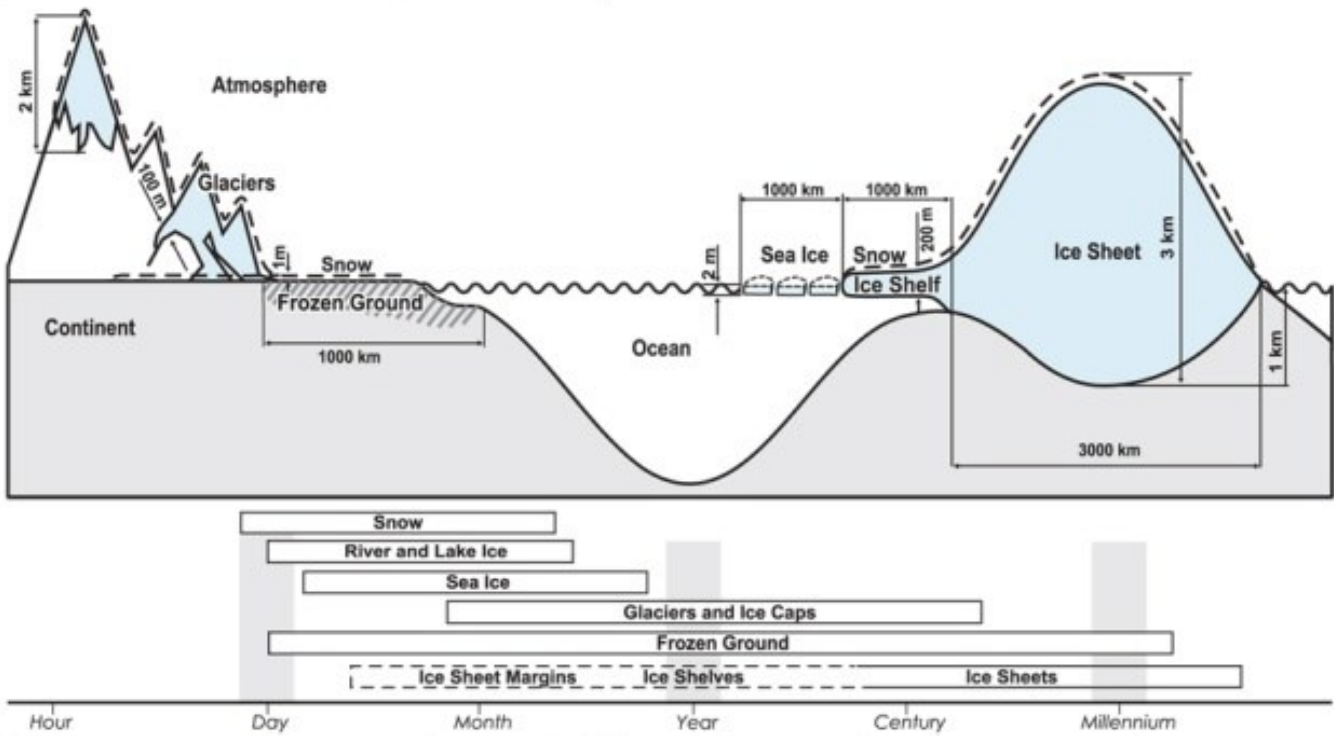


Figure 1-2: Figure from the International Panel on Climate Change (IPCC), a map of cryospheric components and their timescales (Lemke, P. et al., 2007)

To understand the differences between ice sheets and Glaciers, this paper will refer to the National Snow and Ice Data Center's (NSIDC) definitions. Most large bodies of ice are considered to be glaciers, which are made up of precipitation, mainly in the form of fallen snow, which compresses into large, thickened ice masses. Ice sheets are a type of glacier, classified by their enormous size, over 50,000 square kilometers. There are currently only two ice sheets that exist in the world today, located in Greenland and Antarctica, and named accordingly. Within these ice sheets, other glacial formations can exist, such as ice shelves, ice streams, and other forms of glaciers. Below are some bullet points for a better perspective on the differing types and features of glaciers (National Snow and Ice Data Center, 2013).

- **Ice Shelves**- The portion of an ice sheet that extrudes off of land into the sea. The continent of Antarctica is flanked by these shelves, as no land coastline emerges from the ice for the majority of the continent.
- **Ice Caps**- A scaled down ice sheet. These cover less than 50,000 square kilometers of surface area. A good example is the comparison between Greenland and Iceland, where Greenland represents an ice sheet, while Iceland only contains an ice cap, due to its smaller size.
- **Ice Streams (Outlet Glaciers)**- Much like a river, these channel ice into more rapidly moving masses than the surrounding glacial body.
- **Icefields**-A scaled down ice cap. The flow of these is influenced mainly by the underlying topography of their locations.
- **Other Glacier Types**
 - **Mountain**-Often flowing out of icefields, these occur in mountainous regions such as the Himalayas.

- **Valley**-Commonly originating from mountain glaciers or icefields, these spill into valleys, looking more like tongues.
- **Piedmont**-Much like a river delta, these occur as valley glaciers open into relatively flat plains, spreading into bulb-like lobes.
- **Cirque**-These occupy bowl-like hollows on mountainsides and tend to be wider than they are long.
- **Hanging**-Clinging to mountainsides, they resemble kitchen aprons.
- **Tidewater**-Valley glaciers that extend out into the sea.

The table below shows the estimated masses of ice sheets, ice shelves, glaciers, and ice caps throughout the planet.

Table 1-1: Percent of global land surface area and sea level equivalent of the cryospheric components of the Greenland and Antarctic Ice Sheets, along with the glaciers of the world
 [a](Fretwell et al., 2013) [b](Bamber et al., 2013) [c] (Arendt et al., 2012)

Cryospheric Component	% of Global Land Surface	Sea Level Equivalent (meters)
Antarctic Ice Sheet [a]	8.30%	58.3
Greenland Ice Sheet [b]	1.20%	7.36
Glaciers [c]	0.50%	0.41

Climatic alterations occur slowly, as ecosystems generally take time to change, yet recent findings show a significant increase in the acceleration of mass loss of the Greenland Ice Sheet (GrIS) in the last decade (Chen et al., 2006; Luthcke et al., 2006; Rignot et al., 2011; Thomas et al., 2011; Velicogna and Wahr, 2006; Zwally et al., 2005). If these trends continue, and the fresh water contained within the GrIS releases into the sea, there is alarming potential for concern. Consequences of this outcome consist of a global rise in sea level coupled with a decrease in seawater salinity. Oceans are already seeing an increase in height, with approximately 28% of this change attributed to the GrIS (Lemke, P. et al., 2007). In the years to come, however, the GrIS has a great potential to wreak havoc on low lying coastal areas around the globe.

According to the International Panel on Climate Change, there is enough ice on the GrIS alone to raise the global sea level by 7 meters (Bamber et al., 2013). As the ice melts and is carried off into the sea, water is added to the oceans. Enough added water, and the sea rises. Parts of Holland, Thailand, and the American southeast, as well as numerous other locations around the globe, are all susceptible to fluctuations in the sea. Less developed coastal nations are even more vulnerable. The rising tides attributed to this phenomenon would flood houses and businesses, literally inundating the low-lying coastal economies. This will not happen all at once, but gradually, as tides become higher and storm surges more intense. Figure 1-3, Figure 1-4 and Figure 1-5 all show the effects that a rise in sea level of 1 to 6 meters around the globe.

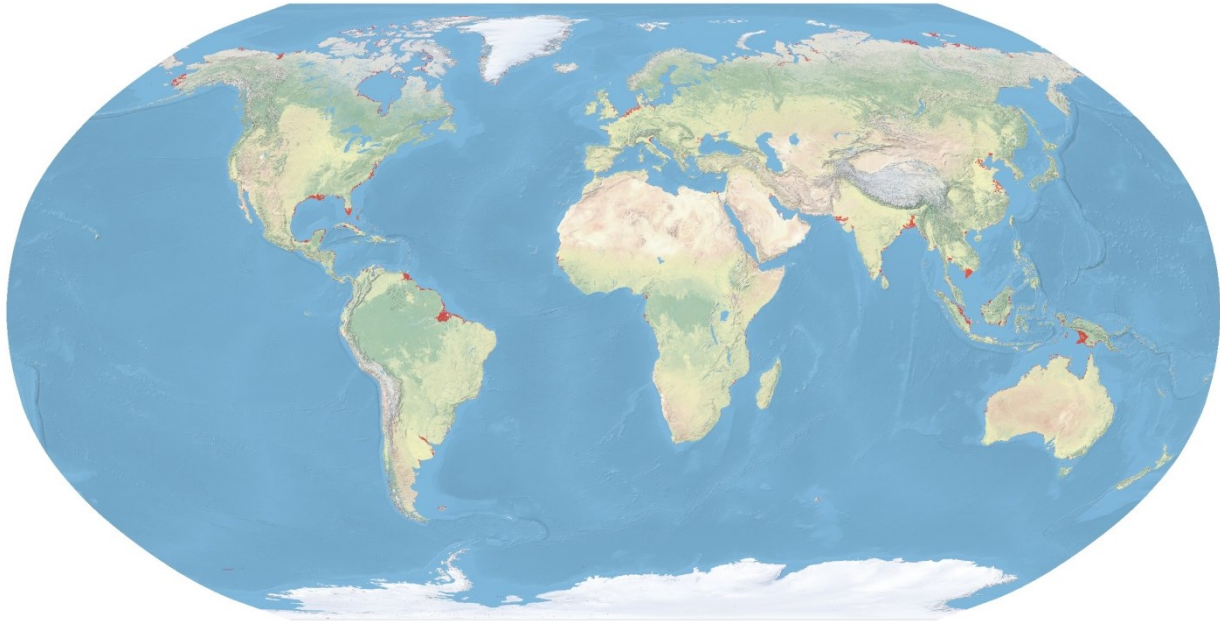


Figure 1-3: Figure from the Center for Remote Sensing of Ice Sheets (CreSIS), University of Kansas, showing worldwide susceptibility to a global sea level rise of 6 meters

The decrease of salinity is also of interest, since the oceans' temperatures are influenced by the amount of salt in the marine ecosystem. The lower levels of salt in the Northern Atlantic could alter the movement of water throughout the entire ocean. It is this thermohaline circulation that keeps European cities warmer than their Russian and North American latitudinal counterparts (Latif et al., 2006; Wanner et al., 2001). Consider Milan, Italy, for example. It rests on the same latitude, 45 degrees north, as Montreal, Canada, and both cities have similar elevations. The climate in Milan, however, is, on average, 6 degrees Celsius warmer than Montreal (WeatherSpark, 2013). A lowering of the temperature of Europe would affect crops, the economy, and the general standard of living. This is not to say that Montreal is a terrible place, just a different one, in terms of climate.

In order to avoid a disastrous situation, the disaster must first be anticipated. This way, the adaptation of humanity to these occurrences can be as smooth as possible, with dire outcomes evaded. It is with these thoughts in mind that computer models are developed in attempts to predict future scenarios. In order for these models to be effective, they must use accurate data and take into account an astonishing number of variables. Currently, however, robust predictions of the behavior of ice sheets under climate change remain challenging (Alley and Joughin, 2012). With the addition of meltwater and the thermodynamic interactions with the surrounding ice, these models have the potential to be brought up to speed (Phillips et al., 2013). This meltwater within the ice releases heat, which increases the temperature of the surrounding ice, reduces its viscosity, and therefore increases its speed.

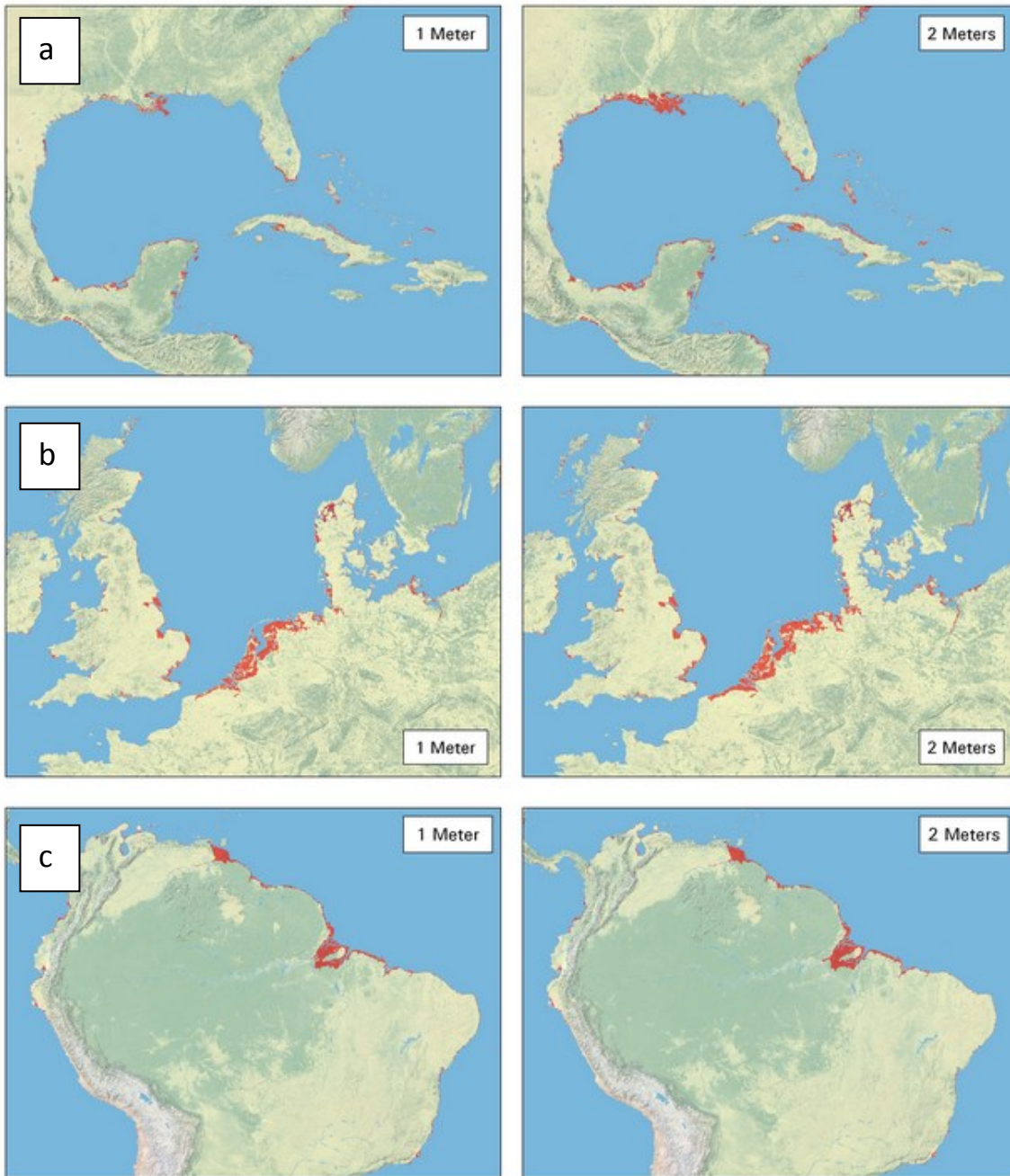


Figure 1-4: Figure from the Center for Remote Sensing of Ice Sheets (CreSIS), University of Kansas, showing sea level rise in a) the Southeastern United States, b) Northern Europe and c) the Amazon Delta, from 1-2 meters

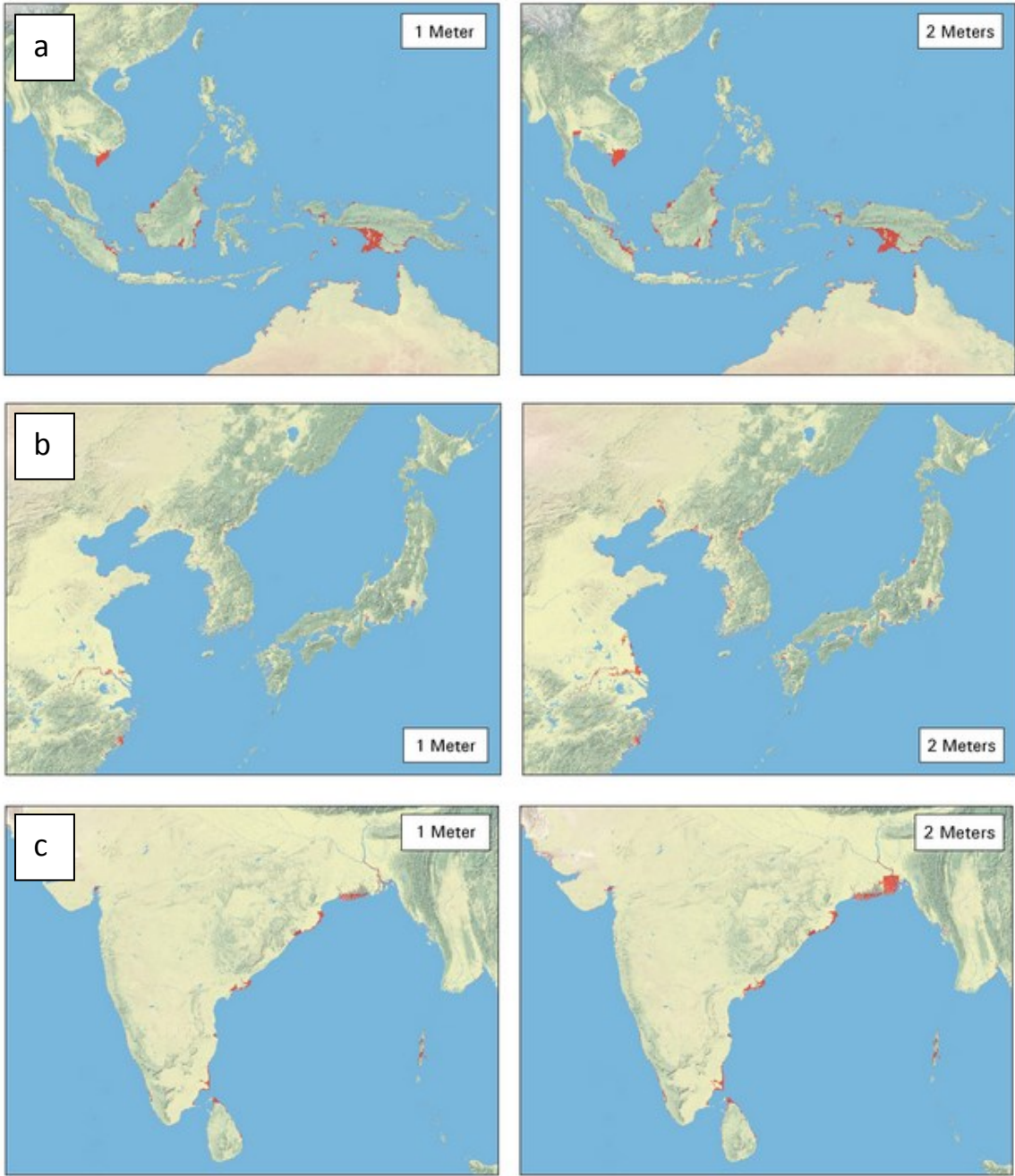


Figure 1-5: Figure from the Center for Remote Sensing of Ice Sheets (CreSIS), University of Kansas, showing sea level rise in a) Southeast Asia, b) East Asia and c) India, from 1-2 meters

1.1 Glacial Network

The first studies of glaciers can most likely be attributed to a Catholic Monk, Sebastian Muenster, in 1561, in southwestern Switzerland. He not only describes the physical features of the nearby Rhone Glacier, but also the surface hydrology, and mentions the entry points of water into the glacier itself (Lamb, 2013). Glacial studies have come a long way since the 1500's, and the growing wealth of knowledge can be traced back to the original observers.

Recently, there have been several studies to track surface elevation and mass changes in the ice sheets of the earth. Global positioning systems (GPS) and remote sensing techniques have enabled researchers to estimate the continually changing mass balance of the cryosphere. Most measurements, however, do not necessarily agree with each other on the quantitative total mass loss of the GrIS, only the qualitative aspect that it is losing mass in correspondence with the thinning ice over time (Thomas et al., 2008).

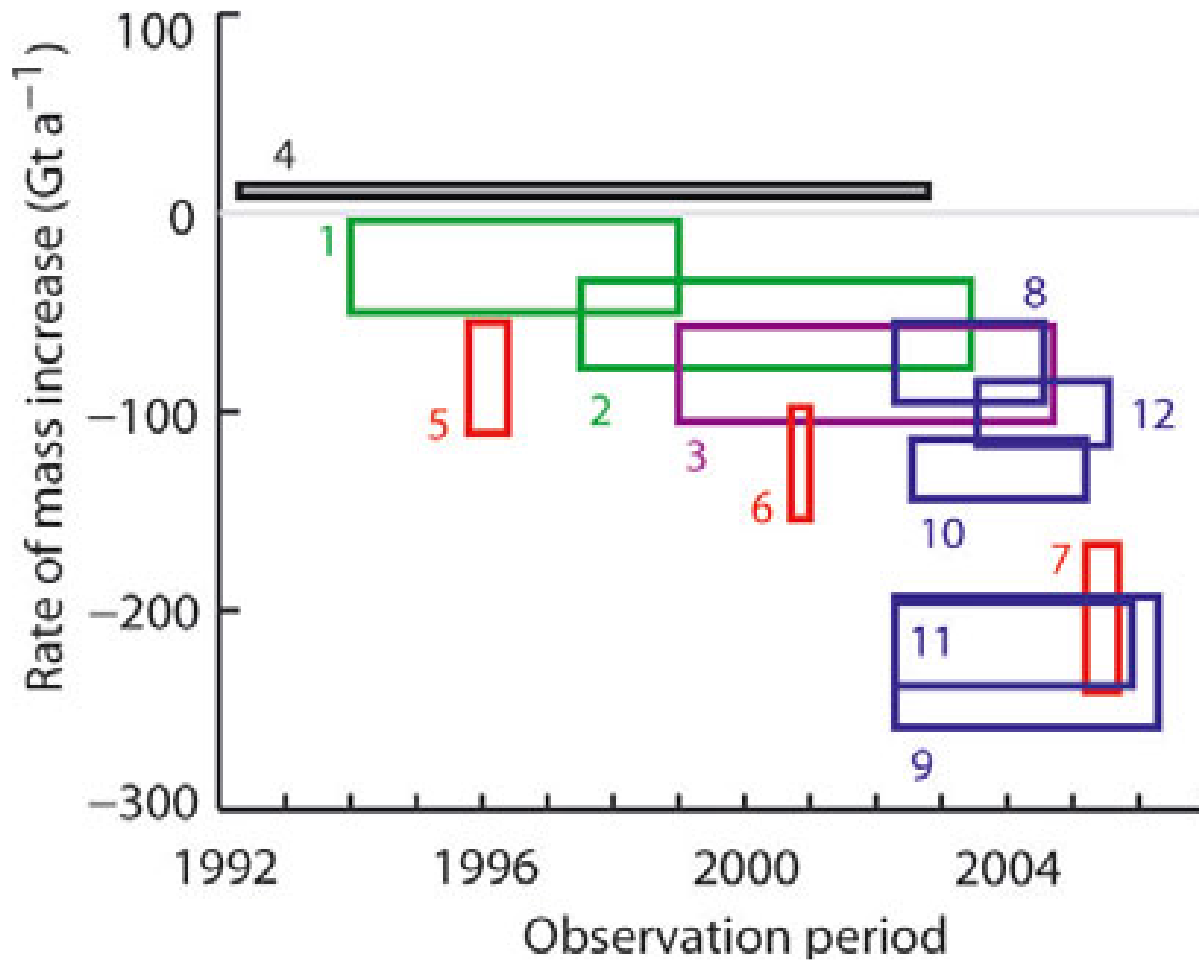


Figure 1-6: Figure from Thomas showing the rates of mass increase of the GrIS estimated on European Remote Sensing data (black), airborne laser-alimeter surveys (purple), mass budget calculations (red), and gravitational changes (blue). These estimations show the time period recorded as well as upper and lower estimates of the rate of mass change. 1 and 2: (Krabill, 2004; Krabill et al., 2000) 3: (Thomas et al., 2006) 4: (Zwally et al., 2005) 5-7: (Rignot and Kanagaratnam, 2006) 8 and 9: (Velicogna and Wahr, 2006): (Ramillien et al., 2006) 11: (Chen et al., 2006) 12: (Luthcke et al., 2006)

European remote sensing satellites, ERS-1 and ERS-2, have been using radar altimetry data (SRALT) to obtain surface elevation heights of the GrIS. They have shown thinning on the margins of the ice sheet and a gain in mass at higher elevations in the interior of Greenland (Johannessen et al., 2005; Zwally et al., 2005).

Another mission that is currently in place is the gravity recovery and climate experiment, better known as GRACE. NASA, along with the German Center for Air and Space Flight, launched twin satellites to precisely measure changes in the gravitational pull of the earth. By circling the earth in identical orbits and tracking miniscule changes in the distance between the two satellites, geodetic measurements can be recorded. Even at a distance of 220 kilometers, the system can detect a change in distance of approximately one-tenth of a human hair. This approach cuts right to the chase of measuring mass change, since the higher the gravitational pull of the earth at a location, the more mass is located there (Steitz, 2002).

Glaciers and ice sheets consist of two major regions where they either gain or lose mass. The accumulation zone, where mass is gained through a net surplus of precipitation, occurs at higher altitudes than its lower equivalent, the ablation zone. This ablation zone is where the ice sheet loses its mass. The majority of the loss comes through the processes of calving and meltwater runoff. Calving, the separation of a block of ice from the main body of the glacier, accounts for about half of the GrIS ablation (Cuffey and Patterson, 2010). This method of calving typically occurs at fringes of the ice sheet, where it is in water, and produces

icebergs that drift off into the sea. Sublimation of the ice also occurs in the ablation zone, as the ice transitions straight from its solid to its gaseous state.

The other main component of ablation rests with the melting of the ice itself (Cuffey and Patterson, 2010). The melt seasons on the GrIS have become longer and longer since the 1980s, providing more and more meltwater each year for the ice sheet (Huff, 2006; Markus et al., 2009). As the ice warms, it absorbs energy, to the point where it changes phases, through melting, from solid form to liquid. The water produced through this process then enters the hydrological system of the ice sheet. This cryo-hydrologic system contains three main parts, the supraglacial, englacial, and subglacial networks, each of which contains a portion of the journey from surface meltwater to its release from the glacial network. These components will be discussed in more detail later on in this chapter.

The warming of the GrIS is only exacerbated by positive feedback loops, especially when it comes to albedo. As the ice melts and becomes liquid, its color changes, from white to blue. The energy input onto the earth by the sun is then retained more by the blue water than by the white ice. The white color of the ice reflects more sunlight than the darker water; thus occurrence of liquid water on the surface exacerbates the heating of glaciers and ice sheets.

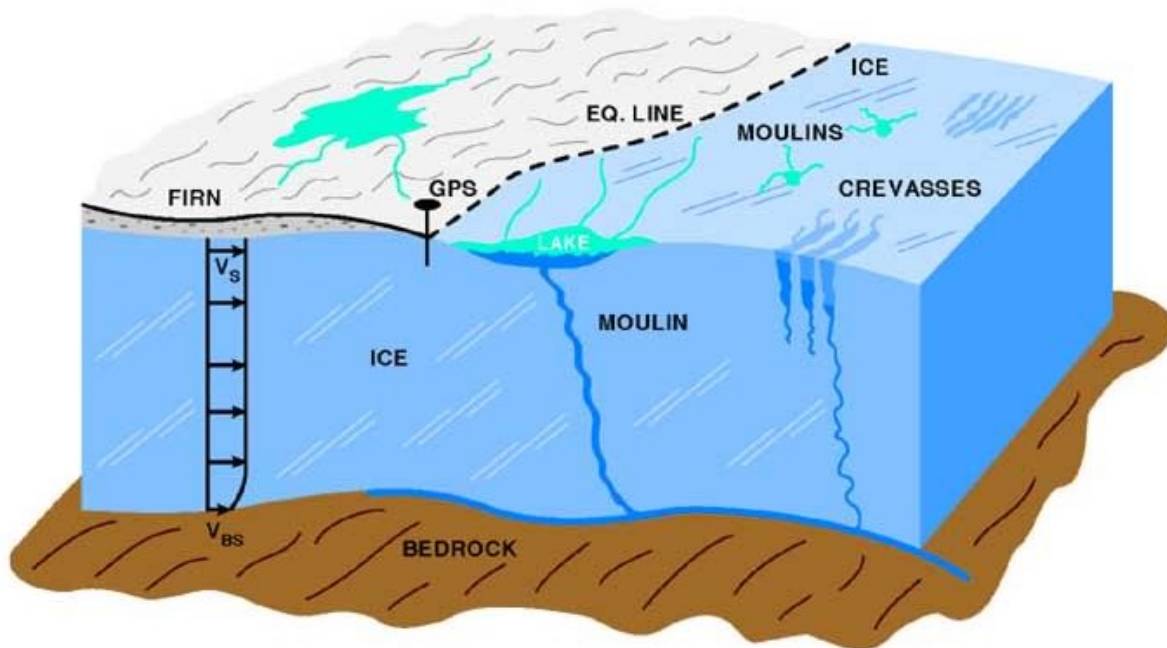


Figure 1-7: Figure from (Zwally et al., 2002) showing a schematic of the glacial water system. The supraglacial network is shown on the top, while the englacial network can be seen in the crevasses and moulin within the ice, and the subglacial system where the water at the bottom of the ice meets the bedrock.

1.1.1 The Supraglacial Network (On the Surface)

The surface of the glacier and its supraglacial network is the most well known of the three stages, since it can be readily and easily observed. Starting with surface melt, due to energy from solar radiation and sensible heat flux, the hydrologic cycle begins (Cuffey and Patterson, 2010) This network of streams and lakes is comparable to an ordinary river system (Shreve, 1972). The difference, though, is how the water exits the network. This happens in a manner not dissimilar to that of a karst region (eroded limestone), where water filters down through crevasses and moulins to the englacial network (Fountain and Walder, 1998; Shreve, 1972).



Figure 1-8: Figure from (Phillips, 2010), taken by Konrad Steffen in 2007, showing a Moulin where water exits the supraglacial network and enters the englacial network

1.1.2 The Englacial Network (Contained Within the Ice)

Once the meltwater enters these moulins and crevasses, it is now characterized as being in the englacial network.

In 1972, Shreve hypothesized englacial pressure gradients within the ice, through which water would flow until it reached the terminus of the glacier (Shreve, 1972). This pressure is created by the ice overburden pressure, as well as the steepness of the bed, and suggested that the water flowing through the ice remained within the ice for a significant period of time, with overburden pressure even causing water to flow uphill in some cases.

That same year, Roethlisberger produced a steady state solution for Jokuhlaups from the 1960's (Roethlisberger, 1972). Jokuhlaups are glacial outburst floods, typically large and sudden releases of water from the englacial system. Using quantum mechanics equations for the conservation of mass, energy, momentum, and inertia, he calculated conduit dimensions for a single conduit, which, he argued, is the steady state solution for the englacial network.

Four years later, in 1976, Nye used the same approach as Roethlisberger, this time for a transient solution, instead of a steady-state solution (Nye, 1953). He neglected the heat transfer between these conduits and the surrounding ice, which is the focus of this paper. He also concluded that an arboresque system is the solution, whereby conduits feed into one another, and the three dimensional result resembles a tree-like structure.

Fountain and Walder, in 1998, also reported an arborescent network for the englacial distribution of water, which adjusts in size due to the amount of water

flow (Fountain and Walder, 1998). This arborescent system of fluid flow, like a pipe system, is developed with the origin of small conduits and streams near the glacier surface. These smaller conduits converge, creating a larger conduit, which draw in the other smaller channels and subsequently becomes a conduit with a large amount of volume flowing through it. They also suggest a non-arborescent basal network, which is described in Figure 1-9.

Most recently, in 2013, Phillips described the cryo-hydrologic cycle in general, noting that liquid water contained within the englacial network can significantly modify the temperature of the ice for long periods of time (Phillips et al., 2013). It was shown that repeated meltwater pulses can increase the ice temperature significantly on decadal time scales. Temperature critically controls mechanical properties of the ice, such as viscosity, which decreases as temperature increases, and therefore increases the ice flow rates for the same driving stresses.

Prior to this work, water flow through cold ice was neglected in studies, and deemed insignificant. Surface melting on the GrIS is common up to 1400m in elevation, and this subsequently drains through the ice sheet (Catania and Neumann, 2010). Catania and Neumann observed, through ice-penetrating radar data, that more melting had occurred than estimated by the potential energy released due to surface meltwater. They also observed persistent moulines that were capable of establishing well connected drainage pathways.

Boon & Sharp also examined meltwater propagation through cold ice and the abruptness of the drainage (Boon and Sharp, 2003). Unlike water flowing through temperate glaciers, where the ice is already at the pressure melting point, water flowing through cold ice is likely to freeze, and release its latent energy into the

ice. In this cold ice, fracture propagation was necessary to form these initial pathways, but insufficient to establish a permanent connection between the ice surface and bed.

Alley also determined that deep water fractures can propagate through cold ice, and confirmed that water in the supraglacial network, in streams, ponds and lakes, is necessary for Moulin formation (Alley et al., 2005). This water within the cold ice can drastically influence the properties of the ice, and that is where this thesis comes in, to improve the understanding of the englacial water system.

1.1.3 The Subglacial Network (Beneath the Ice)

Fountain and Walder suggest a small arborescent network underneath the ice sheet, where water flows, as well as a much larger non-arborescent system where water flows much slower beneath the glacier, as seen in Figure 1-9 (Fountain and Walder, 1998). The arborescent system carries the subglacial water out more quickly than the non-arborescent network, yet both exist, independently of each other.

Basal sliding from this water contained beneath the glaciers and ice sheets is another mechanism to enhance the flow of ice, and it is within this subglacial network where this occurs. An increase in meltwater, which then enters the cryo-hydrologic cycle, would drive the increase in basal sliding (Zwally et al., 2002). This meltwater would not drive acceleration of the ice in the basal sliding, but also the increase in temperatures within the ice.

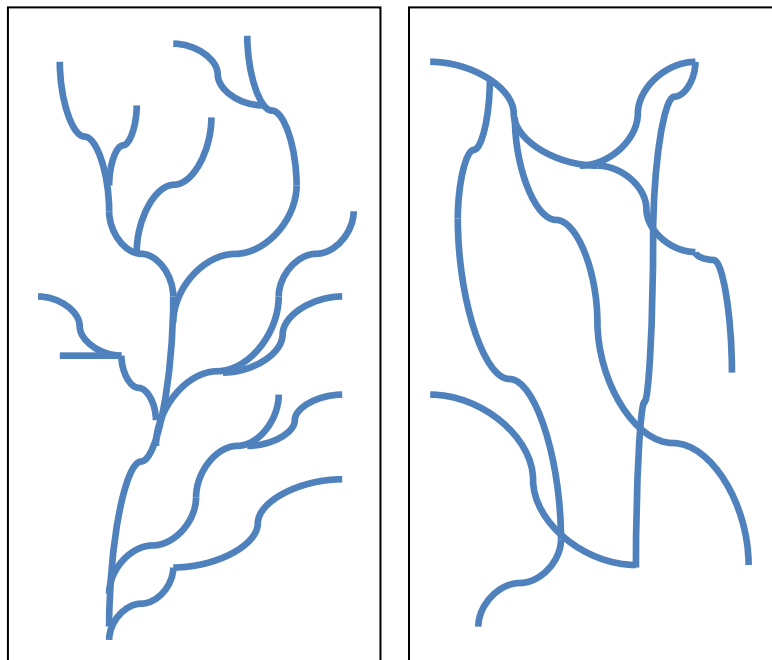


Figure 1-9: At left, an arborescent network is shown, while a non arborescent network is shown at right. Both are proposed mechanisms for water flow beneath ice sheets

1.2 Research Motivation

With the importance of the englacial network established and cryo-hydrologic warming recognized, the research motivation for this thesis can be examined. The growth and reduction of conduits within cold ice due to frictional heating are not well known, and have been estimated based on outdated parameters. As stated, the cryo-hydrologic cycle can increase the temperature of ice sheets and glaciers for a significant amount of time after a large meltwater event. This temperature then reduces the viscosity, which is much lower in cold ice than in temperate ice, and increases the velocity in which this cold ice flows. This, in turn, increases the mass loss from glaciers and ice sheets.

This thesis will examine the thermodynamic interactions between conduits contained within cold ice and the very ice that surrounds them. Small scale experiments, using laboratory generated ice, are run to further study these relationships and previous parameter assumptions. These experiments are compared with a simple numerical model, based on Fourier's law of heat conduction and frictional heating between the water and ice.

2 Experimental Overview

Recent work has demonstrated the potential warming influence of englacial water bodies on the Greenland Ice Sheet ((Alley et al., 2005; Boon and Sharp, 2003; Catania and Neumann, 2010; Phillips et al., 2013; Phillips, 2010). The equilibrium line has been ascending in altitude, by more than 250 meters, and generating an inland propagation of areas receiving melt by about 20km in southwest Greenland. This work is meant to improve the understanding of the thermodynamic interactions between englacial water bodies and surrounding ice in polythermal glaciers and ice sheets. This is done by conducting experiments focusing on measuring heat transfer from water filled conduits in cold ice, and used to validate numerical models of heat transfer from englacial conduits to cold ice. These experiments were conducted at both the University of Colorado Boulder and at a cold-room facility at the NASA Goddard Space Flight Center (NASA GSFC) in Greenbelt, Maryland.

The goal of these experiments was to explore the physics of heat exchange between flowing and stagnant water in englacial conduits and the surrounding cold ice. The important heat exchange processes involved are conductive loss of energy from the conduit and supply of energy by viscous/turbulent dissipation in water flowing through the conduit. Conduit growth is anticipated when the energy supply is sufficient. Otherwise, the conduit is expected to refreeze. The experimental plan included both refreezing and conduit growth regimes. The experiments were crafted upon a theoretical analysis which established the threshold water discharge rate in a conduit above which conduit growth can

occur. Further calculations examining this critical flow rate can be seen in Section 5.1.

Even in the case where refreezing occurs, the ice temperature surrounding the conduit will increase due to the release of latent heat by refreezing water. Using the assumption of radial symmetry, a numerical model was developed to quantify the temperature distribution in the ice. The model uses an implicit finite-difference approach to solve the heat equation within the ice, and also tracks the time-varying conduit radius based on an energy-balance condition at the conduit wall. A variable time-step is used to ensure that the conduit wall moves by one node in each time-step, which facilitates accurate tracking of the conduit radius evolution.

The first set of experiments focused on a refreezing regime. Ice temperature and water flow rate data were collected from the experimental setup in Figure 4-3 and compared to the numerical analysis. The tests began with initial conduit diameters of 9.53mm, with varying ice temperatures from -12 to -26 Celsius, and initial flow rates in the range of 1.18×10^{-4} - 1.31×10^{-4} m³/s. The critical flow rate for growth, depending on estimated parameters in the model, varies from 1.31×10^{-4} to 5.26×10^{-4} m³/s depending on initial ice temperatures and other parameters. Section 5.1 shows more information.

To freeze the water, a concept of freezing in lifts was used, and initial lifts of 6.35mm were implemented for the initial experiment. Thermocouples were placed within the ice by augering holes to their desired depths and freezing them in place, although this method proved less than optimal. The thermocouples shifted and froze radially away from the conduit, leaving their locations uncertain

until all experiments were complete. In the second round of testing, the experimental setup was modified, and the thermocouple placement method was vastly improved. The differences between the experimental setups can be seen in Figure 3-2.

In the trials where the conduit froze completely in on itself, the conduit was re-augered out to its initial dimensions, and the experiment was setup to run again. In the conduit expansion cases, an aluminum rod was inserted into the expanded conduit, water poured around it, and left to refreeze, whereupon the rod was removed, leaving a conduit 9.53mm in diameter, and the experiment was set up to run again. Table 2-1 highlights all tests run, with their initial ice temperatures and flow rates.

Table 2-1: Table of all tests run, including the initial ice temperature and initial flow rate of water through the conduit

Test Regime	Initial Ice Temperature (°Celsius)	Initial Flow Rate (m³/s)
Stagnant	-13.4	0
	-14.4	0
	-18.8	0
	-18.7	0
	-26.1	0
	-26.0	0
Low Flow	-14.0	1.18E-04
	-14.3	1.29E-04
	-14.9	1.29E-04
	-19.3	1.18E-04
	-19.9	1.31E-04
	-20.1	1.94E-04
	-20.6	1.62E-04
High Flow	-1.66	2.52E-04
	-4.53	2.52E-04
	-4.60	2.52E-04
	-5.43	2.52E-04
	-5.51	2.52E-04
	-5.73	2.52E-04
	-6.03	2.52E-04
	-9.55	2.52E-04
	-10.74	2.52E-04

3 Experimental Rationale

Only one previous laboratory study has been done in order to examine water flow through englacial conduits. These first experiments were conducted in a cold-room facility at the Institute of Low Temperature Sciences, Hokkaido University, Japan. The physics of heat exchange in those experiments focused on the water temperature change, and did not delve into the changing temperature profiles of the surrounding ice (Isenko et al., 2005). Isenko concluded that water flowing through englacial conduits tends toward the equilibrium temperature exponentially, and that the presence of sediments within these englacial passageways increases this equilibrium temperature. The tests shown here did not involve the temperature change of water through the length of ice, as it was initially close to equilibrium temperature, Table 4-4, and no sediments were present during the laboratory tests at Colorado and NASA GSFC.

The rationale behind the dimensions and overall physical properties of the experiments were based on many factors. The initial goal was to focus on creating a large ice sample with a circular conduit for water to flow through. Experimental limitations included the size of the cold-room being used. The University of Colorado had a small Kenmore chest freezer which could be used for smaller-scale experimental trials, and NASA GSFC provided a larger cold-room setup which was used to run the larger flow rate tests. Another factor was that the experimental setup had to be able to run multiple trials in order to produce more experimental results. The need for the ice sample housing to remain in a precise location to run additional tests was therefore necessary, in order for repeatability to be established.

The ice sample could have been refrozen, but the length of time required for refreezing was determined to be too long for our purposes. A method of auguring the conduit once the trial had finished was developed, and a long drill bit was used to return the conduit to its initial dimensions.

An issue that required consideration in comparing the experiments to the numerical model was the need to retain a constant temperature in the ice sample, and the combination of an adequate cold-room facility and insulation of the sample was needed. The facilities at NASA GSFC provided much more stable temperatures than the freezer at CU, yet variations in temperature for the ice samples used and run at CU were aided by the insulation used in protecting the ice sample. Chest freezers, like the one used at CU, fluctuate in temperature on a frequent defrost cycle, and obtain a large amount of heat whenever the lid is opened and shut. Larger facilities, like the one used at NASA GSFC, operate on a much less frequent defrost cycle, and contain enough space to add sufficient thermal mass, which also keeps temperature fluctuations to a minimum.

Once these issues were addressed, the profile of temperatures within the ice sample had to be considered. Initially, simple drilling into the ice sample was used, and thermocouples were inserted and frozen in place. As stated previously, this proved less than ideal, as the thermocouples were displaced by the heaving of the freezing water. In the subsequent experimental setup, the lifts were frozen in a different style, and the thermocouples could be manually adjusted until they were frozen in their final locations. This method can be seen in Figure 4-29.

Once the ice sample was set up and the ice profiles monitored, the temperatures of the flowing water had to be obtained, along with the flow rate of the water. In

the initial stagnant water case, this proved to be easy, as the flow rate was zero, and an additional thermocouple was inserted into the side of the conduit, where monitoring of the water temperature was straightforward. In the following low flow rate experiments, the water temperature was recorded at the outlet, and flow rate was monitored using the technique shown in Figure 4-7. Temperature gauges were fabricated and installed in the final radial experiments at NASA GSFC, and are shown in Figure 4-13.

The iterations of experimental containers for the ice sample consisted of an expandable box, where the entire ice sample was frozen at once, and the side walls allowed to expand as the ice froze, releasing the stress from the container walls. The ends were kept at a constant location, where the conduit ends remained in place, in order to allow for re-augering of the conduit. This proved insufficient, since the water temperature monitoring profile was inadequate and the expansion of the box allowed for large fluctuations of ice temperature in the sample. The above problem was fixed by using a small, acrylic container with rigid walls and thick insulation, and the method of freezing the ice in lifts was then implemented. The downside to this setup, however, was the fact that the sample was rectangular in shape, and the thermocouple placement was less than ideal. This system did, however, generate good results for the stagnant and low flow regimes, and proved much easier to re-auger than the larger ice samples of the subsequent experimental containers. This insulated box container can be seen in Figure 4-4. Finally, the pvc systems were developed, and fit all of the criterion for the experimental trials. The smaller pvc system can be seen in Figure 4-15 and the larger pvc system can be seen in Figure 4-15. A comparison of the different experimental containers is shown in Figure 4-1.

Table 3-1: Comparison of experimental containers

Requirement	Experimental Container			
	Expandable Box	Insulated Box	Small PVC	Large PVC
Ice Sample	Yes	Yes	Yes	Yes
Multiple Trials	Yes	Yes	Yes	Yes
Constant Ice Temperature	No	Yes	Yes	Yes
Ice Profile Monitoring	Yes	Yes	Yes	Yes
Water Temperature Monitoring	No	No	Yes	Yes

Further schematics of the experimental containers are shown in Figure 3-1, and the dimensions and differences between the insulated box and the pvc systems can be seen.

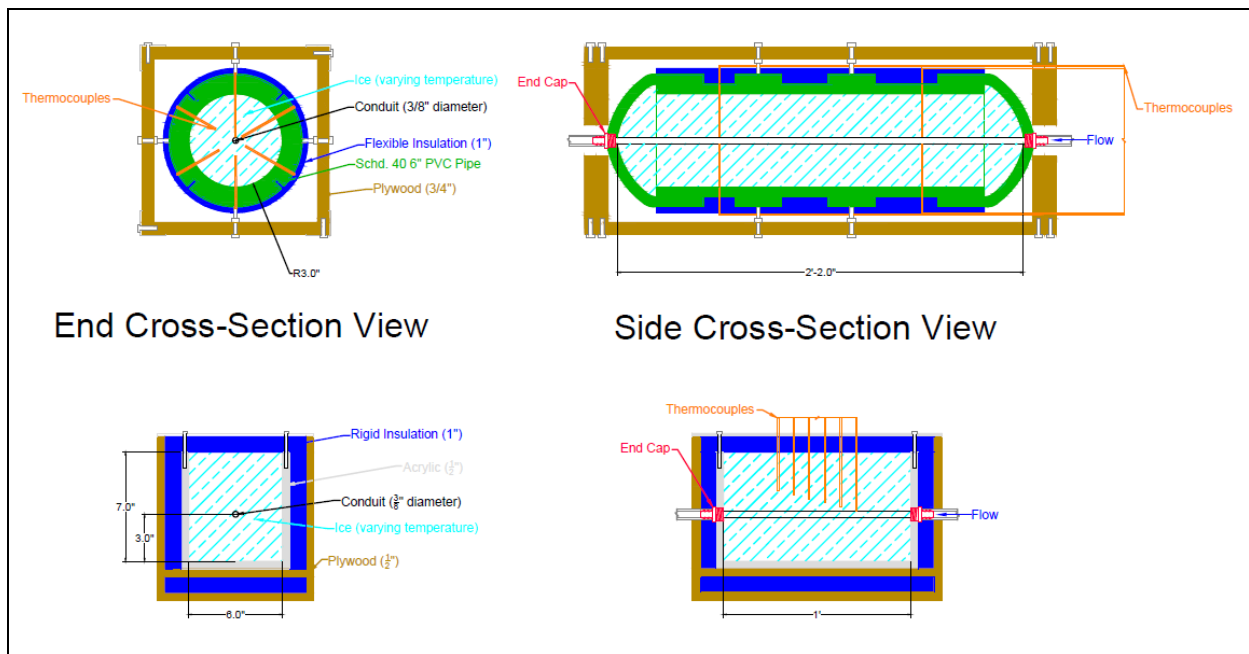


Figure 3-1: Schematic of insulated box and small pvc experimental containers used in the stagnant, low water flow, and high water flow tests

These experimental containers were then used in separate experimental setups, which differed based on which regime was being tested. The three regimes examined were the stagnant water case, low flow case, and high flow case. A comparison of these three regimes can be seen in Figure 3-2, and further details can be found in the next section of this thesis.

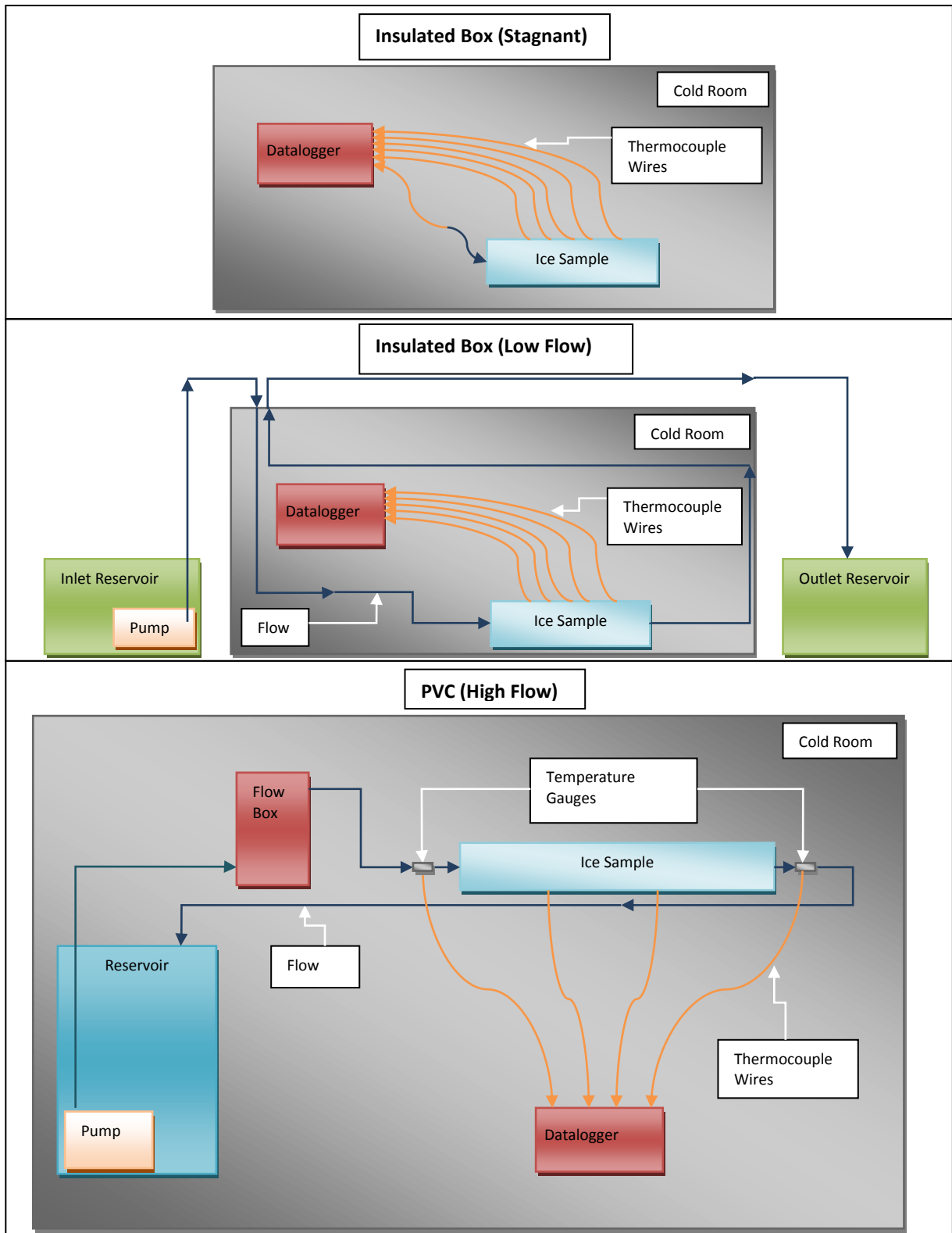


Figure 3-2: Comparison of experimental schematics for the stagnant, low water flow, and high water flow tests

4 Experimental Setups

4.1 Preliminary Trials

The initial expandable box container and trials provided valuable insight and experiences in the design and further iterations of the experiments to follow. Figure 4-1 shows an initial stagnant water test being run at the facility at NASA GSFC, where thermocouples can be seen in the ice, as well as attached to the ends to collect the water temperature as it freezes. This ice sample was frozen all at once, in a large chunk of ice, and the pressure from the side walls were released as the water froze. This was done by creating a box of plywood, 152.4mm x 152.4mm x 304.8mm, and lining it with a flexible pond liner, installing end caps for the conduit to pass through, and fabricating a metal housing of slotted angle for support.

Bolts were attached to the side panels of the box, and screwed in to apply initial pressure on the side walls to contain the water. These were then relaxed, as the ice froze, 12-24 hours into the freezing process. Figure 4-2 shows a view from above of an ice sample in the expandable box, with the conduit illuminated through the ice sample, and thermocouples along the length.

This conduit and thermocouple setup was used in the subsequent insulated box experimental technique. Some cracking of the ice can also be seen in Figure 4-2, and these large discontinuities, formed as the water froze from the outside inward, providing additional pressure on the exterior ice, were a contributing factor to the redesign of the ice housing for the subsequent experiments. While

this expandable box system may have applications for other experiments or uses, the lack of insulation and discontinuities within the ice provided results that were not used in the qualitative analysis of this project.

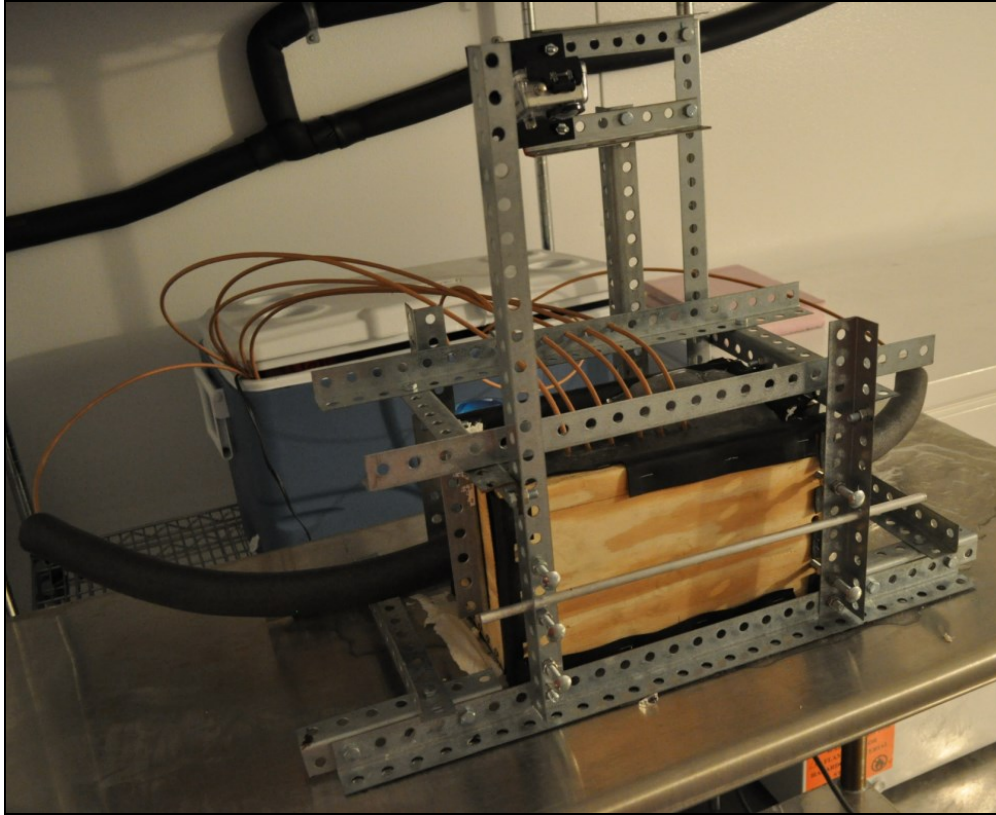


Figure 4-1: Preliminary expandable box experimental container used for initial stagnant and low flow trials at NASA GSFC



Figure 4-2: Air-filled conduit illuminated through expandable box system after augering conduit to initial dimensions, but prior to the addition of stagnant or flowing water

4.2 Stagnant Water Tests

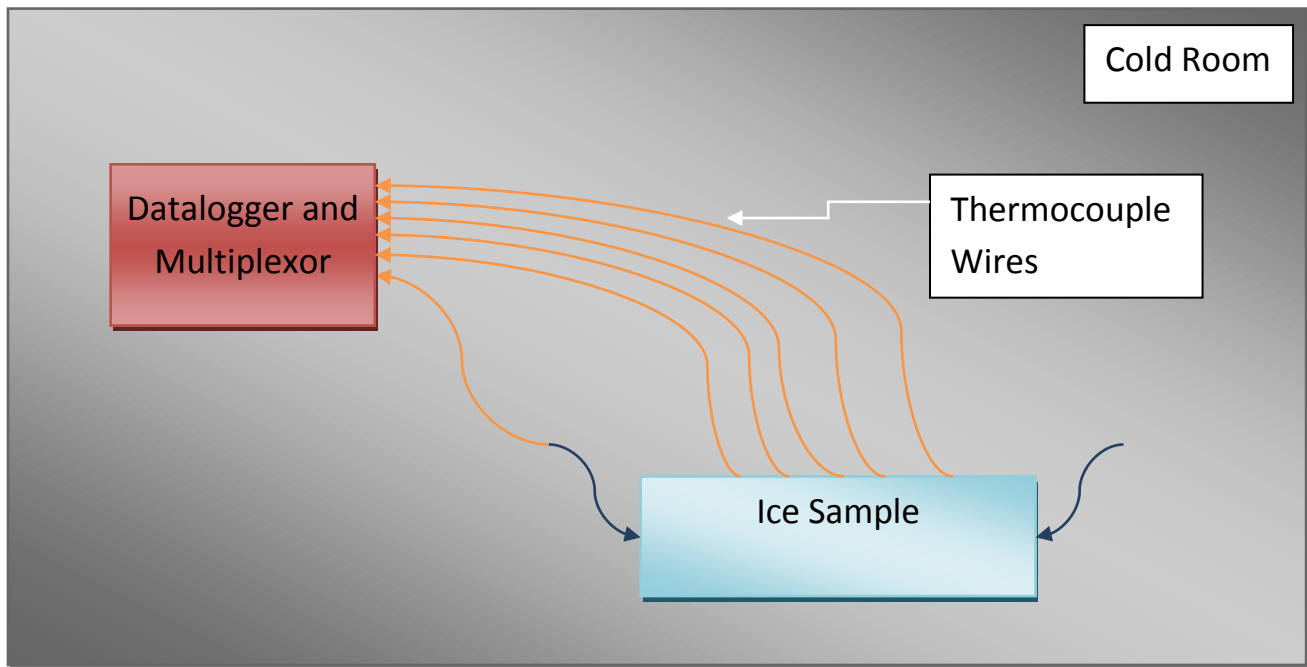


Figure 4-3: Stagnant water experimental schematic showing the ice sample and the monitoring system for recording temperatures within the ice in the cold room atmosphere of CU Boulder

The initial stagnant water tests consisted of a fairly uncomplicated setup, with the entire experiment contained within the cold room freezer at CU, as shown in Figure 4-3. The stagnant water tests used the insulated box ice sample, which was stored in the freezer, along with all tubing and datalogging materials. The initial conduit was formed by placing an aluminum rod through the ends of the ice sample and letting the ice freeze around it. To prevent the expansion as the water froze, the water was added in layers, so as not to exert an undue amount of stress on the container. These lifts, as stated before, were 6.35mm in height. The thermocouples were installed by drilling holes in from the top of the sample once the ice had frozen, placing the thermocouple tips into these holes, and re-freezing the thermocouples into place, where they could record the ice temperature data.

The bit used to re-drill the conduit can be seen in Figure 4-5, with a razor blade in the picture for scale. The freezer used in the CU Boulder laboratory was a Kenmore Elite Heavy Duty chest freezer. The datalogger collecting the thermocouple information was a Campbell Scientific CR10X, with an attached



Figure 4-4: Pictures of insulated box container used in both stagnant and low water flow tests

AM32B multiplexor. The ice within the sample had a square cross section of 152.4mm in height by 152.4mm in width, with a length of 304.8mm. Short lengths of tubing were installed on the end caps of the conduit, and water was poured into these tubes, entering and filling the conduit completely, and allowed to freeze, releasing latent heat into the surrounding system. An additional thermocouple was placed directly into the end of the tube to record the water temperature initially, and then through time as the conduit water froze. This system used the insulated box, with original testing being done at the cold room facility at NASA Goddard Space Flight Center and the expandable box setup.

The pictures shown in Figure 4-4 reveal the setup for the small box, where the insulation is clamped in place by plywood supports and the clear acrylic box contains the ice sample. End caps are threaded in place to prevent the system from leaking while it is running, and also provide support for the re-drilling of the conduit. A longer sample was not feasible in the CU freezer, since the re-drilling of the conduit after each experiment required the drill to be placed horizontally into the freezer to keep a level hole.

A drill rig setup was used and worked quite effectively to auger the conduit back to its initial dimensions. This consisted of a power hand drill mounted on a platform at a specific height. The bit was horizontal, and could be used to drill through the ice. Removing the container from the freezer for drilling was deemed infeasible, since the ice sample would be exposed to a much higher temperature and experience melting, if only slightly, around the edges. The top cap of this box setup contained holes for the six installed thermocouples to pass through, and connect the ice to the datalogger.

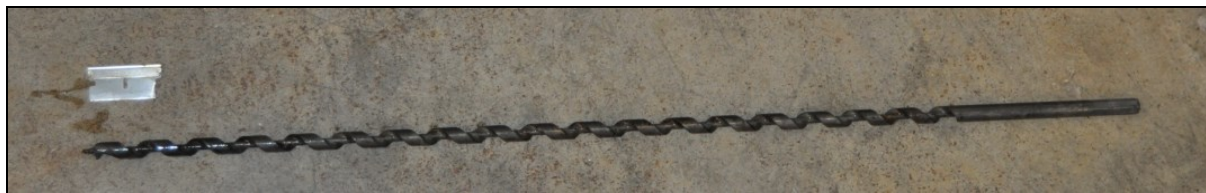


Figure 4-5: Auger bit used to re-drill the conduit for the insulated box container. The bit is 9.53mm in diameter and 609.6mm in length

4.3 Low Water Flow Rate Tests

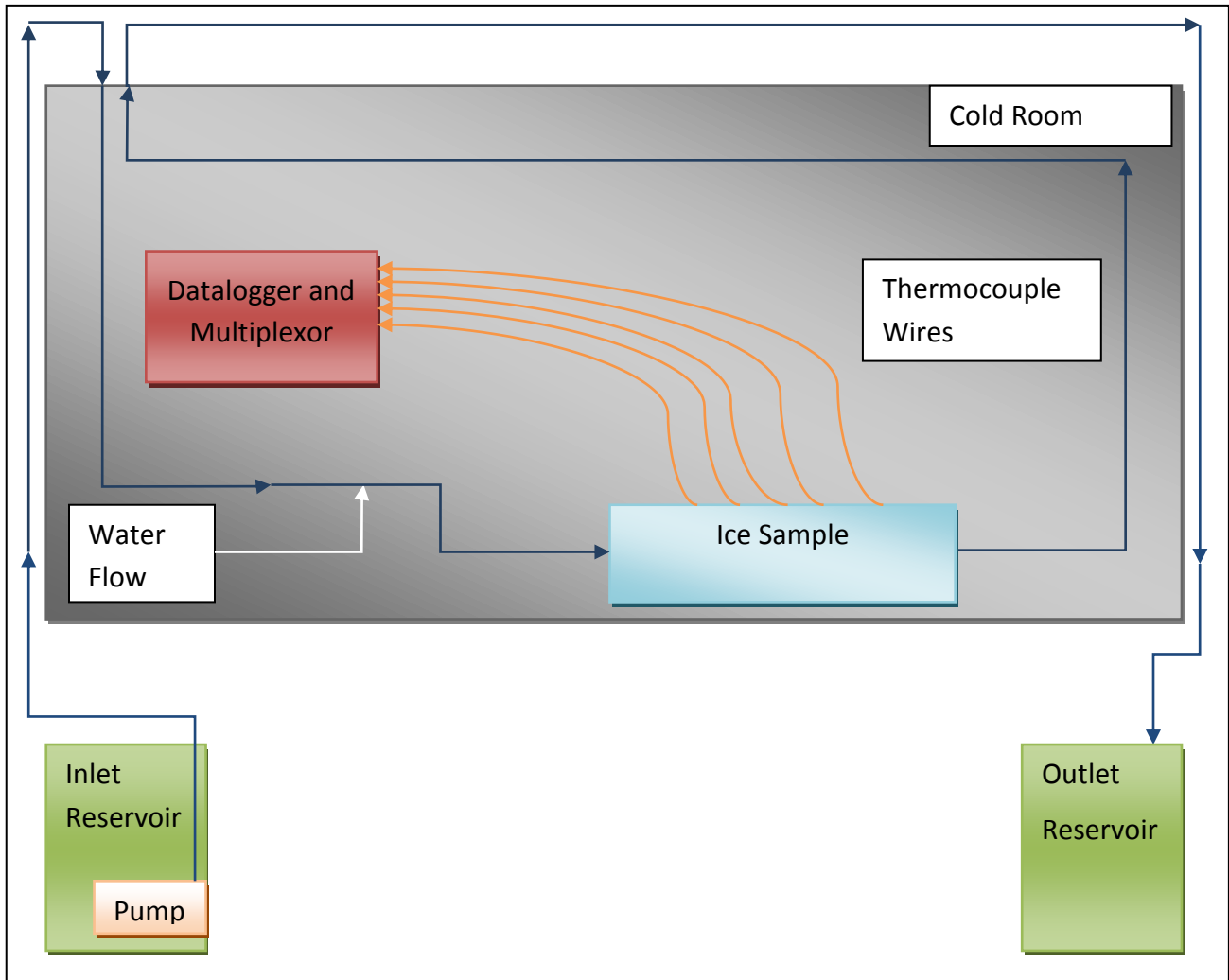


Figure 4-6: Low flow experimental schematic showing the ice sample, ice temperature monitoring system and path of flowing water through the cold room atmosphere at CU Boulder

The low water flow experiments were run in the same experimental container as the initial stagnant water experiments, in the insulated box as seen in Figure 4-4, yet the low flow experiment could not be entirely contained within the cold room freezer at CU. The freezer was thus fabricated to accommodate flow into and out of the lid. This meant the water reservoirs would have to be placed outside the cold room, and the flowing water cooled externally by ice. The pump was placed

in the inlet reservoir, while a monitoring system used to determine the flow rate through the experimental time was used in the outlet reservoir. This monitoring system tracked the rise in water level through time, to determine the flow rate, and also measured the outlet water temperature of the system. Rotameters can be seen in a photograph of the experimental setup in Figure 4-10, but with the low output of total head by the pump, the rotameters created too much head loss through the pipe system, so an alternative flow monitoring system was devised for these experiments. This monitoring system can be seen below in Figure 4-7.

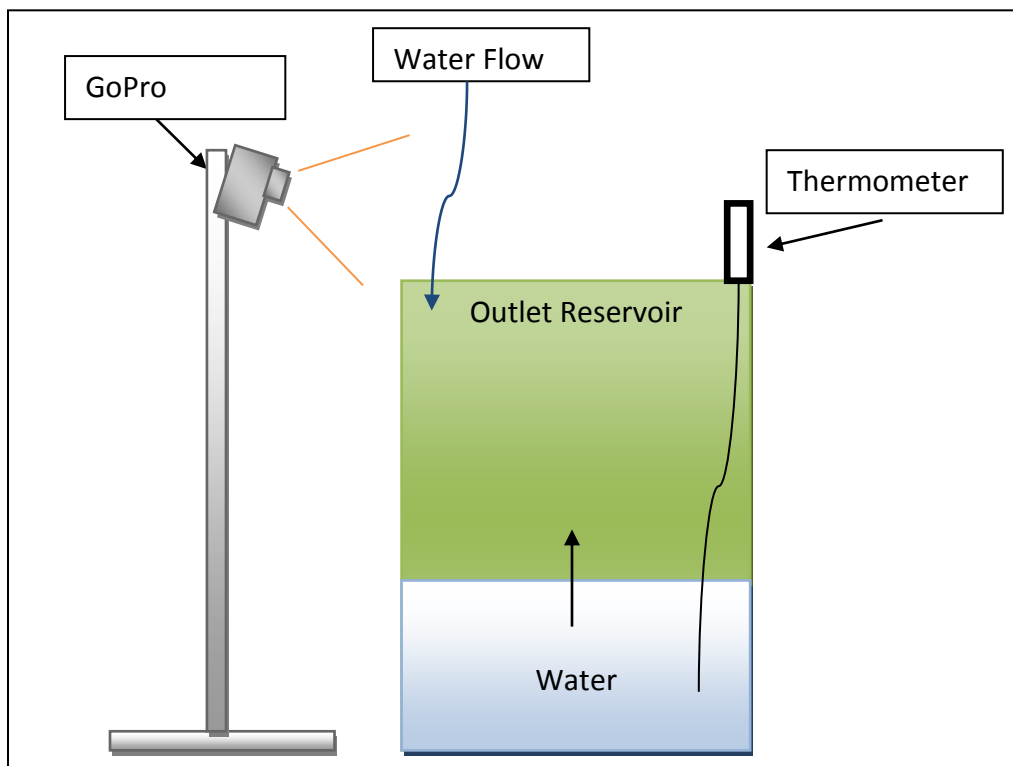


Figure 4-7: Low flow monitoring system consisting of video camera tracking changing water level height as it enters the outlet reservoir, as well as a thermometer tracking the temperature of the outlet water

The monitoring system is comprised of a mounted GoPro video camera to track the change in height of water within the $1.89 \times 10^{-2} \text{ m}^3$ bucket to calculate the total flow rate through the system. The thermometer also recorded the outlet

temperature of water upon leaving the experimental system. Note: The outlet reservoir used a $1.89 \times 10^{-2} \text{ m}^3$ bucket, whose radius varies with height, and this was taken into account through the experimental flow rate calculations. Further visualizations for the monitoring system can be found in Figure 4-8 and Figure 4-9.

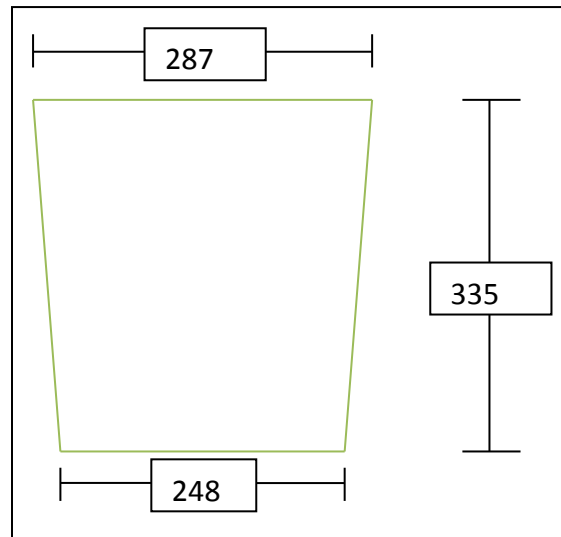


Figure 4-8: Diagram of outlet reservoir bucket (units in mm and are not to scale) used in determining the volume change associated with a changing water level height as seen in Figure 4-7



Figure 4-9: GoPro video camera snapshot of outlet reservoir bucket for low water flow experiments. A thermometer and ruler can be seen, as well as water flowing into the outlet reservoir

For further results on the monitoring system and its outputs, the graphs can be seen from Figure 4-26 to Figure 4-28. The flow rate from the GoPro video camera was calculated by tracking the change in time per 10 centimeter rise in water level height of the bucket, which led to stepwise function behavior. This function was not the most ideal for input into the theoretical model so the flow rate was idealized by fitting a third degree polynomial equation to the data, and these values were used when input into the numerical model.

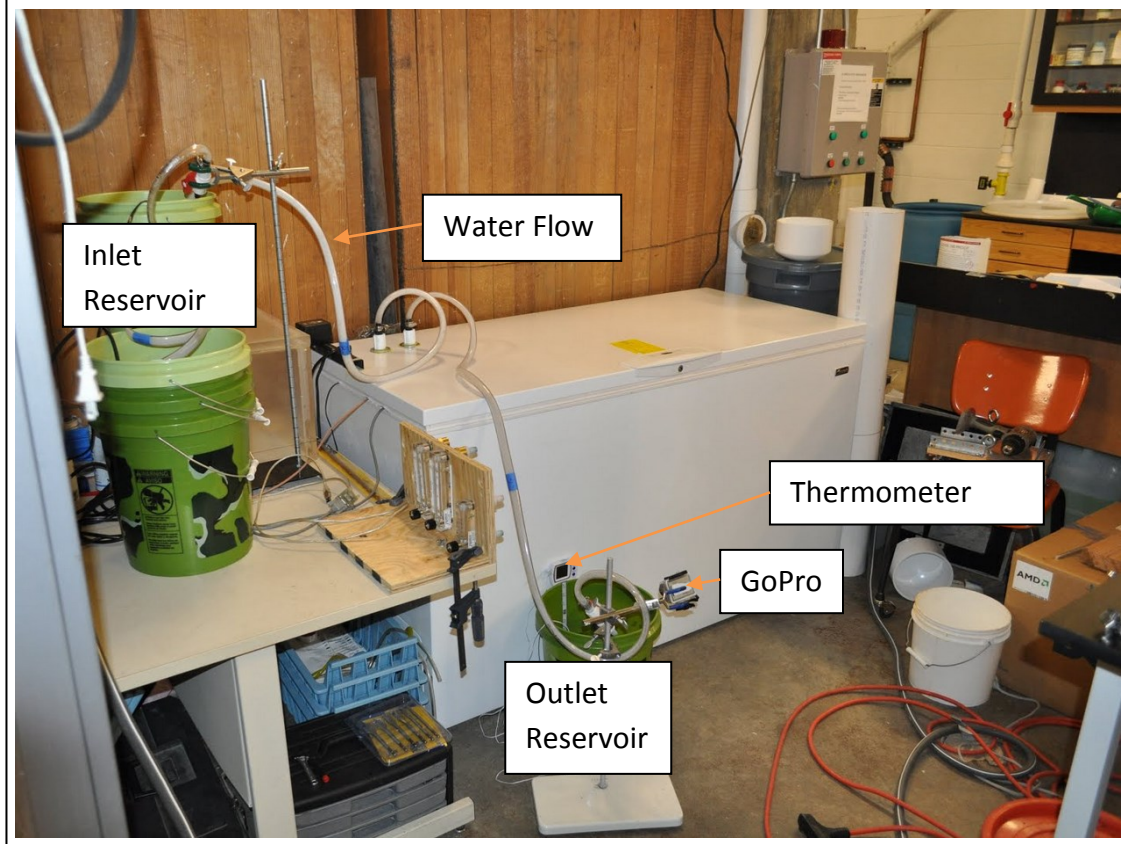
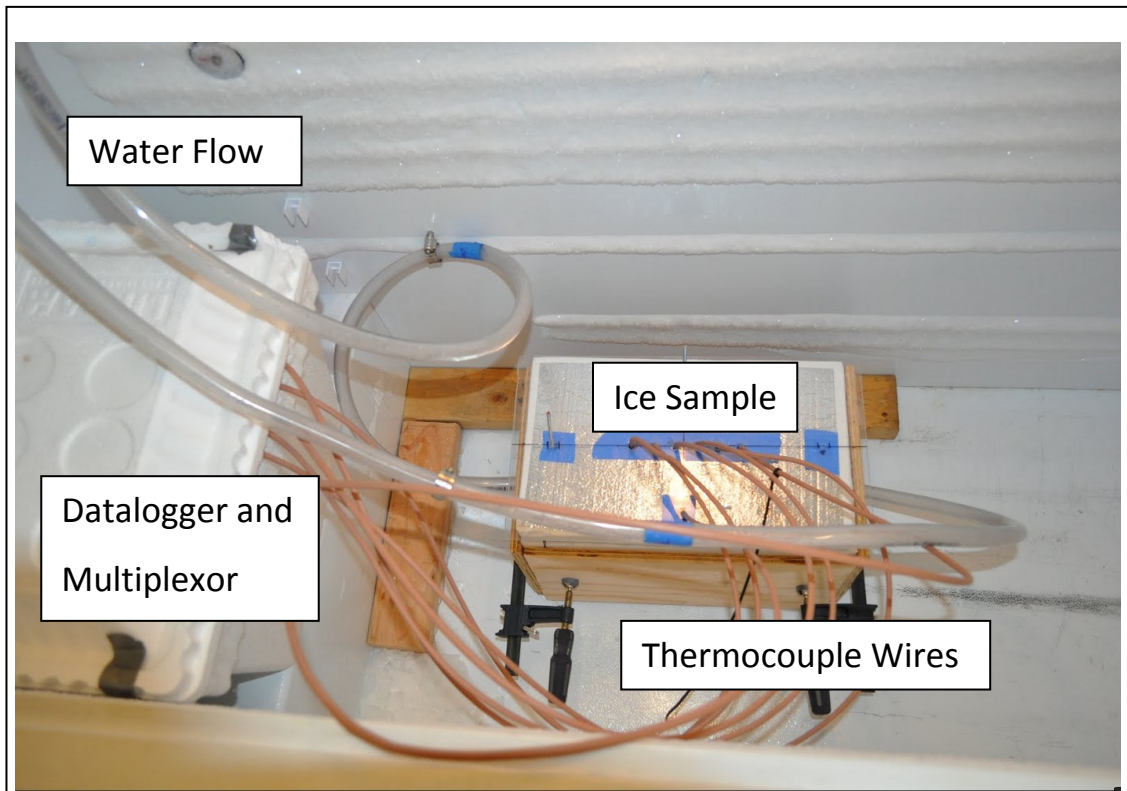


Figure 4-10: University of Colorado low flow experimental setup detailing the physical housing of the ice sample as well as the inlet and outlet reservoirs

4.4 High Water Flow Rate Tests

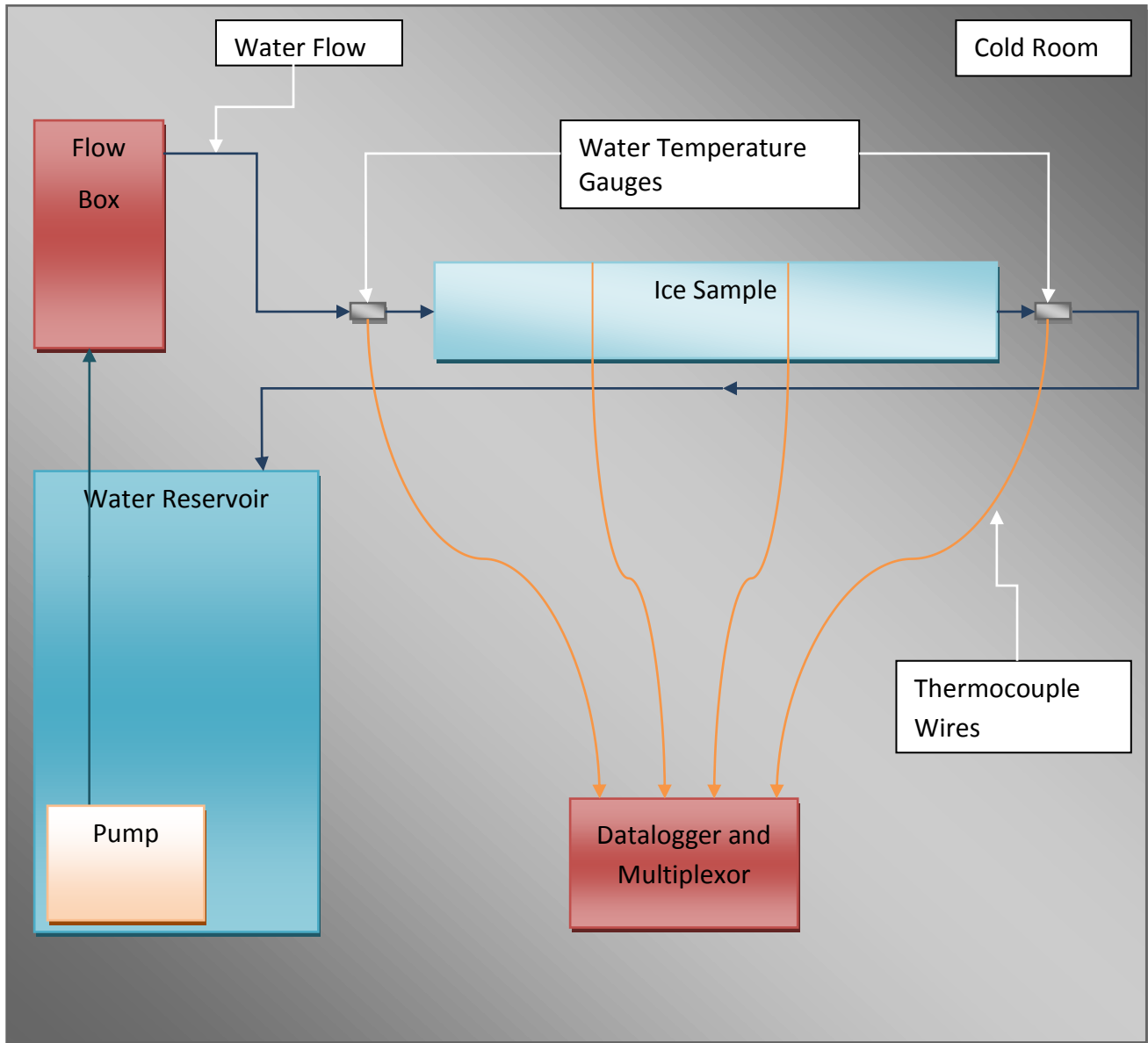


Figure 4-11: High flow experimental schematic showing the ice sample and monitoring system for the high flow water tests run at NASA GSFC

The higher flow rate tests were run at a cold room facility at NASA GSFC. These tests followed the same general approach as the low flow tests run at CU, but the larger environment at NASA GSFC facilitated substantially longer and higher flow rate trials. The cold room facility in the cryospheric lab provided much lower fluctuations in temperature throughout the experiment, and provided enough room to work within the entire cold environment. To run these tests, water is stored in the cold room in the cold water reservoir, along with the ice sample, water temperature gauges, and datalogger/multiplexor box.

When the test is ready to run, the pump, tubing and flow box are brought into the cold room (They become too rigid and breakable when stored in the cold room between experimental trials, so they are stored in a warmer environment and brought in only when the tests are run). To keep the water at a temperature as close to freezing as possible, the cold water reservoir is stored in the freezer, and the reservoir freezes on the surface. The surface must be chiseled out in order to place the pump in the liquid prior to testing, as the reservoir tends to freeze between trials. The flow box must be leveled so the flowmeter is vertical, and can measure the flow rate accurately.

The tubing is tightened to all of the inlet and outlet end caps, so that the entire system is sealed, and the water can flow freely from the cold water reservoir, up the pump, through the flow box, into the water temperature gauge, through the ice sample, out of the other water temperature gauge, and finally back into the cold water reservoir, where it is recycled and allowed to flow through the system once more, as seen in Figure 4-11. The thermocouples installed in the ice sample are routed back to the datalogger and multiplexor, to record the ice and water

temperature every 30 seconds. The temperatures being recorded are the inlet and outlet temperatures, ice profile temperatures, and ambient freezer temperature.

Figure 4-12 shows the physical setup in the cold room at NASA GSFC. Only the top of the pump system can be seen over the top of the reservoir in Figure 7-12. A computer is also shown in this picture and is used to record in real time the thermocouple temperature readings. A GoPro camera is clamped in place to record the flow rate during testing, much like the previous slow flow test, here monitoring both the flowmeter and cold water reservoir temperature. The camera can be seen attached to the water reservoir, just above the ice sample.

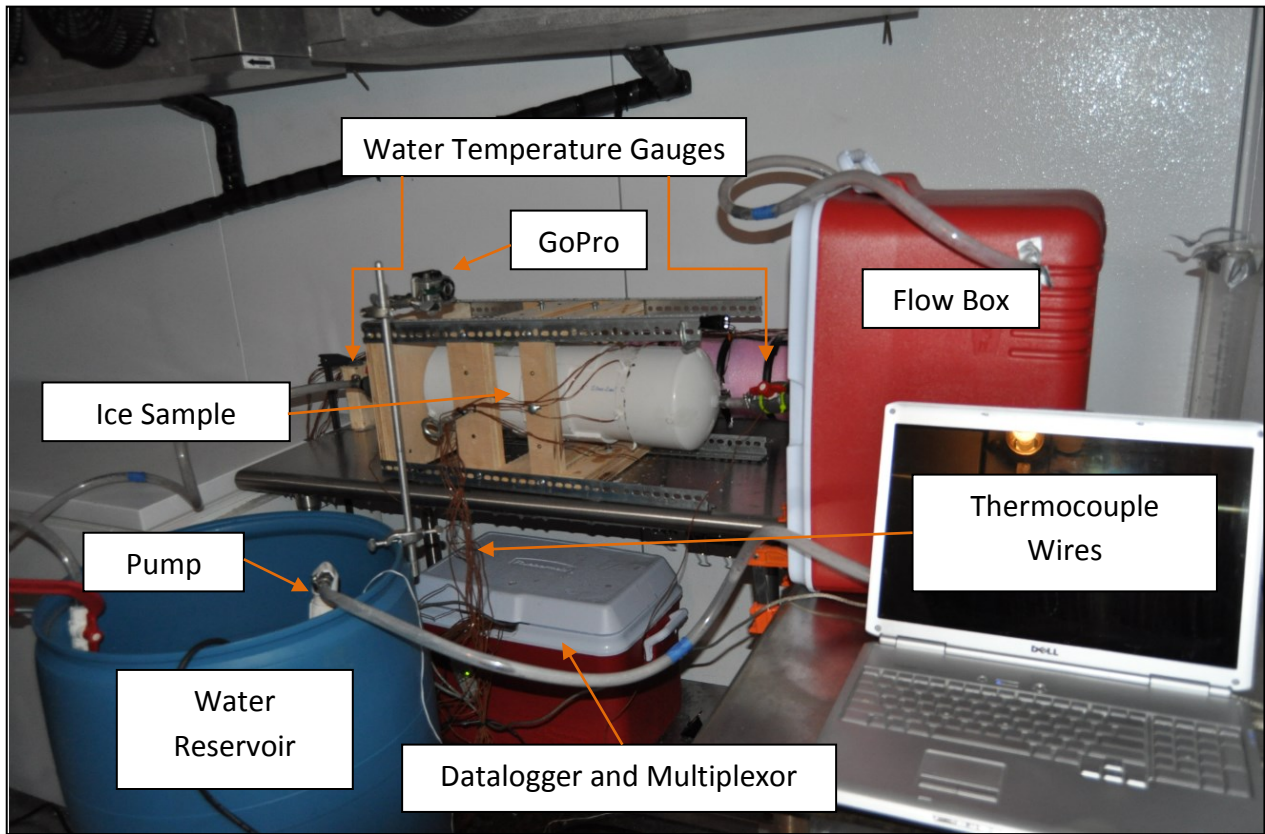


Figure 4-12: NASA GSFC high flow experimental setup detailing the layout of the testing from the pump to the flow box, through the ice sample and back to the water reservoir

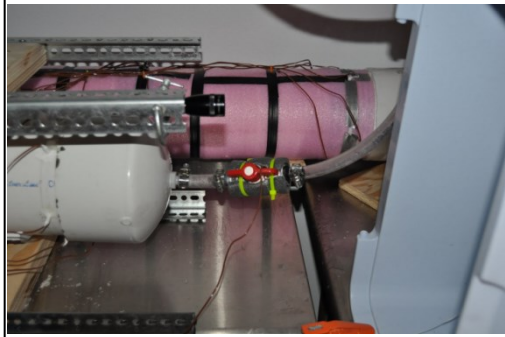
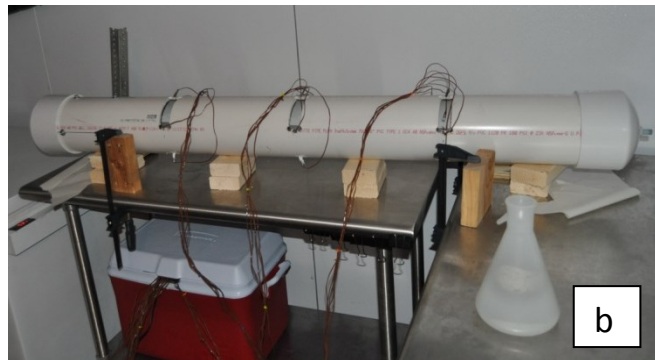


Figure 4-13: Water temperature gauges, at the outlet of the large pvc experiment and inlet of the small pvc experiment

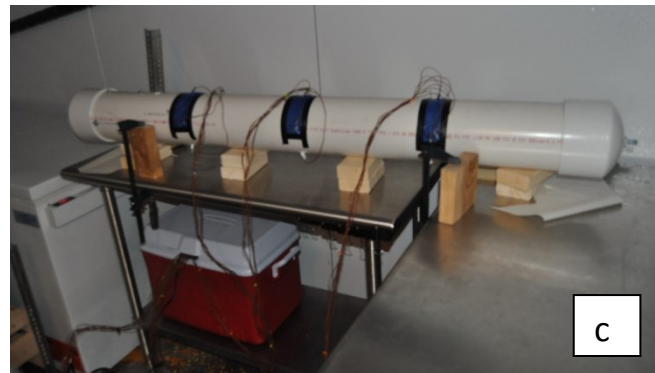
Figure 4-13 shows a close up of the water temperature gauges being used, attached to the inflow of the smaller radial PVC experimental container and outflow of the larger radial PVC experimental container. A level and threaded rod can also be seen in the top picture, which are both used for conduit redrilling purposes, as well as leveling the experiment to the horizontal plane before the water is added. The temperature gauges consist of a valve with a thermocouple installed through a hole in the bottom. The valve is sealed open, and the thermocouple placed in the middle of the flow stream, and then made watertight.



Figure 4-14 shows the large flow rate experimental setup. First, rectangular holes were drilled out of the PVC walls of the conduit-ice system container to provide for access to the thermocouples at the three different profiles throughout the sample. Next, holes are drilled into the PVC walls and the thermocouples are placed into the setup. Then, water is



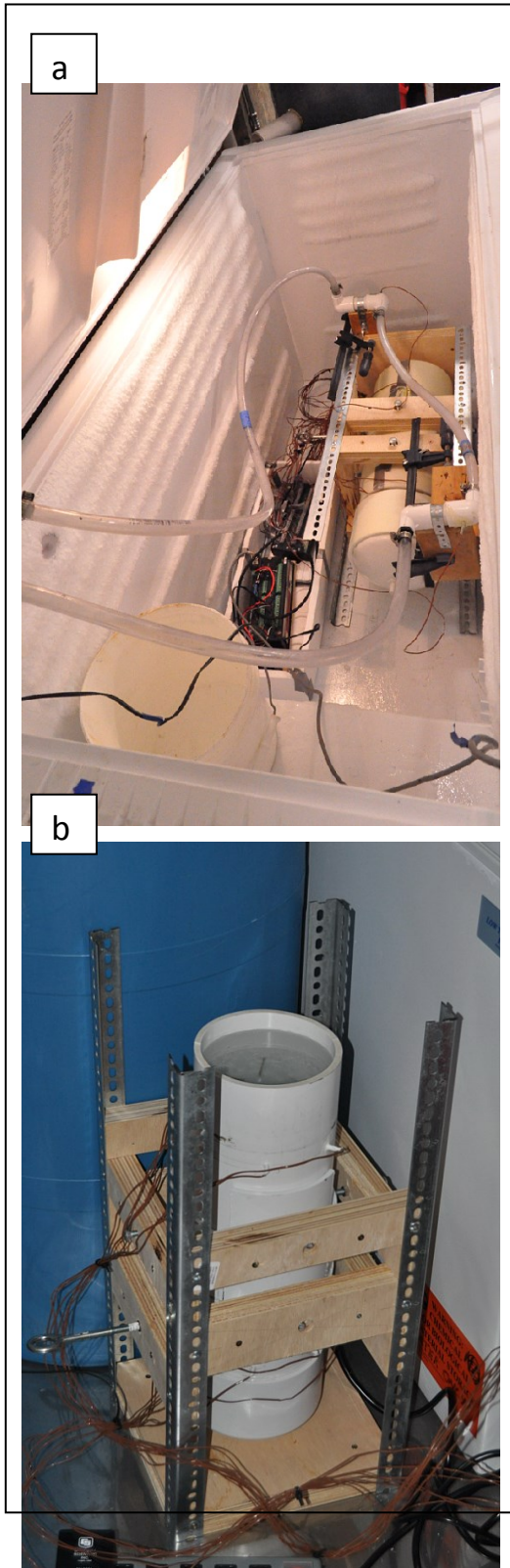
frozen, again in layers, and the thermocouples are manipulated into place with pliers as the ice level rises in the sample. These locations are found by measuring the distance of



the thermocouples from the rectangular holes, and once again upon completion of the trials when the setup is taken apart, and the photos digitized as seen in Figure 4-29. Once the ice level reaches the bottom of the hole, the sample is then waterproofed. Holes are drilled in from the top, in order for the sample to be used multiple times.

Figure 4-14: Large pvc setup during fabrication showing a) initial access to interior of sample b) during thermocouple installation, and c)waterproofing of container

This setup did not produce results that can be easily examined since the conduit



through the ice sample did not remain in a straight line. Upon completion of testing, when the setup was taken down, the cross-sections were examined at the thermocouple profile locations, and the conduit was found to be located at varying locations from the walls of the container. This can be attributed to the meandering of the conduit from the water flow through the ice amplified by difficulties in initial drilling. Figure 4-15 at left shows the small radial PVC experimental setup being tested at the CU facility and in the process of freezing in lifts at NASA GSFC.

Figure 4-15: Small pvc setup a) in CU lab before beginning of experimental testing and b) during the freezing in lifts stage at NASA GSFC (below)

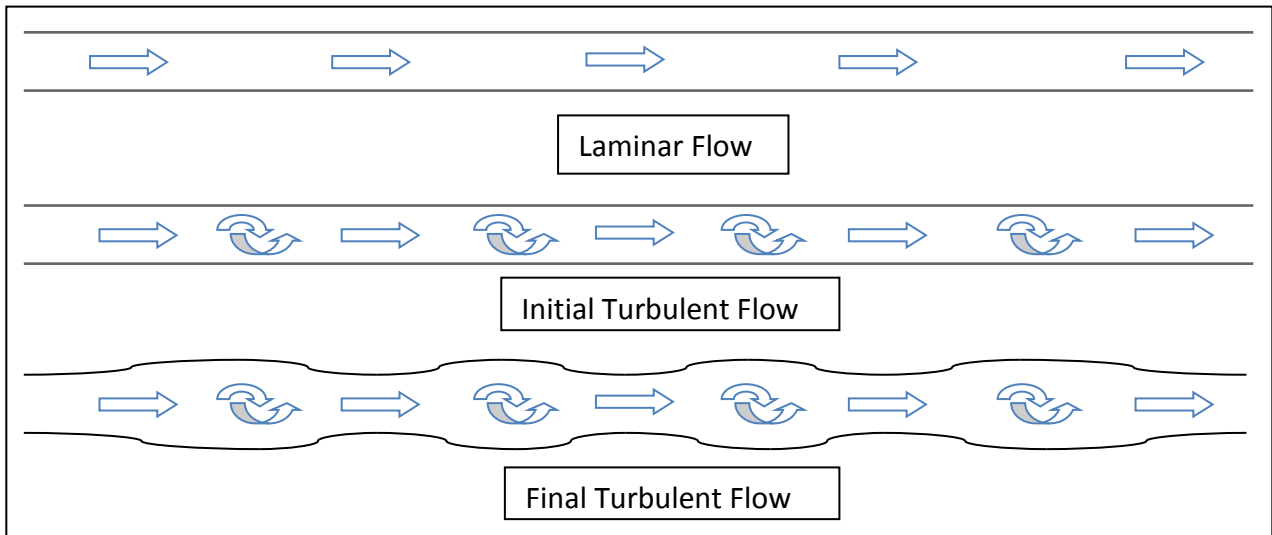


Figure 4-16: Evolution of conduit cross-section from initial laminar flow to turbulent flow and scalloping of conduit walls



Figure 4-17: Photo of subglacial conduit beneath Hansbreen, a polythermal glacier in Norway, exhibiting scalloping behavior. Photo credit to J.D. Gulley (Gulley et al., 2013)

The turbulent flow of water through the conduit generates flow paths of the water that are not in straight lines, as laminar flow would, as shown in the top representation in Figure 4-16. The conduit starts, initially, with straight boundaries that resemble a smooth pipe, as seen in the top initial laminar flow figure above. Then, as the turbulent flow starts, and the conduit begins to expand, eddies form and carve out dimples and coffer-like structures, or scallops, form around the edge of the conduit. This progression is shown in Figure 4-16, and the final conduit, upon draining the experiment of all water, matches the experimental observations. See Figure 4-18 and Figure 4-20. This physical process is vital to the understanding and modeling of the experiments, and is examined further in Section 5.1.

Figure 4-17 is a photo of a glacial Moulin at the outlet of a glacier and shows the effects of turbulent water flow through a glacier. The eddies generated on the ice water interface carve out scallops in the ice. It is for this reason that the friction

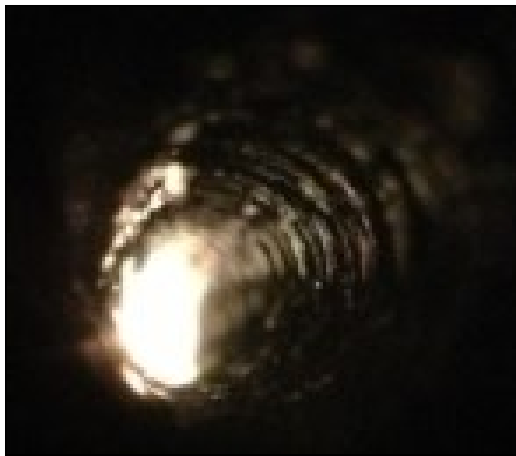


Figure 4-18: Initial conduit geometry of high flow test after reaugering of conduit

factor for these englacial conduits and moulins is on the rough side of the Darcy-Weisbach scale. The friction factor for these englacial conduits far exceeds typical values observed for engineered pipes, wherein reduction of friction losses is desirable (Gulley et al., 2013)

Figure 4-18 documents the conduit before the high flow through the ice and Figure 4-19 shows the conduit cross-section after the flow has been stopped and the conduit emptied.

The conduit can initially be seen to be somewhat rough around the edges, yet has a 9.53mm radius along its entire length. Upon completion of the test, however, it can be seen that the ice water interface is very smooth, yet does not have a uniform radius the entire length. It can also be seen to exhibit properties very similar to the scalloping in

Figure 4-17 and has the behavior demonstrated in Figure 4-16. A feasible, robust method for measuring this radius, in the experimental setup shown, was not developed. Short of x-ray computed tomography, an exact radius for this experimental setup, with the ability to run multiple tests with the same ice sample, proved elusive. Figure 4-20 shows the final conduit upon a preliminary flow trial through the expandable box setup, and corroborates the eddy generation and scalloping behavior suggested above.

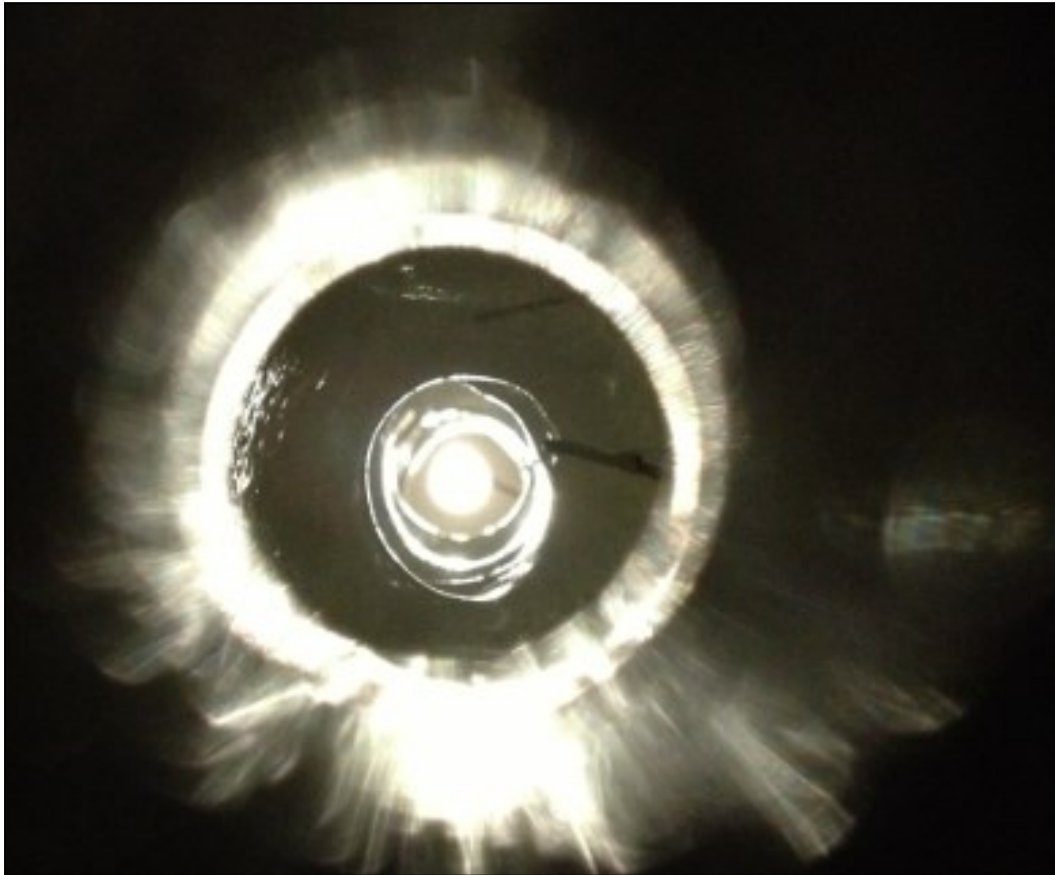


Figure 4-19: Final conduit geometry of high flow test showing cross-sectional variations through flow path and scalloping due to turbulent flow

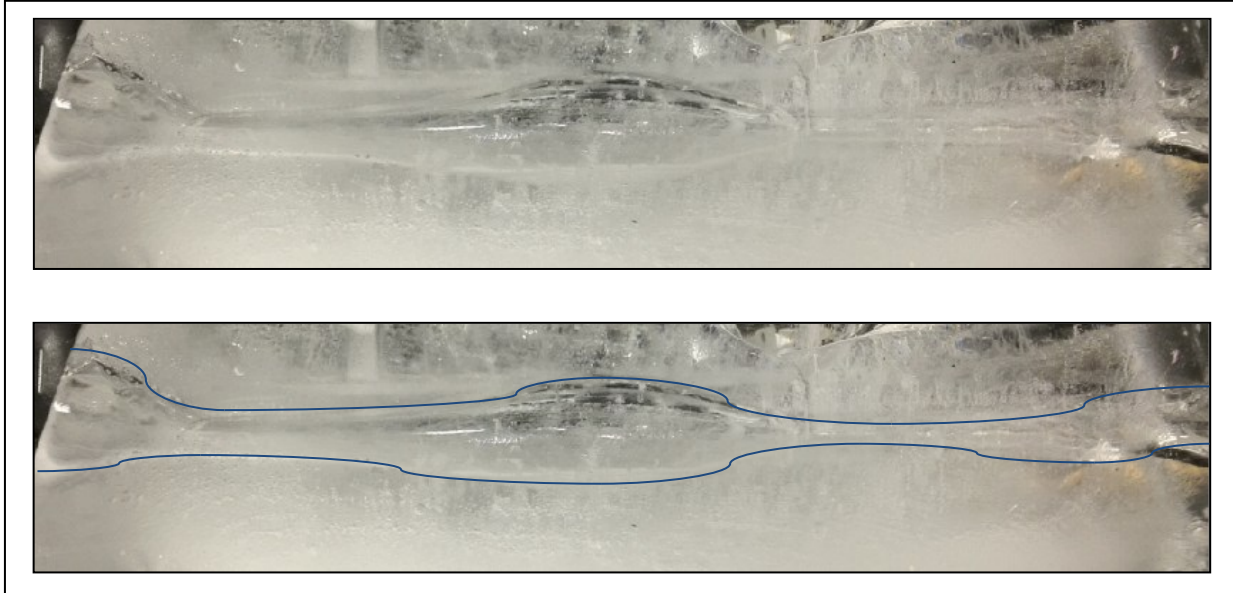


Figure 4-20: Final conduit after flow through ice in expandable box system showing lengthwise cross-sectional variation of scalloping due to turbulent flow

4.5 Results (Stagnant Experiments)

The stagnant water tests were run with one profile of thermocouples set along the length of the conduit, as shown in Figure 4-21. The thermocouples were located at distances away from the conduit center as follows: 14.2mm, 24.6mm, 29.5mm, 37.3mm, 42.2mm and 44.5mm. These somewhat odd-seeming thermocouple locations are the result of the thermocouple installation errors, when the freezing water heaved them out of their intended positions. These values were obtained upon the completion and dismantling of the test by marking the location on the thermocouple wire where it entered the ice and measuring the length from that point to the thermocouple tip.

The thermocouples recorded temperature values through time as the test was run, with the initial time of 0 seconds as the point when the water first came in contact with the surrounding ice. The following graphs, from Figure 4-22 to Figure 4-24, show ice temperature profiles through time for three different experiments, as latent heat was released from the freezing water within the conduit.

The initial ice temperatures of the stagnant water experiments are shown in Table 4-1 and range from -13.4 degrees Celsius to -26.0 degrees Celsius.

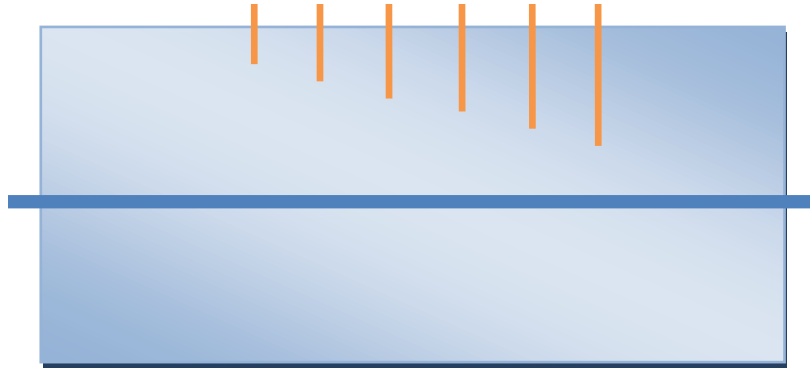


Figure 4-21: Length-wise cross-section of thermocouple locations in insulated box for stagnant water testing

Table 4-1: Initial ice temperatures of stagnant water experiments

Stagnant	
Initial Ice Temperature (°Celsius)	
	-13.4
	-14.4
	-18.7
	-18.8
	-26.0
	-26.1

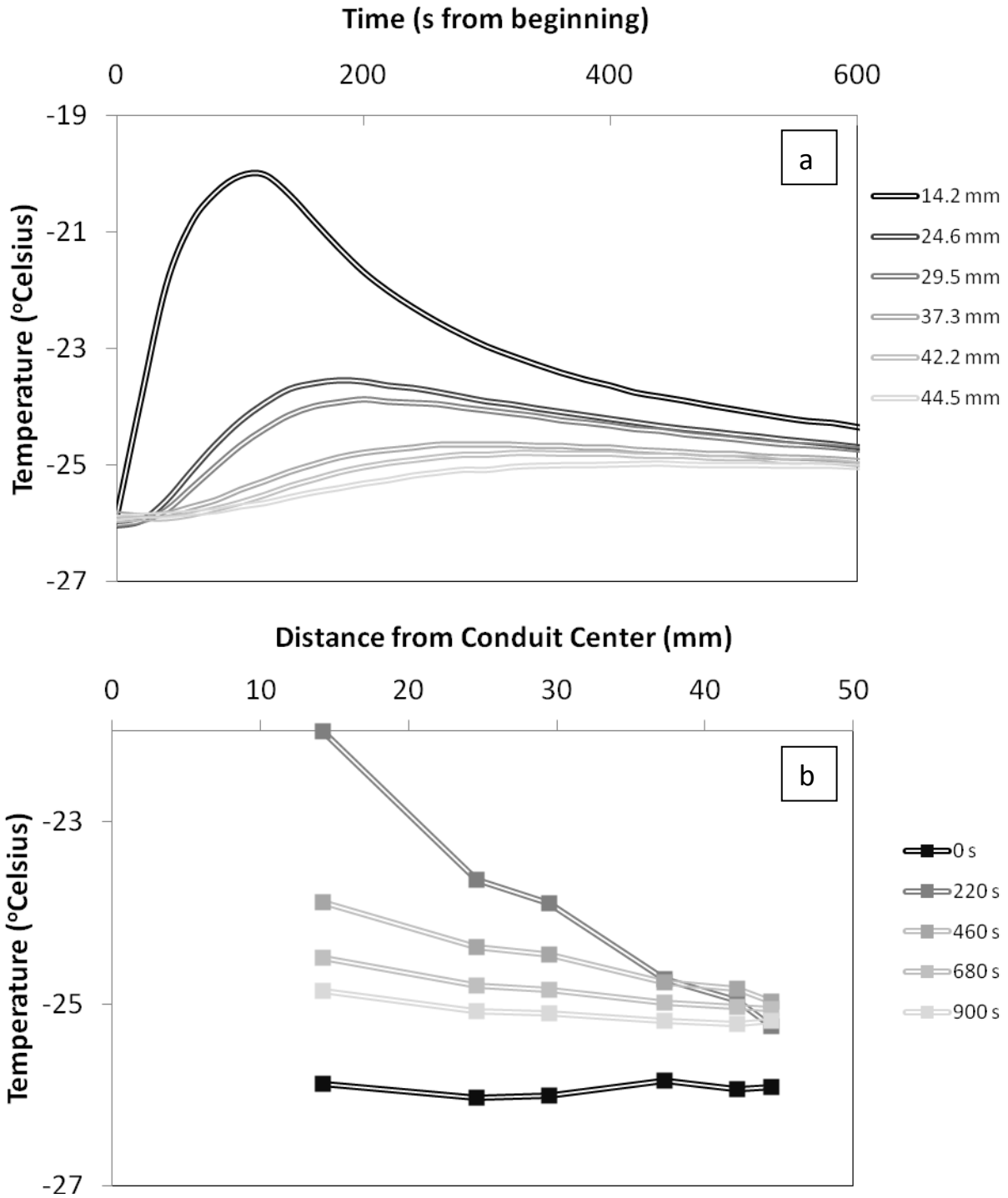


Figure 4-22: Stagnant water test results from -26.0° Celsius ice showing a) individual thermocouple temperature recordings through time and b) temperature profiles of the ice through time

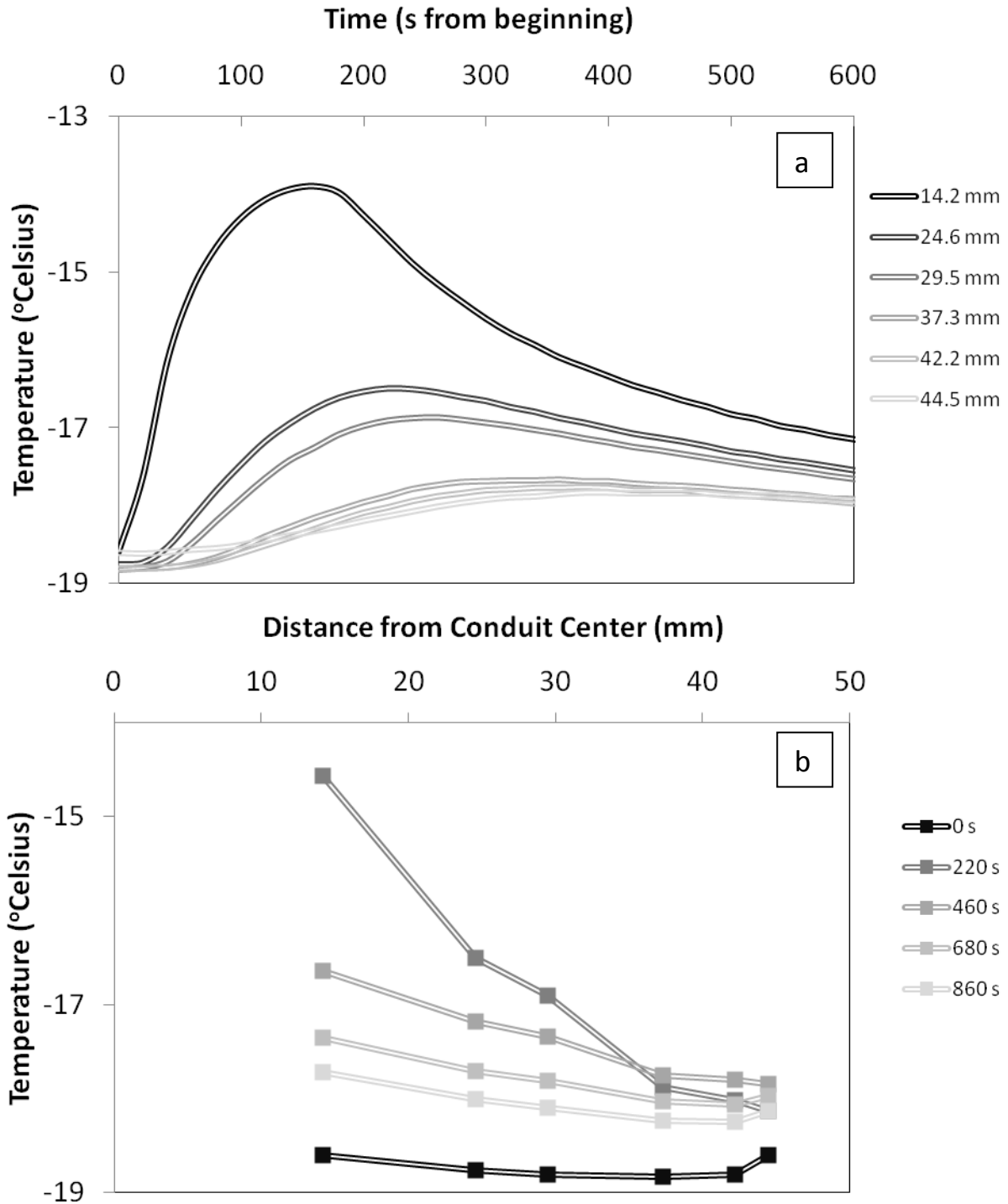


Figure 4-23: Stagnant water test results from -18.7° Celsius ice showing a) individual thermocouple temperature recordings through time and b) temperature profiles of the ice through time

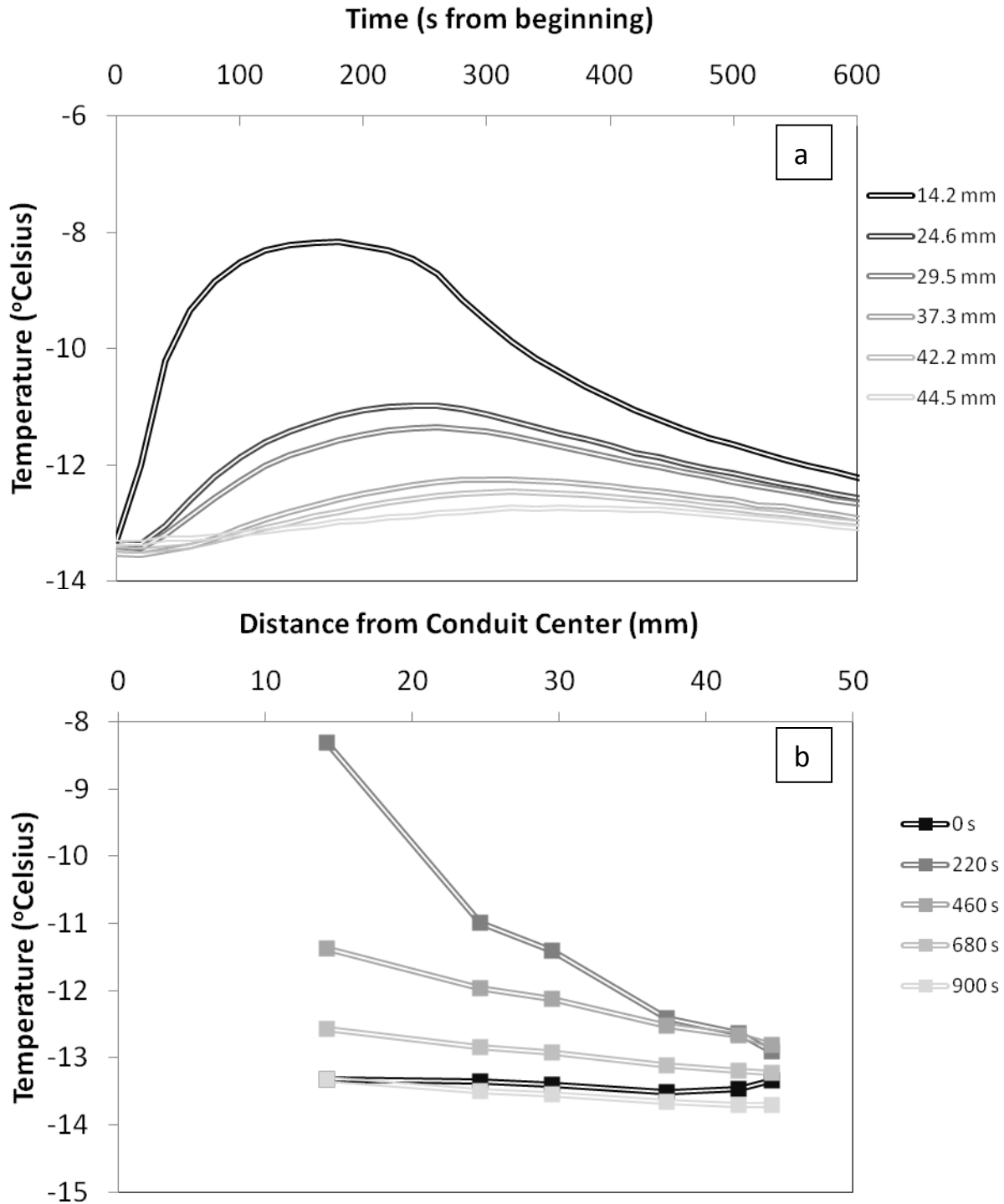


Figure 4-24: Stagnant water test results from -13.4° Celsius ice showing a) individual thermocouple temperature recordings through time and b) temperature profiles of the ice through time

4.6 Discussion (Stagnant Experiments)

The results from the stagnant test show an initial increase in the temperature of all thermocouples along the conduit length as the latent heat from the water is released into the surrounding ice. Once the conduit freezes, and no more energy is provided to the system, the thermocouples return to just above their initial values, retaining the energy input into the system due to the insulation. As qualitative results go, the thermocouples behaved as predicted, with the closest thermocouple responding to the additional heat in the system faster than the thermocouples farther away from the conduit center in all trials.

Due to the small ice sample size, and lack of confining stress during freezing, creep can be neglected in all of the experiments. Given the freezing of the ice in layers, and the small amount of time the trials take to run, the stresses in the ice were relieved as it froze. Since only 76.2mm of ice existed above the conduit center, the ice held its structure well after the conduit had been redrilled. This matched observations during testing, as the conduit was typically drilled the day before the trial was run. Prior to running the trial, the 9.53mm rod used to initialize the conduit for the first test was once again run through the conduit, and showed that the conduit had maintained its 9.53mm diameter in the absence of water, as it passed freely through the conduit, thus verifying that no creep closure occurs.

See Section 6.1 for further comparisons among all stagnant water tests, along with numerical model predictions.

4.7 Results (Low Flow)

The low water flow tests were also run with one profile of thermocouples set along the length of the conduit, as shown below in Figure 4-25, which is identical to the stagnant water tests. The thermocouples were also located at distances away from the conduit center as follows: 14.2mm, 24.6mm, 29.5mm, 37.3mm, 42.2mm and 44.5mm. The ice sample from the stagnant water testing was used for the low flow water tests. The thermocouples recorded temperature values through time as the test was run, with the initial time of 0 seconds as the point when the water first came in contact with the surrounding ice.

The following graphs, from Figure 4-26 to Figure 4-28, show ice temperature profiles through time for three different experiments as latent heat and viscous heat due to friction with the side walls are released from the freezing water within the conduit, as well as the measured flow rates through time from the monitoring system shown in Figure 4-7. The results from the flow rate monitoring system were not smooth, as the monitoring system provided only a general approximation of the flow rate. The flow rate from the GoPro video camera was calculated by manually tracking the change in time per 10 centimeter rise in water level height of the bucket, which led to stepwise function behavior. An idealized value through time was used from a third order polynomial trend line and replicated the physical behavior of the flow rate through the noise. The pump used to provide the flow was a ViaAqua PowerHead Pump, whose flow rate decreased as the conduit froze in on itself, providing additional head loss through the system as time progressed, and was not the most consistent.

The initial ice temperatures of the stagnant water experiments are shown in Table 4-2 and range from -14.3 degrees Celsius to -20.6 degrees Celsius.

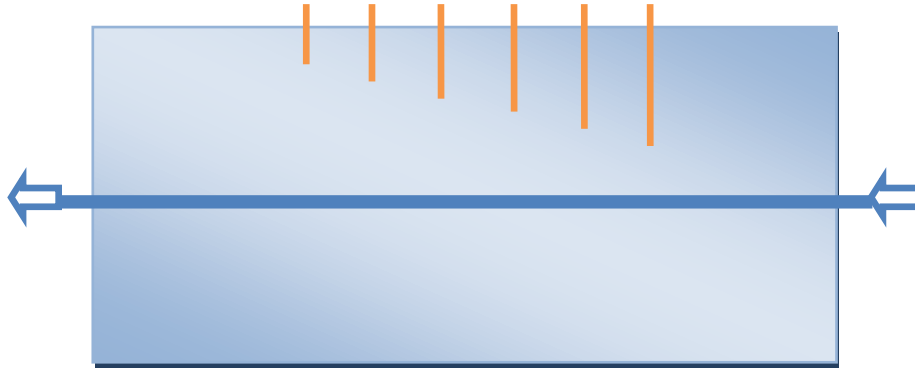


Figure 4-25: Cross-section of thermocouple locations in insulated box for the low water flow experiments and their respective locations in relationship to the flow of water

Table 4-2: Initial ice temperatures, flow rates, and closure times of low water flow experiments

Low Flow		
Initial Ice Temperature (°Celsius)	Initial Flow Rate (m³/s)	Conduit Closure Time (s)
-14.0	1.18E-04	250
-14.3	1.29E-04	200
-14.9	1.29E-04	260
-19.3	1.18E-04	200
-19.9	1.31E-04	200
-20.1	1.94E-04	200
-20.6	1.62E-04	170

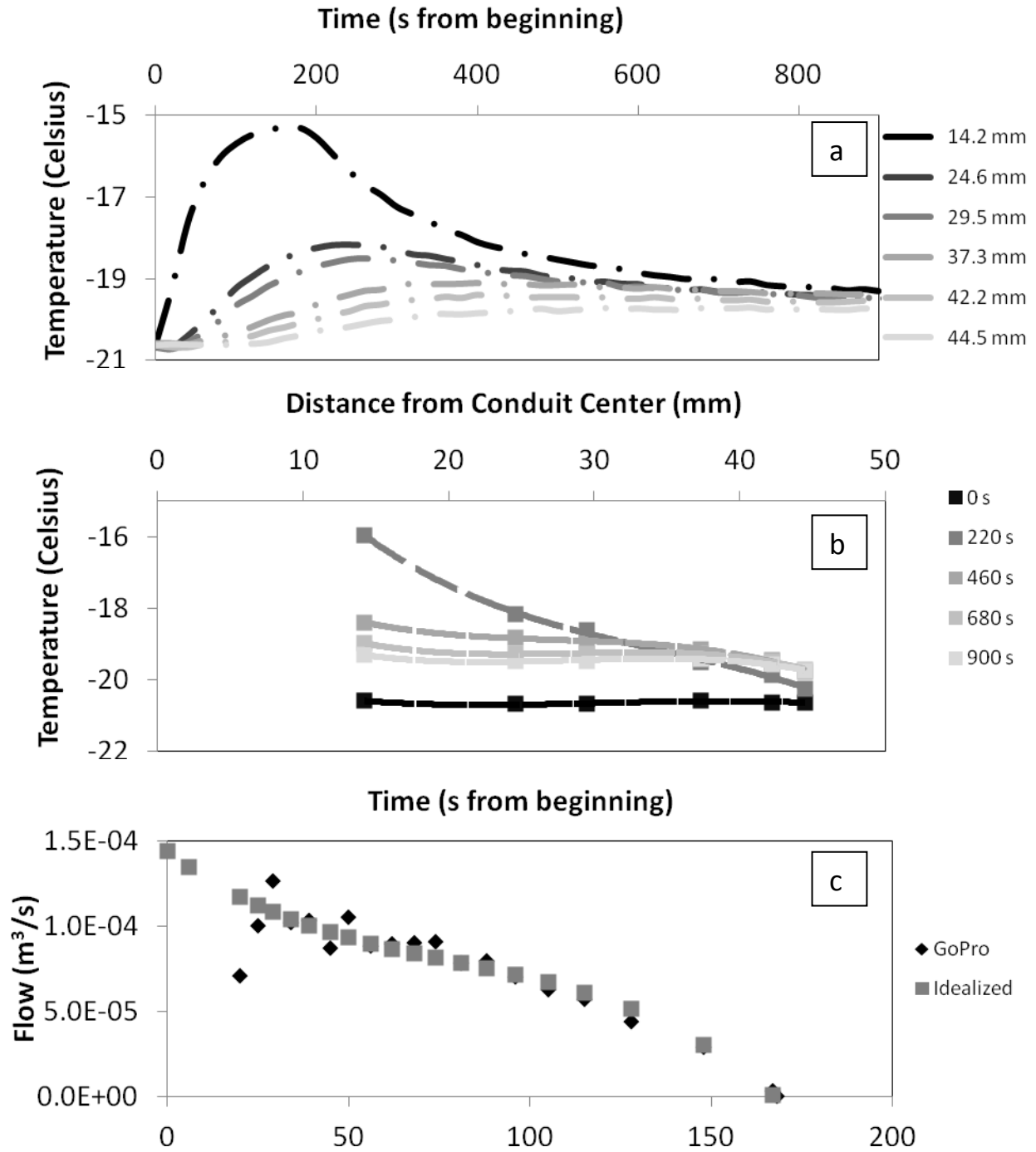


Figure 4-26: Low water flow test results from -20.6° Celsius ice showing a) individual thermocouple temperature recordings through time b) temperature profiles of the ice through time and c) flow rate of water within the conduit through time

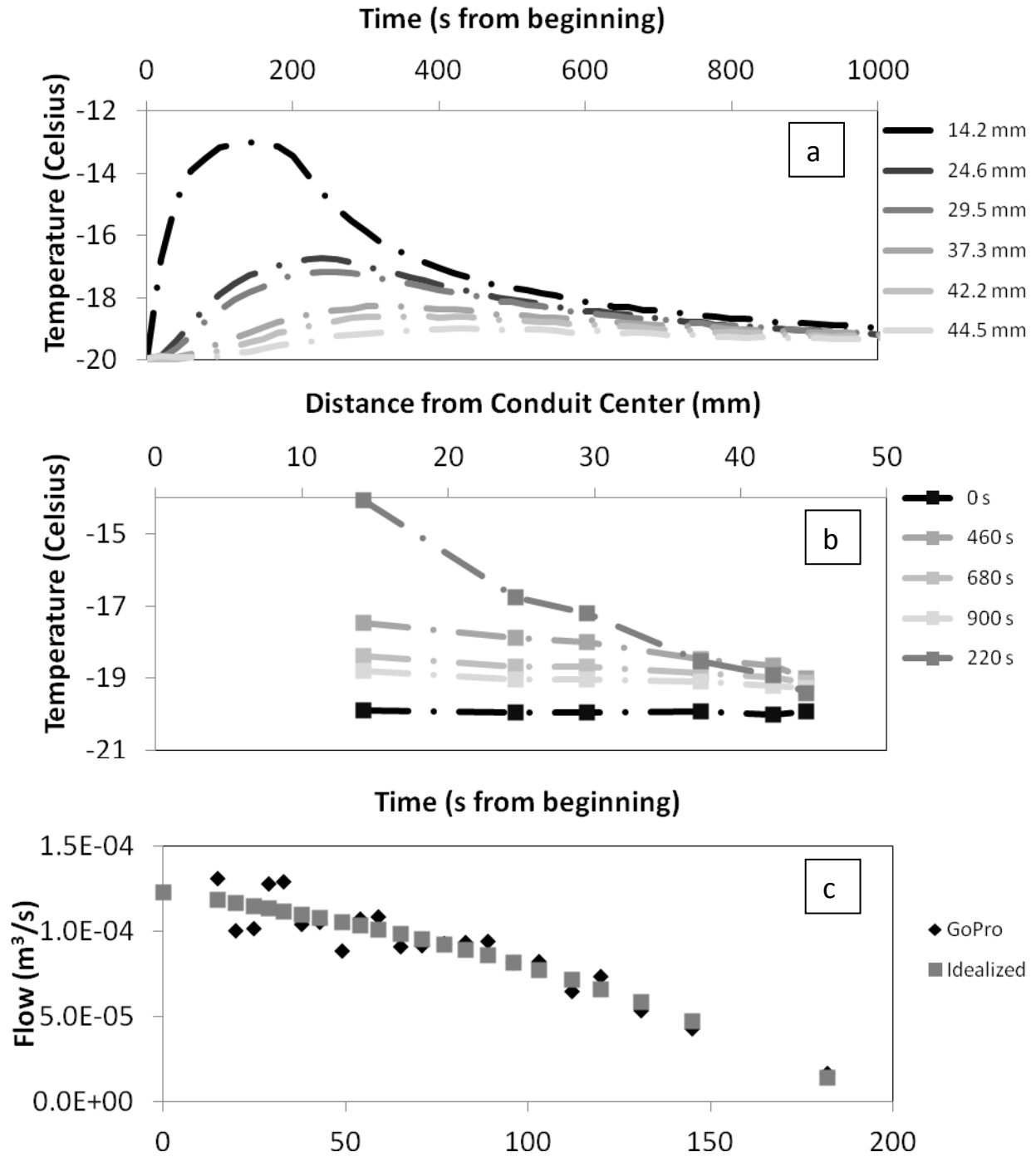


Figure 4-27: Low water flow test results from -19.9° Celsius ice showing a) individual thermocouple temperature recordings through time b) temperature profiles of the ice through time and c) flow rate of water within the conduit through time

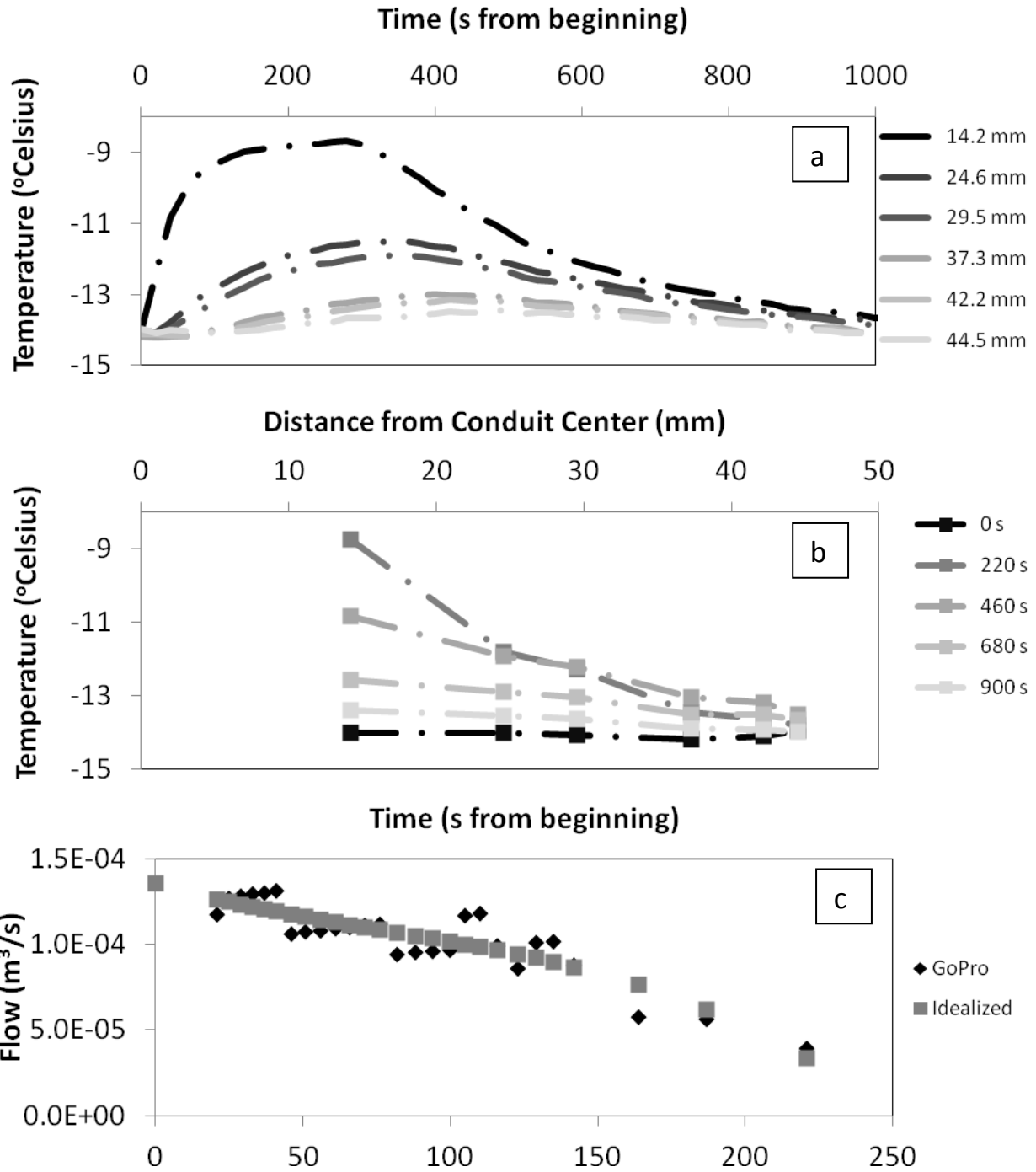


Figure 4-28: Low water flow test results from -14.0° Celsius ice showing a) individual thermocouple temperature recordings through time b) temperature profiles of the ice through time and c) flow rate of water within the conduit through time

4.8 Discussion (Low Flow)

The low flow results are strikingly similar to the stagnant water tests, as the heat generated by turbulent/viscous dissipation in the flowing water is not enough to overcome the conduit closure by freezing. Had the ice been at a lower temperature, the pump would have been able to provide conduit growth, as predicted in Table 5-5.

Although the conduit diameter through time could not be recorded, it can be inferred through the loss of flow rate through time in every low flow experiment that the conduit is closing by freezing in on itself. Referring to the critical flow rate value in Section 5.1, these results are not surprising, as the low flow rate used in these experiments is well under the critical value needed to push the conduit into the expansion regime, and all tests run at this flow rate were indeed in the conduit closure regime.

Creep was neglected as a form of conduit closure as well in the flow experiments, for precisely the same reason as described in the stagnant test discussion, since its impact in these experimental trials proved negligible.

See Section 6.3 for further comparisons among low water flow rate tests, along with their numerical model predictions.

4.9 Results (High Flow)

The high water flow tests were run with two profiles of thermocouples set at two different cross-sections within the ice along the conduit. This is demonstrated in Figure 4-29. Two profiles were used in an effort to quantify the advection heating as the water flowed through the ice. Due to the small length of the ice sample, however, the results of the two profiles were too similar for a good comparison. The inlet thermocouples (the profile closest to where the flowing water entered the conduit) were located at distances away from the conduit center as follows: 9.9mm, 27.7mm, 29.2mm and 38.9mm. The outlet thermocouples were located at the following radial distances: 14.7mm, 24.9mm, 26.4mm, 33.8mm and 42.2mm. The temperature values were recorded through time as the test was run, with the initial time of 0 seconds as the point when the water first came in contact with the surrounding ice.

The following graphs, from Figure 4-31 to Figure 4-35, show three ice temperature profiles through time as the latent heat and viscous heat due to friction with the side walls are released from the freezing water within the conduit. The inconsistency in the number of thermocouples shown in Figure 4-29 and the number of thermocouples listed and shown in the graphs is due to the failure of a few thermocouples in each profile as the ice sample was being setup. Enough data was recorded, however, to interpret the results. The distance from the center for each thermocouple was recorded by digitizing the data shown in Figure 4-29, finding the conduit center, and locating the vertical and horizontal distances from that center of each thermocouple.

The pump used to provide the flow was an EBARA Stainless Steel Sump Pump, model 304-SS, with a pump curve shown in Figure 4-30. Throughout the high flow tests, the flow rate did not alter, staying at a constant $2.52 \times 10^{-4} \text{ m}^3/\text{s}$ throughout all tests. The initial ice temperatures of the high water flow experiments are shown in Table 4-3 and range from -1.66 degrees Celsius to -10.74 degrees Celsius.

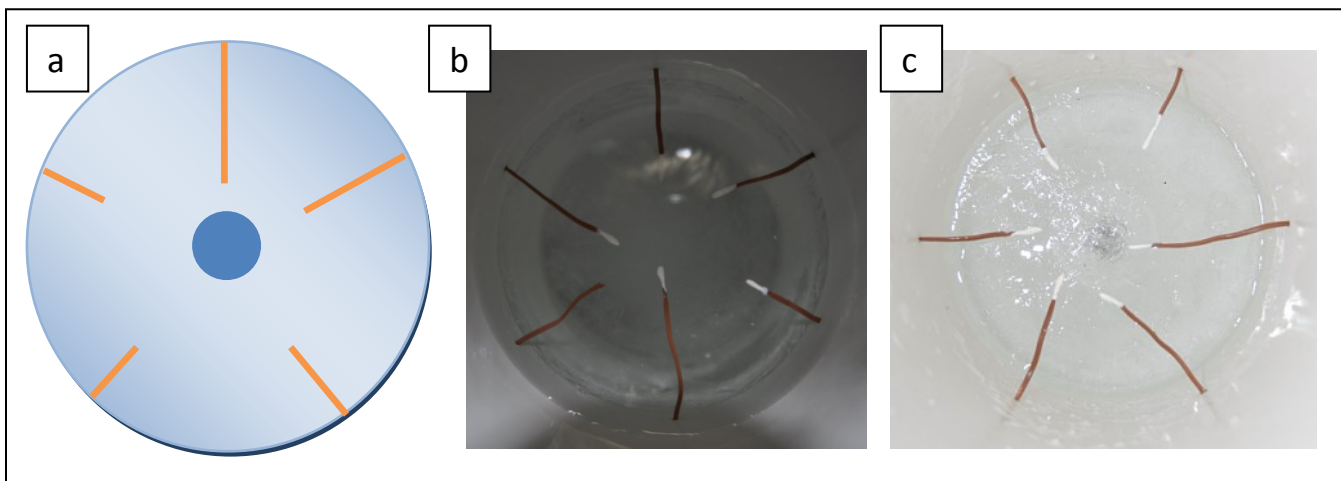


Figure 4-29: Cross-section of thermocouple locations in the high water flow pvc experiments, in a) schematic and photographs of the thermocouples located in the small experiment b) profile located closest to the outlet flow of water and c) profile located closest to the inlet flow of water

Table 4-3: Initial ice temperatures of high water flow experiments that were run with a flow rate of $2.52 \times 10^{-4} \text{ m}^3/\text{s}$

High Flow	
Initial Ice Temperature (°Celsius)	
	-1.66
	-4.53
	-4.60
	-5.43
	-5.51
	-5.73
	-6.03
	-9.55
	-10.74

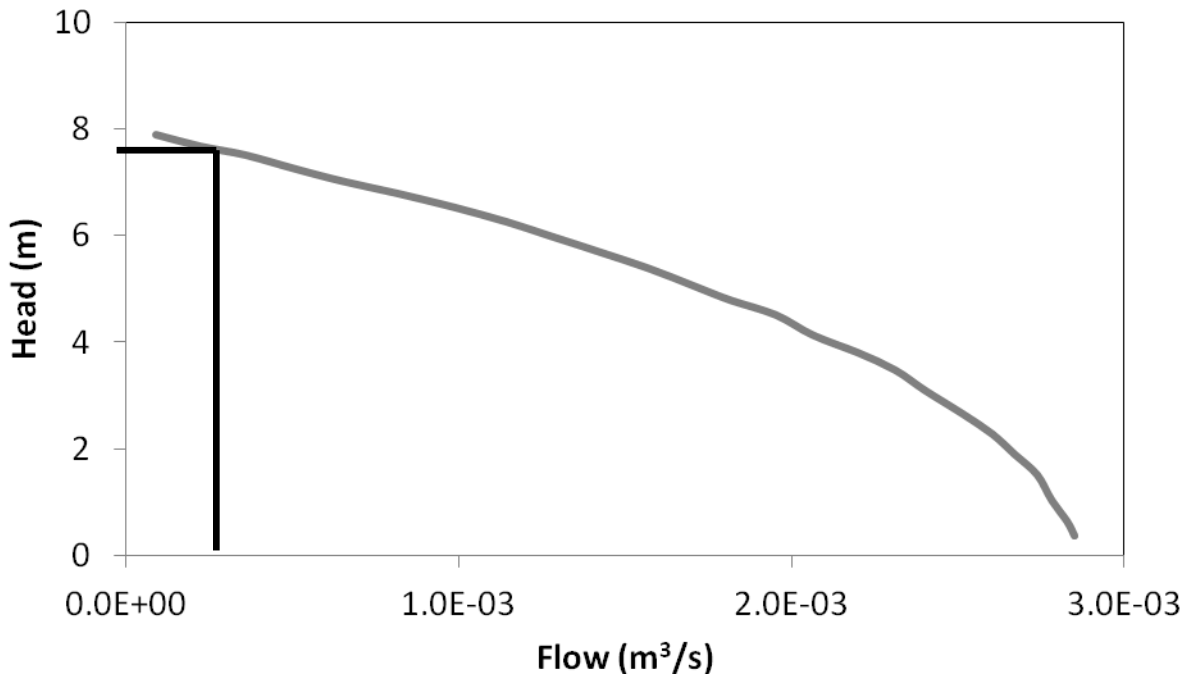


Figure 4-30: EBARA model 304 SS submersible pump curve for high water flow tests, showing the output of $2.5 \times 10^{-4} \text{ m}^3/\text{s}$ and the corresponding head loss through the system at NASA GSFC

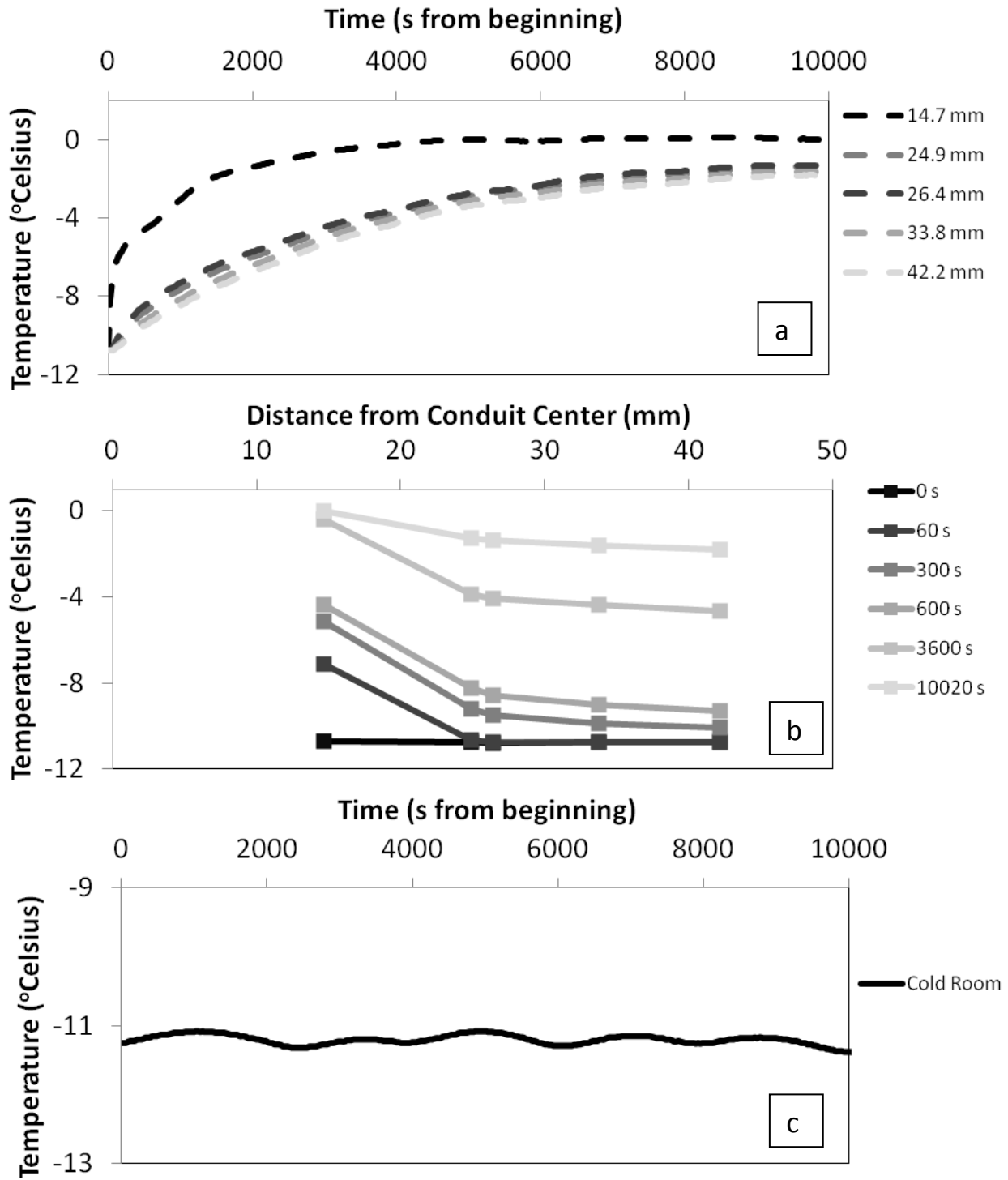


Figure 4-31: High water flow test results from -10.74° Celsius ice, at the temperature profile located closest to the outlet flow of water showing a) individual thermocouple temperature recordings through time b) temperature profiles of the ice through time and c) the temperature of the cold room through time at NASA GSFC0 S

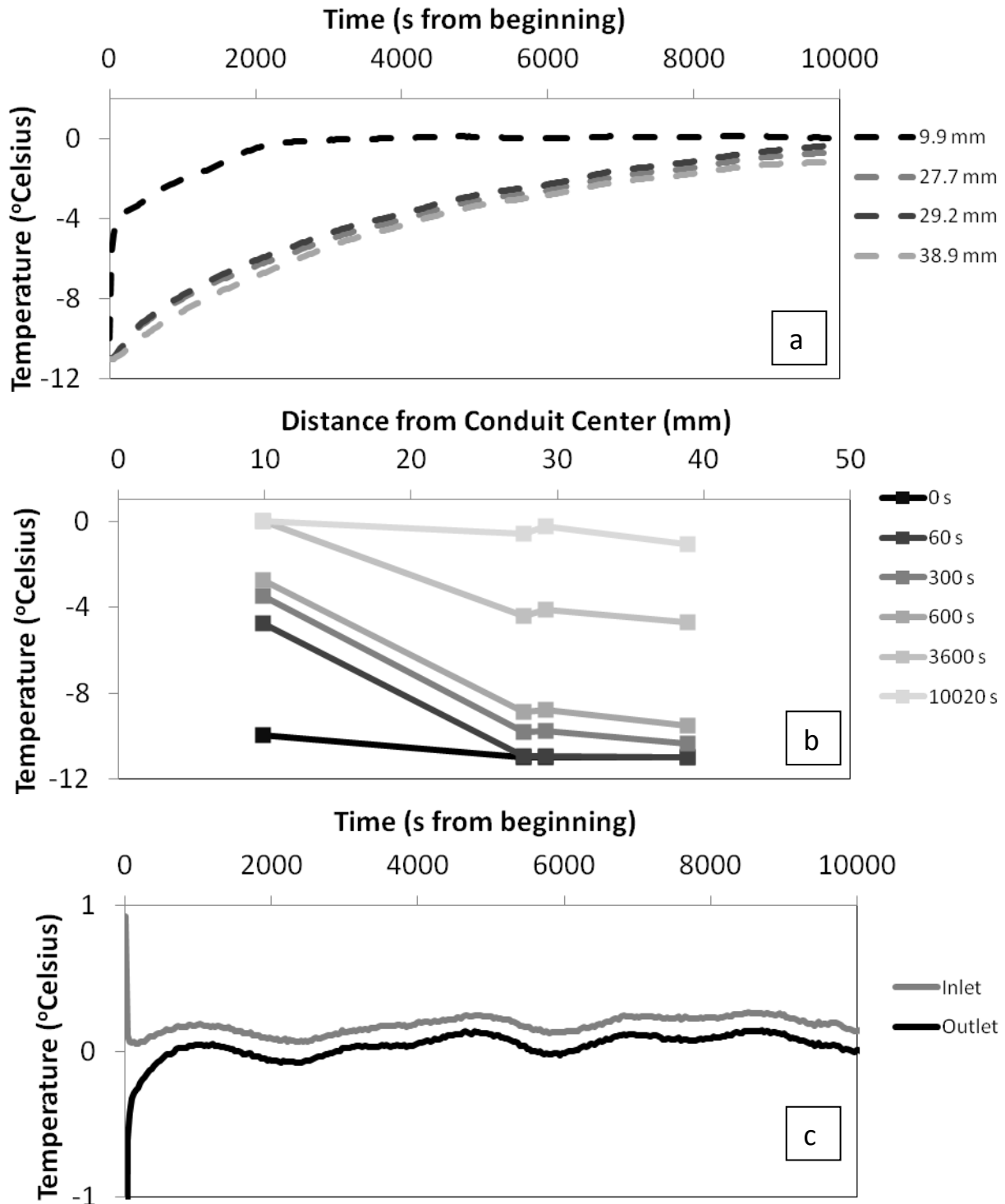


Figure 4-32: High water flow test results from -10.74° Celsius ice, at the temperature profile located closest to the inlet flow of water showing a) individual thermocouple temperature recordings through time b) temperature profiles of the ice through time and c) the temperature of the water flowing through the conduit at the inlet and outlet water gauges through time

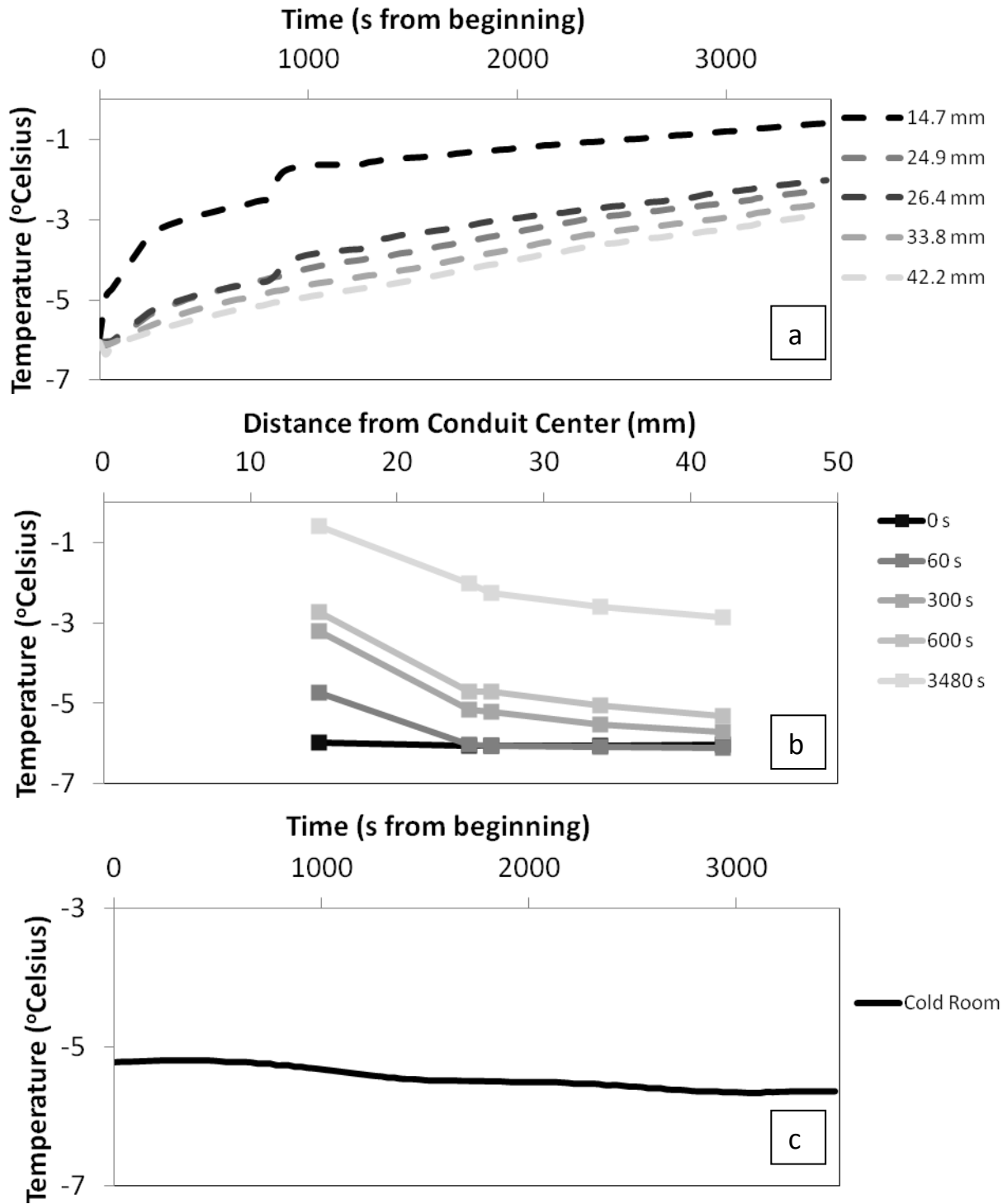


Figure 4-33: High water flow test results from -6.03° Celsius ice, at the temperature profile located closest to the outlet flow of water showing a) individual thermocouple temperature recordings through time b) temperature profiles of the ice through time and c) the temperature of the cold room through time at NASA GSFC

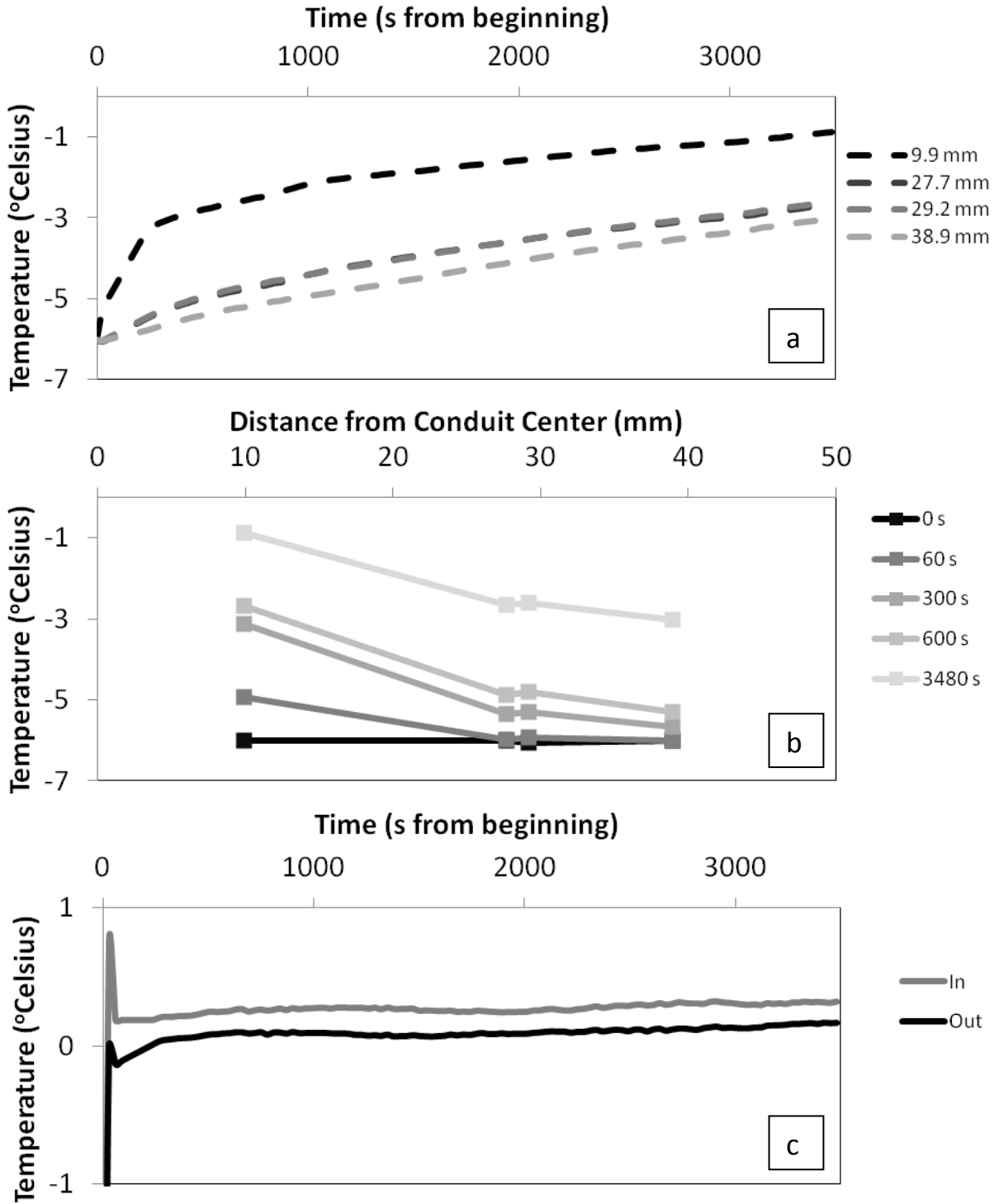


Figure 4-34: High water flow test results from -6.03° Celsius ice, at the temperature profile located closest to the inlet flow of water showing a) individual thermocouple temperature recordings through time b) temperature profiles of the ice through time and c) the temperature of the water flowing through the conduit at the inlet and outlet water gauges through time

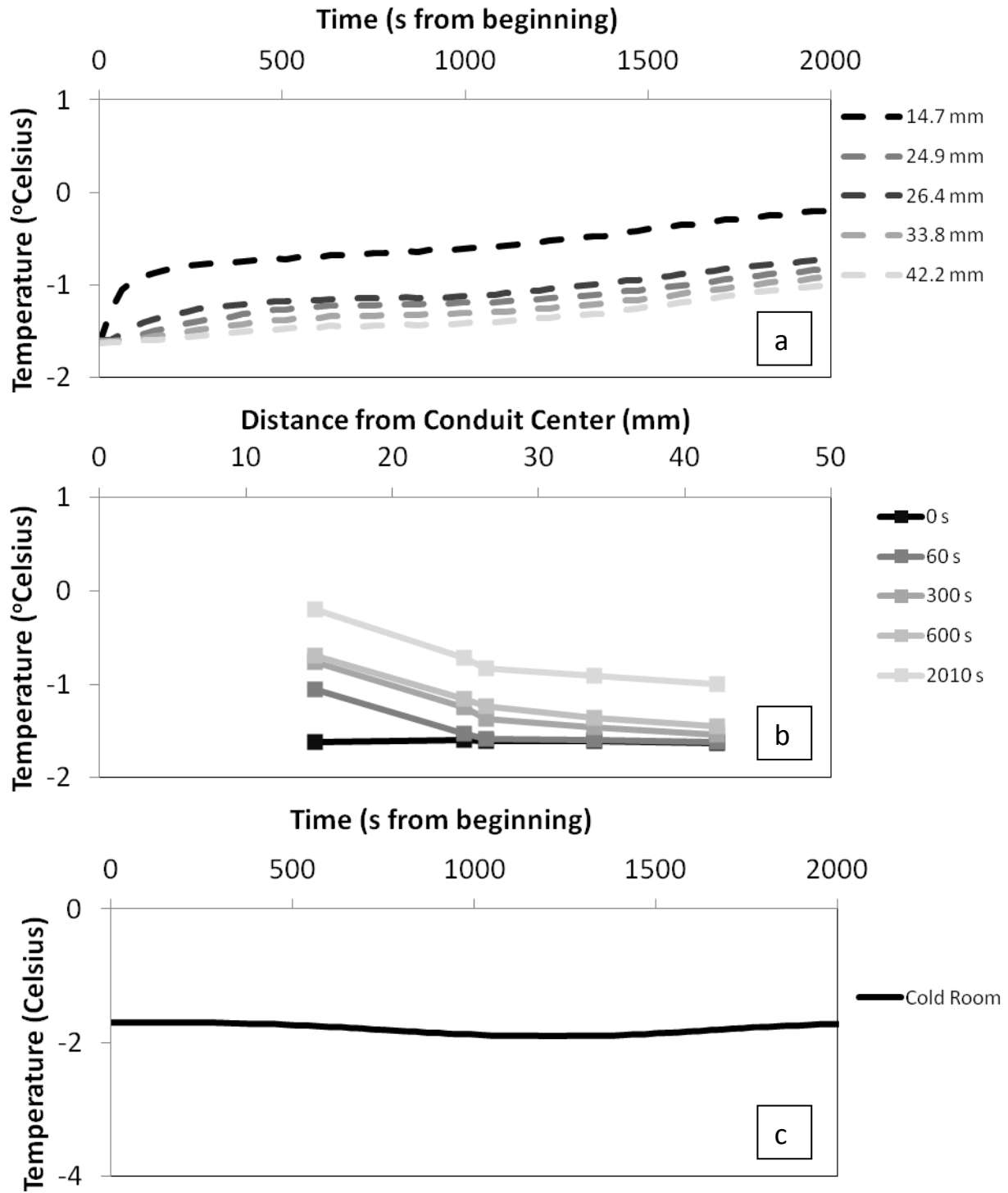


Figure 4-35: High water flow test results from -1.66° Celsius ice, at the temperature profile located closest to the outlet flow of water showing a) individual thermocouple temperature recordings through time b) temperature profiles of the ice through time and c) the temperature of the cold room through time at NASA GSFC

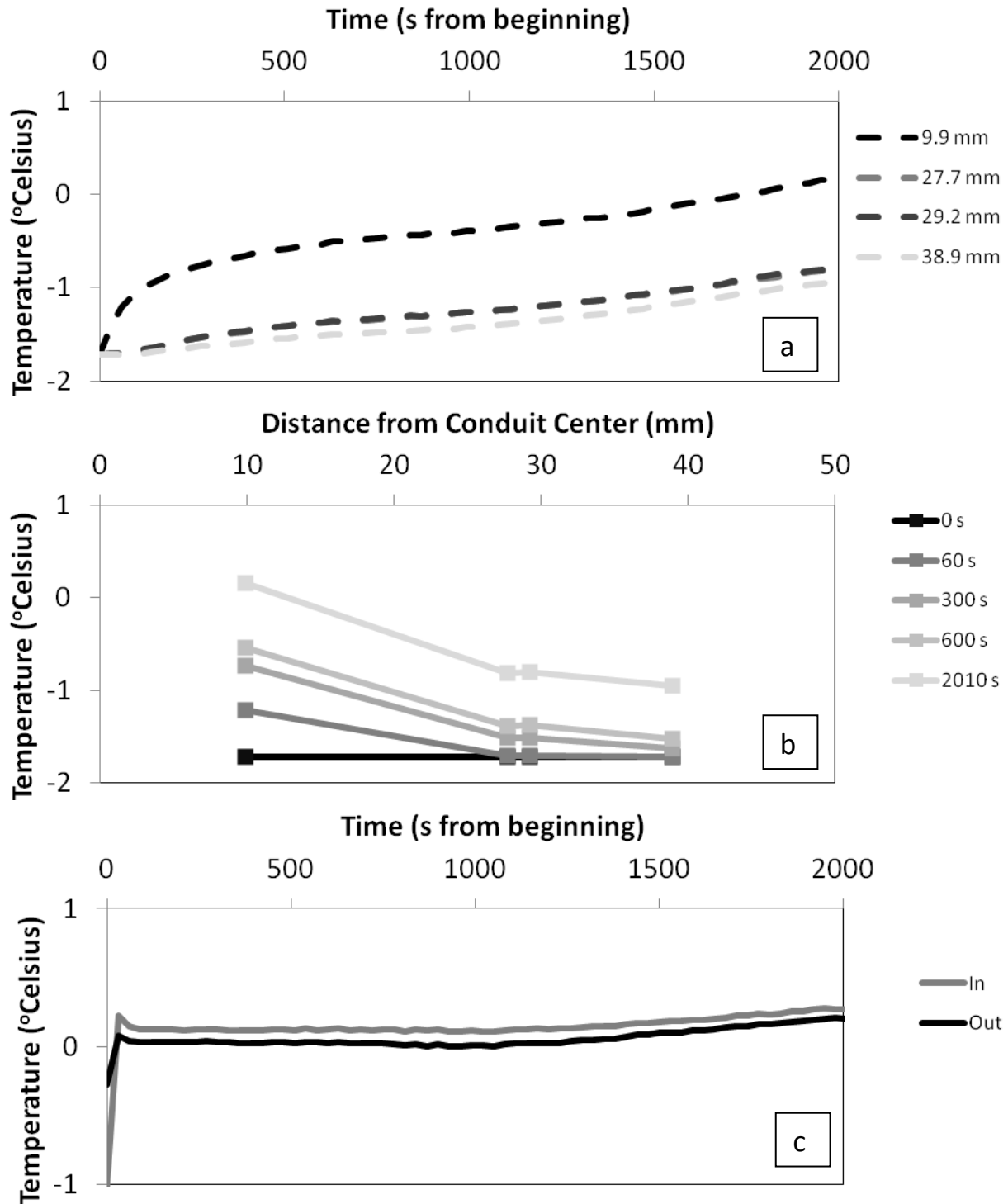


Figure 4-36: High water flow test results from -1.66° Celsius ice, at the temperature profile located closest to the inlet flow of water showing a) individual thermocouple temperature recordings through time b) temperature profiles of the ice through time and c) the temperature of the water flowing through the conduit at the inlet and outlet water gauges through time

4.10 Discussion (High Flow)

Unlike the previous stagnant and low flow water tests, the high flow water tests provided for unlimited conduit growth. The flow rate was held constant during testing with the EBARA pump as compared to the ViaAqua, which was used in the low flow tests. Though the variation of the conduit radius with time was not recorded, it can be inferred throughout the test that the conduit experienced expansion, as the thermocouple located closest to the conduit center experienced temperatures in between those of the water at the inlet and outlet, signifying that the conduit had grown beyond the location of the closest thermocouple in that cross-section.

These findings also matched observations through the test, as seen in Figure 4-20. Creep was once again neglected for the reasons listed previously. Also, no significant differences in the thermocouple recordings were observed between the inlet and the outlet thermocouple profiles. In these short, small-scale experiments, the advection term can be neglected. The water temperature recordings show there was little difference between the inlet and outlet water temperatures, though in all cases, the temperature of the water exiting the system was lower than that of the water entering it. Table 4-4 lists these values.

Table 4-4: Average temperature difference between water entering and exiting the high flow experimental ice sample at $2.52 \times 10^{-4} \text{ m}^3/\text{s}$

Initial Ice Temperature (°Celsius)	Average Water Difference Between Inlet and Outlet (°Celsius)
-1.66	0.08
-4.53	0.13
-4.60	0.10
-5.37	0.15
-5.43	0.13
-5.51	0.15
-6.03	0.17
-9.55	0.20
-10.74	0.13

5 Numerical Model

A numerical model was developed to quantify temperature distribution through the ice and provide a theoretical basis with which to compare the experimental results. To establish the small-scale problem and create a numerical code, a simple, two-dimensional, circular geometry was assumed for the ice, with a circular water conduit in the center, as shown below in Figure 5-1, which shows a two-dimensional cross-sectional schematic for the numerical model, with water through the conduit flowing on the axis which runs into and out of the page.

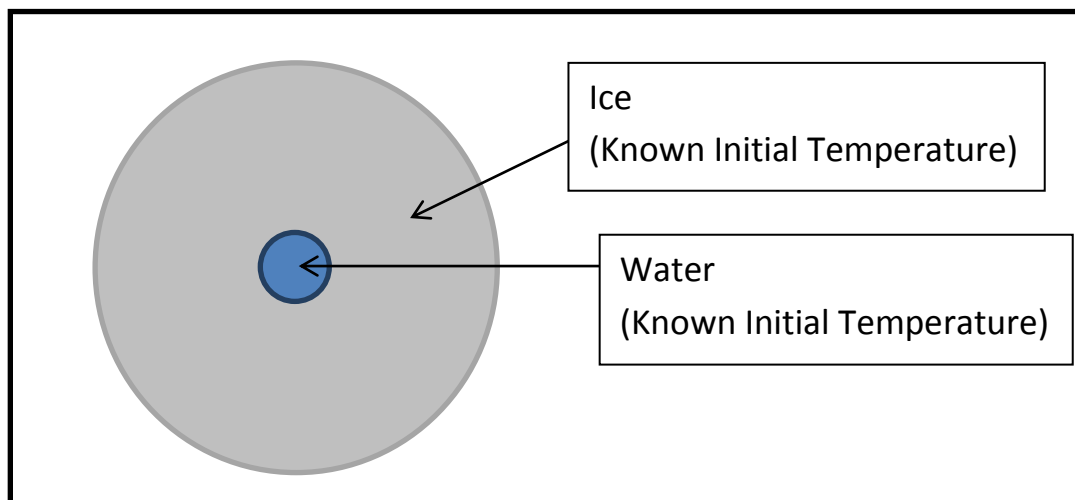


Figure 5-1: Two-dimensional schematic of numerical problem showing radial cross-section of ice and water

Over short distances, the axial variations in water temperature are expected to be small. Furthermore, an ice-water interface can only be at the melting point. Thus the ice temperature is expected to vary only radially. Assuming that ice is an isotropic medium, the energy equation in ice can be further reduced to a one dimensional problem in radial coordinates. The problem can be decomposed into evenly spaced nodes along the radius, for implementation into a numerical

model, and can be visualized as shown in Figure 5-2. Note that this schematic is the radius from the center of the conduit to the exterior boundary of the ice.

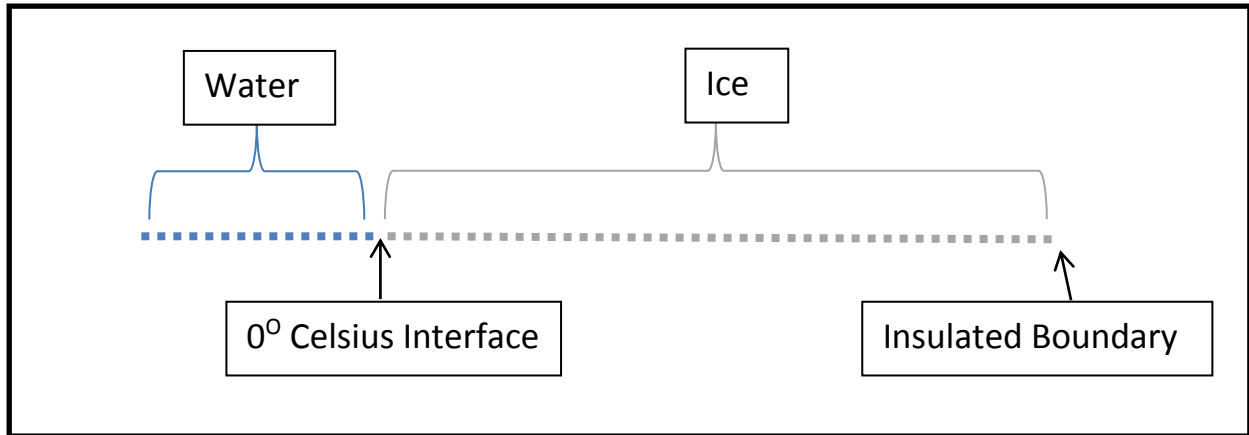


Figure 5-2: One-dimensional schematic of numerical problem showing water and ice nodes, interface between the two, and insulated boundary condition

As mentioned previously, water contained within ice sheets can either be flowing or stagnant. When it is flowing, it will be flowing either into or out of the page (refer to Figure 8-1). From this interaction, the application of heat transfer throughout the ice through time can be known.

The energy equation in water is simplified by assuming that water flowing inside the conduit is at the melting point. The energy equation in water thus does not strictly need to be solved for determining the water temperature. Energy balance in water is maintained in the following manner: mechanical energy dissipated by viscous and turbulent head losses is converted to thermal energy and conducted to the water-ice interface, where it is conducted into the ice surrounding the conduit. This energy balance condition also implies that the thermal energy supplied to the ice at the conduit wall equals the rate of dissipation of mechanical energy, given by:

$$\gamma Q \left| \frac{dh}{dx} \right| = \frac{8\rho f Q^3}{\pi^2 D^5}$$

Equation 5-1

Where γ is the specific weight of water, Q the flow rate, $\left| \frac{dh}{dx} \right|$ the head loss per length of conduit through the system, ρ the density of water, f the Darcy-Weisbach friction factor, D the diameter of the conduit and r the radius of the conduit. Note that the head loss per length of the conduit is obtained by using the standard Darcy-Weisbach friction factor equation for pipe flow.

The energy equation in ice is the heat conduction equation in radial coordinates:

$$\rho_i C_i \frac{\partial \theta}{\partial t} - \frac{1}{r} \frac{\partial}{\partial r} \left(r k_i \frac{\partial \theta}{\partial r} \right) = 0, r > R(t)$$

Equation 5-2

Where θ is denoted to be the ice temperature, r the distance along the one-dimensional space, and t the time. k again represents the thermal conductivity of the medium, ρ the density, and C_p the specific heat capacity. The boundary conditions for solving Equation 5-2 are $\theta = 0$ on $r = R(t)$, where $R(t)$ is the conduit radius, which evolves with time and can be seen in Figure 5-4, while either a no-flux condition or a specified external temperature exist at the outer edge of the ice where $-k \frac{d\theta}{dr} (r = L, t) = 0$. Given the insulated experiment, a no-flux condition was used in the model, as the heat flux from the ice sample was

negligible. The initial condition is a constant initial ice temperature through all ice nodes where $\theta_{initial} = Constant$.

Because there is always a net heat flux across the ice-water interface (i.e. the conduit radius), the conduit radius evolves with time. The equation for the evolution of the conduit radius is obtained from an energy balance at the interface. The energy balance condition at the interface is (note that the conduit radius R varies with time):

$$\gamma Q \left| \frac{dh}{dx} \right| = -2\pi R k_i \left. \frac{\partial \theta}{\partial r} \right|_{r=R} + 2\pi R \rho_w L \frac{\partial R}{\partial t}$$

Equation 5-3

This equation states that the energy supplied to the interface contributes to both melting at the interface and conduction of heat into ice. In the absence of energy supply to the interface from water (e.g. stagnant water in conduit with no viscous/turbulent energy dissipation), Equation 5-3 will consistently produce refreezing or closure of the conduit, because the ice temperature gradient, $\frac{\partial \theta}{\partial r}$ is always negative, leading to a negative $\frac{\partial R}{\partial t}$. A negative temperature gradient in the ice at the conduit wall implies a loss of thermal energy from the water to the ice. When the turbulent/viscous heating is not large enough to negate this loss, refreezing occurs.

Numerical implementation of the above theoretical model will require the solution of the energy equation in ice (Equation 5-2), and evolution of the conduit radius based on Equation 5-3.

Equation 5-2 can be expanded and solved using an Euler-Backward approach. With j representing the individual node number, r_i the radial coordinate of the corresponding node, and n the time level, the discrete form of Equation 5-2 is:

$$\rho_i C_i \frac{\theta_j^{n+1} - \theta_j^n}{\Delta t} - \frac{k_i}{r_j} \left[\frac{r_{j+1/2} \frac{\theta_{j+1}^{n+1} - \theta_j^{n+1}}{r_{j+1} - r_j} - r_{j-1/2} \frac{\theta_j^{n+1} - \theta_{j-1}^{n+1}}{r_j - r_{j-1}}}{r_{j+1/2} - r_{j-1/2}} \right] = 0$$

Equation 5-4

Equation 5-4, expanded out to solve for the temperature profile through time, can be written as:

$$(-\alpha \Delta t) l_j \theta_{j-1}^{n+1} + [1 + (l_j + u_j) \alpha \Delta t] \theta_j^{n+1} + (-\alpha \Delta t) u_j \theta_{j-1}^{n+1} = \theta_j^n$$

Equation 5-5

With the radius terms defined as:

$$r_{j+1/2} = \frac{r_j + r_{j+1}}{2}$$

Equation 5-6

And:

$$r_{j-1/2} = \frac{r_j + r_{j-1}}{2}$$

Equation 5-7

The thermal diffusivity as:

$$\alpha = \frac{k_i}{\rho_i C_i}$$

Equation 5-8

And the extra terms in the expanded Euler-Backward solution as:

$$l_j = \frac{r_{j-1/2}}{\frac{1}{2}r_j(r_j - r_{j-1})(r_{j+1} - r_{j-1})}$$

Equation 5-9

And:

$$u_j = \frac{r_{j+1/2}}{\frac{1}{2}r_j(r_{j+1} - r_j)(r_{j+1} - r_{j-1})}$$

Equation 5-10

Actual values used are presented in Table 5-1. To define the boundary conditions of the solution in a one-dimensional case, both the first and second type boundary conditions, or Dirichlet and Neumann conditions, are invoked. Under certain circumstances, a third boundary condition, the Stefan condition, is used, which includes the work required to change the density of the material undergoing the phase change. When the system pressure is much less than 3.04E-6 kPa, however, as it is in these experimental cases, this condition can be neglected (Lunardini, 1981). In the numerical model, the radius extends from the center of the conduit ($r = 0$) to the outer edge of the ice. At $r = 0$, and within the conduit ($r \leq R(t)$), the temperature is held constant at 0 degrees:

$$\theta(r \leq R(t), t) = T_1(t) = 0$$

Equation 5-11

And at the Insulated boundary, the flux is set to zero, as:

$$-k \frac{d\theta}{dr}(r = L, t) = 0$$

Equation 5-12

The initial ice temperature at all nodes is known and input into the model, providing initial conditions to run the code from. Compiling this system of equations, a tridiagonal system of equations for ice temperatures results in each time-step, and is solved using the Thomas algorithm. These theoretical temperatures are recorded and stored in every time step and compared to the experimental values.

With inputs of initial ice and water temperature, the numerical model is run using these boundary conditions, following the method portrayed in Figure 5-5. For the initial radius, the temperature value of the water nodes was set to zero. To incorporate the changing interface boundary location, a variable time-step method was used, moving the interface one node per iteration of the code. In order to determine the time required for the interface node to move by one timestep, either by freezing in on itself or expanding outward, the rate of change in radius is determined at the end of every time-step, using Equation 5-3, leading to:

$$\frac{\partial R}{\partial t} = \left(\gamma Q \left| \frac{dh}{dx} \right| + 2\pi R k_i \left. \frac{\partial \theta}{\partial r} \right|_{r=R(t)} \right) / (2\pi R \rho_w L)$$

Equation 5-13

Using this term, along with the given node spacing of .01 mm for dr , shown in Table 5-1, the timestep can be calculated using Equation 5-14:

$$\partial t = \left| \frac{\partial R}{\partial R / \partial t} \right|$$

Equation 5-14

Once the value of the timestep is calculated, the numerical model predicts whether or not the conduit within the ice will re-freeze in on itself or expand outward. This is determined based on the sign of the energy flux at the interface, where growth occurs for positive values, and refreezing for negative values, depending on the dominating term, either the conductive heat transfer or the turbulent/viscous heating. Because the temperature gradient in the ice at the conduit wall is always negative, it implies a loss of thermal energy from the water to the ice. When the turbulent/viscous heating is not large enough to negate this loss, refreezing occurs. The radius of the conduit is then moved one node accordingly, while the temperature of water-filled nodes within the conduit remains constant at 0 degrees.

Table 5-1: Initial Parameters for Numerical Model

Initial Parameters		
Density (Water)	999.8	kg/m ³
Density (Ice)	916.8	kg/m ³
Specific Heat (Ice)	2.11	kJ/kgK
Thermal Conductivity (Ice)	2.18	W/mK
Latent Heat	335	kJ/kg
Node Spacing	0.01	mm
Initial Radius	4.76	mm

A flow chart for the process used in the numerical model is shown in Figure 5-5 and used for the stagnant, low water flow, and high water flow tests. The numerical model is run to the final time that the experiments were run. Figure 5-3 shows profiles of theoretical temperatures through time, from both a stagnant experiment in the refreezing regime, and a high water flow experiment in the conduit growth regime.

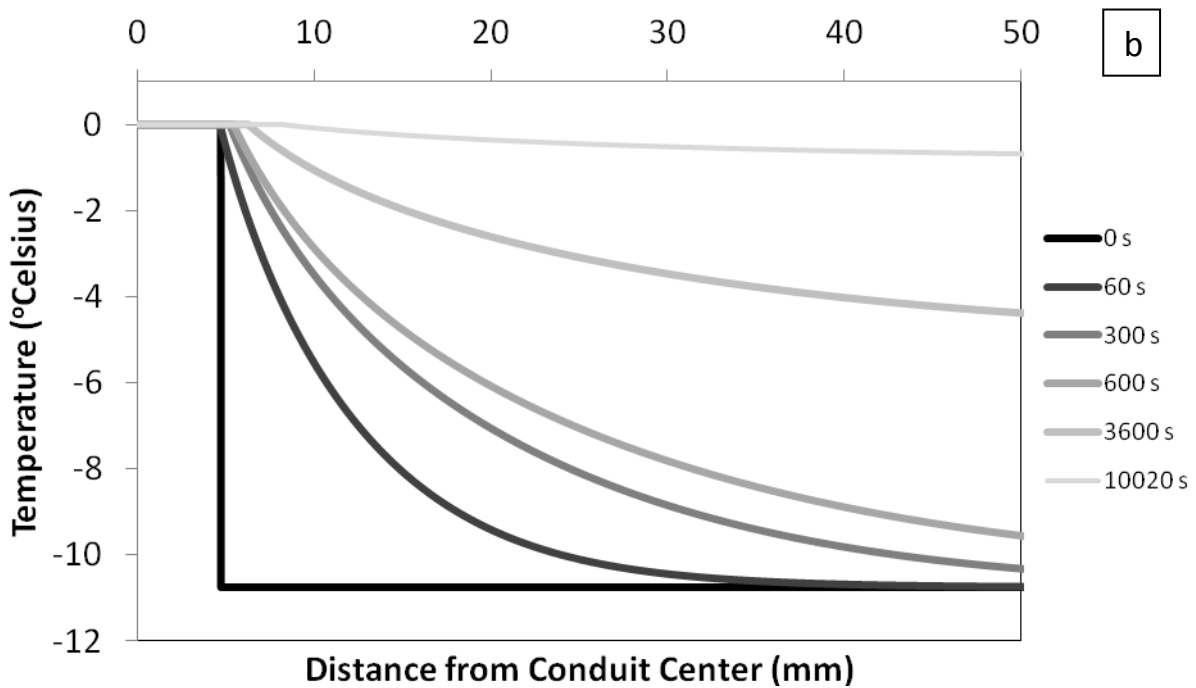
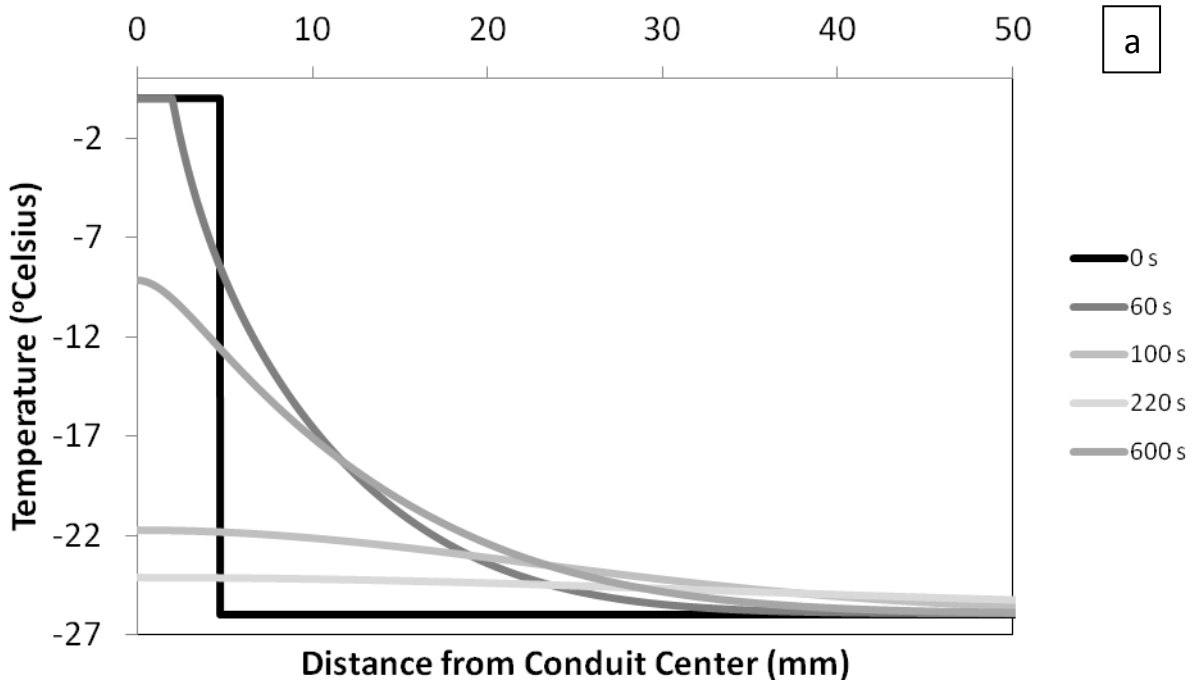


Figure 5-3: Theoretical profile of temperature across the experimental radius at different times showing a) stagnant experiment with initial ice temperatures of -26.0° Celsius and b) high water flow experiment below with initial ice temperature of -10.74° Celsius and flow rate of $2.25 \times 10^{-4} \text{ m}^3/\text{s}$

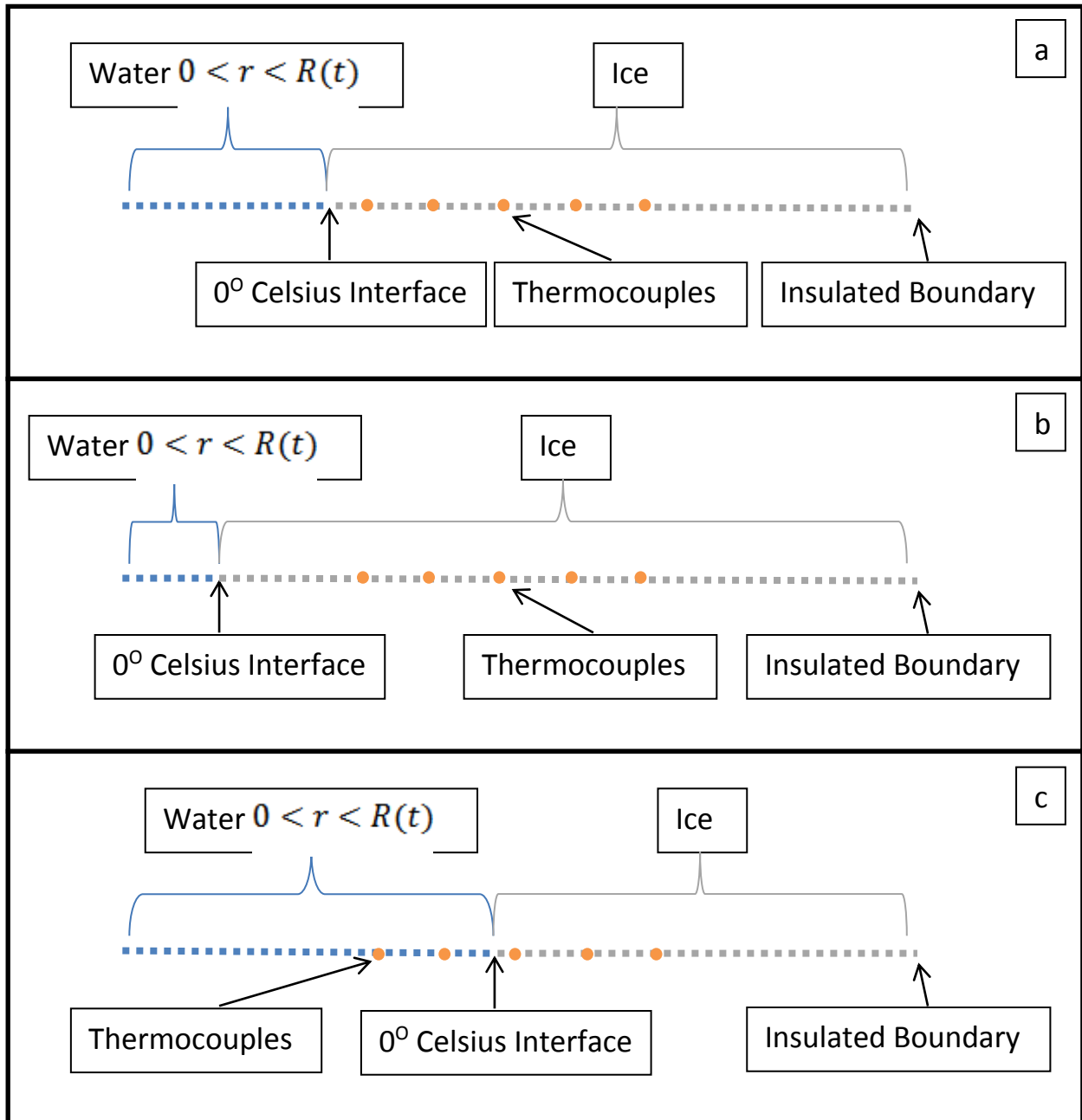
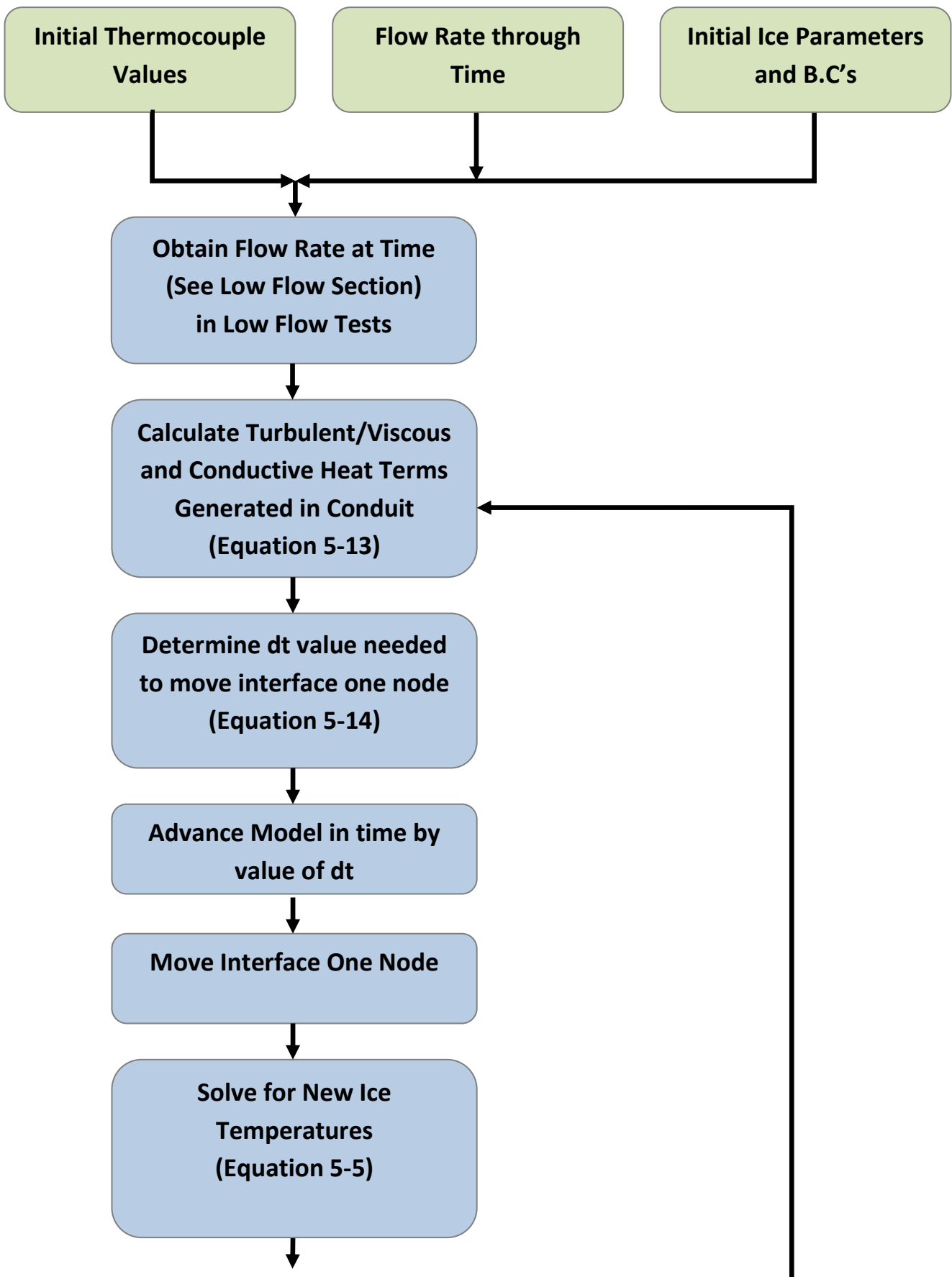


Figure 5-4: Schematic of one dimensional node layout for a) initial conduit dimensions b) conduit dimensions during refreezing of the conduit and c) conduit dimensions during conduit expansion by turbulent heat generation



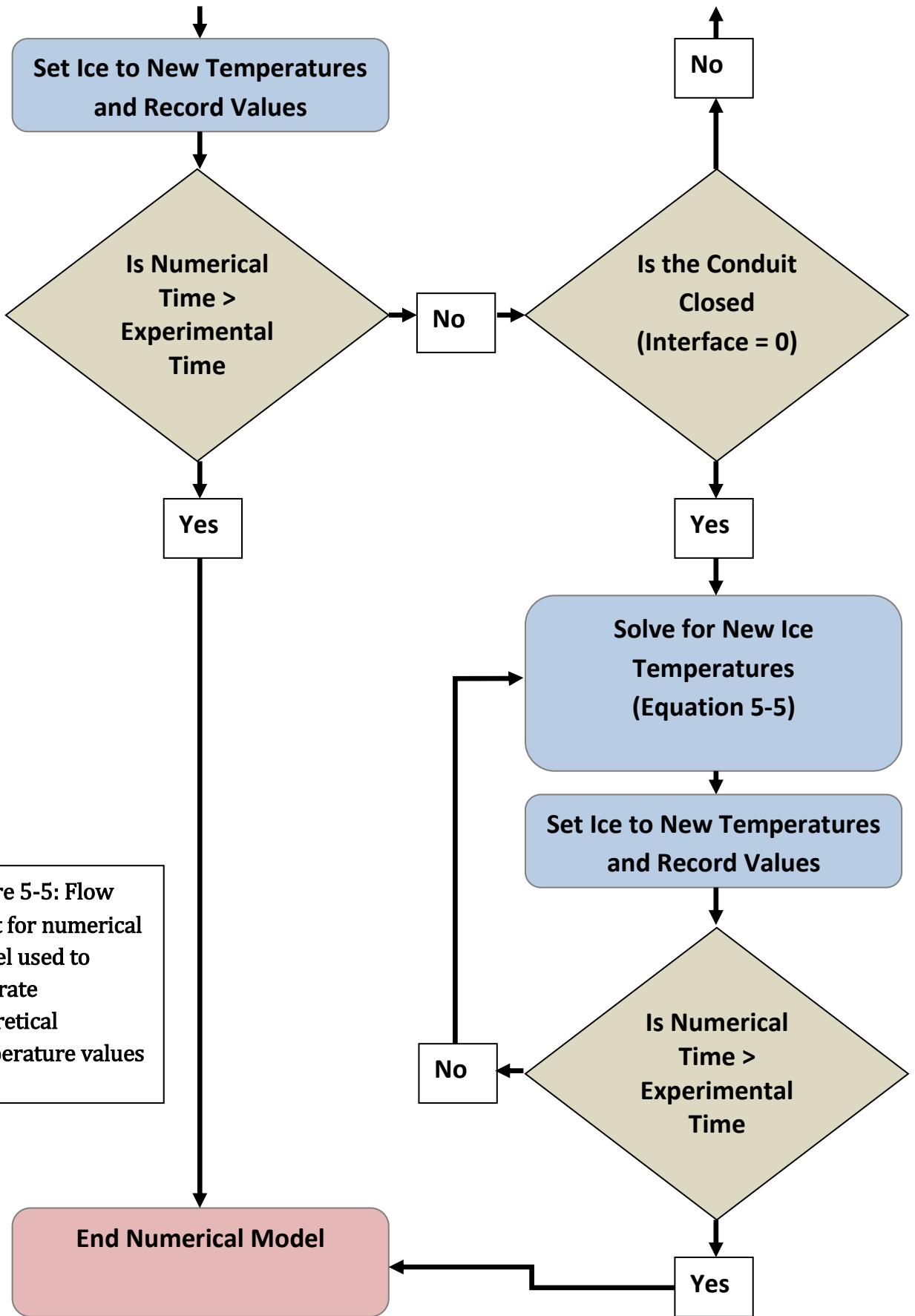


Figure 5-5: Flow chart for numerical model used to generate theoretical temperature values

5.1 Critical Flow Rate

When determining the regime of water flowing through an englacial conduit, it is necessary to have an approximate measure to predict the initial "critical" flow rate where no change in conduit geometry occurs (i.e. the heat flux from the conduit is balanced by the heat supplied by turbulent/viscous dissipation at early time). For the numerical model, an arbitrary node spacing was generated, which impacts the calculation of an initial critical flow rate, by affecting the estimate of temperature gradient at the interface. A new calculation is used to solve for an initial critical flow rate.

In this instance, for the physical experiments being run, the mechanism controlling growth is the heat generated by turbulent/viscous "friction" losses as water flows through the conduit and against the ice walls. The closure mechanism is the conductive heat flux between the ice and water. Creep is neglected in the experimental case due to the negligible overburden stress of the ice, which was only 76.2mm thick.

Considering the flux at the surface between a region bounded by a circular cylinder, at small time values $t \ll R^2/\kappa$ as used by (Carslaw, H. S., and J. C.

Jaeger., 1959), and shown in the appendix is:

$$F_{\text{wall}} = \frac{k\Delta T}{R} \left\{ \frac{1}{\sqrt{\frac{\pi\kappa t}{R^2}}} + \frac{1}{2} - \frac{1}{4} \sqrt{\frac{\pi\kappa t}{R^2}} + \text{H.O.T} \right\}$$

Equation 5-15

Where the thermal diffusivity is:

$$\kappa = \frac{k}{\rho C_p}$$

Equation 5-16

Integrating this flux term over a small time interval Δt , the integrated flux becomes:

$$\int_0^{\Delta t} F_{\text{wall}} dt = 2\pi k(T_f - T_o) \left\{ 2 \sqrt{\frac{\Delta t R^2}{\pi \kappa}} + \frac{1}{2} \Delta t - \frac{1}{6\sqrt{\pi}} \Delta t^{\frac{3}{2}} + \text{H. O. T} \right\}$$

Equation 5-17

F_{wall} denotes the heat supplied from the ice surrounding the conduit to the water contained within it, T_f the temperature of the fluid within the conduit, T_o the temperature of the surrounding ice, Δt the timestep, R the radius of the conduit, κ the thermal diffusivity, and k the thermal conductivity.

For a small timestep, the term $\frac{\kappa \Delta t}{R^2} \ll 1$, so the higher order terms (H.O.T) are neglected, and only the first term in the brackets in Equation 5-17 is used, leading to an integrated wall flux of:

$$2\pi k(T_f - T_o) \frac{2\sqrt{\Delta t}}{\sqrt{\pi\sqrt{\kappa}}} R$$

Equation 5-18

Which can then be written as:

$$4kR(T_f - T_o) \frac{\sqrt{\pi\Delta t}}{\sqrt{\kappa}}$$

Equation 5-19

The term driving conduit expansion is then used as the integrated energy dissipated from water flow, and is written as:

$$\gamma_w Q \left| \frac{dh}{dx} \right| \Delta t$$

Equation 5-20

The head loss term in equation is defined, with a Darcy-Weisbach friction factor, and is calculated per unit length along the pipe as:

$$\left| \frac{dh}{dx} \right| = \frac{f}{2R} \frac{Q^2}{2g(\pi R^2)^2}$$

Equation 5-21

For equilibrium to occur, the wall flux term in Equation 5-19 must be equal to that of the term in Equation 5-20, and the minimum value of Q allowing for conduit expansion can be solved by:

$$\gamma_w Q \frac{f}{2R} \frac{Q^2}{2g(\pi R^2)^2} \Delta t \geq 4kR(T_f - T_o) \sqrt{\frac{\pi\Delta t}{\kappa}}$$

Equation 5-22

Solving to isolate the flow rate term Q , the equation becomes:

$$Q^3 \geq 4kR(T_f - T_o) \frac{\pi^{5/2} 4gR^5}{\sqrt{\kappa\Delta t} \gamma_w f}$$

Equation 5-23

This situation, however, is less than ideal because there is some Δt when the energy dissipated from the water flow is greater than that of the heat flux from the ice. However, if this value of Δt is so large that the condition $\frac{\kappa\Delta t}{R^2} \ll 1$ is violated, then the expression for the conductive heat flux must be modified to one that is valid at later times. It becomes necessary to impose an arbitrary Δt in order to find the minimum value of Q that will allow for conduit growth. It is therefore necessary to define a unitless constant a (smaller than 1) such that:

$$a = \frac{R}{\sqrt{\kappa\Delta t}}$$

Equation 5-24

The minimum value of the flow rate to provide for conduit expansion is then written as:

$$Q \geq \sqrt[3]{\frac{16k(T_f - T_o)\pi^{5/2}R^5 a}{\rho_w f}}$$

Equation 5-25

This flow rate is extremely dependent on the radius of the conduit, yet is also dependent on the friction factor associated with the interface between the water and ice. The friction factor used here, and in the entirety of this thesis, is the

Darcy-Weisbach friction factor. This is typically calculated by obtaining the Reynolds number and relative roughness of the pipe through which the fluid is flowing. The Reynolds number is calculated using the velocity of the flowing fluid, f , the diameter of the conduit through which the fluid flows, D , and the kinematic viscosity, ν , and shown in below in Equation 5-26:

$$Re = \frac{vD}{\nu}$$

Equation 5-26

Which can also be written as:

$$Re = \frac{2Q}{\pi R \nu}$$

Equation 5-27

For a smooth pipe, as used in the conduit refreezing regimes, the friction factor can be calculated from the Blasius equation, where:

$$f = 0.3164Re^{-0.25}$$

Equation 5-28

In all other cases, the relative roughness of the pipe is needed and calculated using a ratio of:

$$\text{Relative Roughness} = \varepsilon/D$$

Equation 5-29

Where ε is a property of the conduit walls, and D the diameter of the conduit.

Once the Reynolds number and relative roughness of the system are known, the

Moody Diagram, shown in Figure 5-6, and is used to determine the friction factor throughout the system.

Unfortunately, due to an unknown relative roughness, both at the beginning of the flow of water through the conduit in our experiments, as well as in field studies, there is no consensus on what this relative roughness, or friction factor, should be for englacial conduits. It is then that the friction factors found in (Gulley et al., 2013) will be taken into account, as well as observational results from the experiments in the high flow comparison discussion (Section 4.10), and qualitative evidence from the laboratory experiments, as seen in the final conduit geometry of the high flow test (Figure 4-19).

It should be noted that the Darcy friction factor values used in this study are not shown on the Moody Diagram, since typical engineering applications will not involve such high relative roughness values in the design of a pipe system. Table 6-1 shows previous Darcy-Weisbach friction factors used.

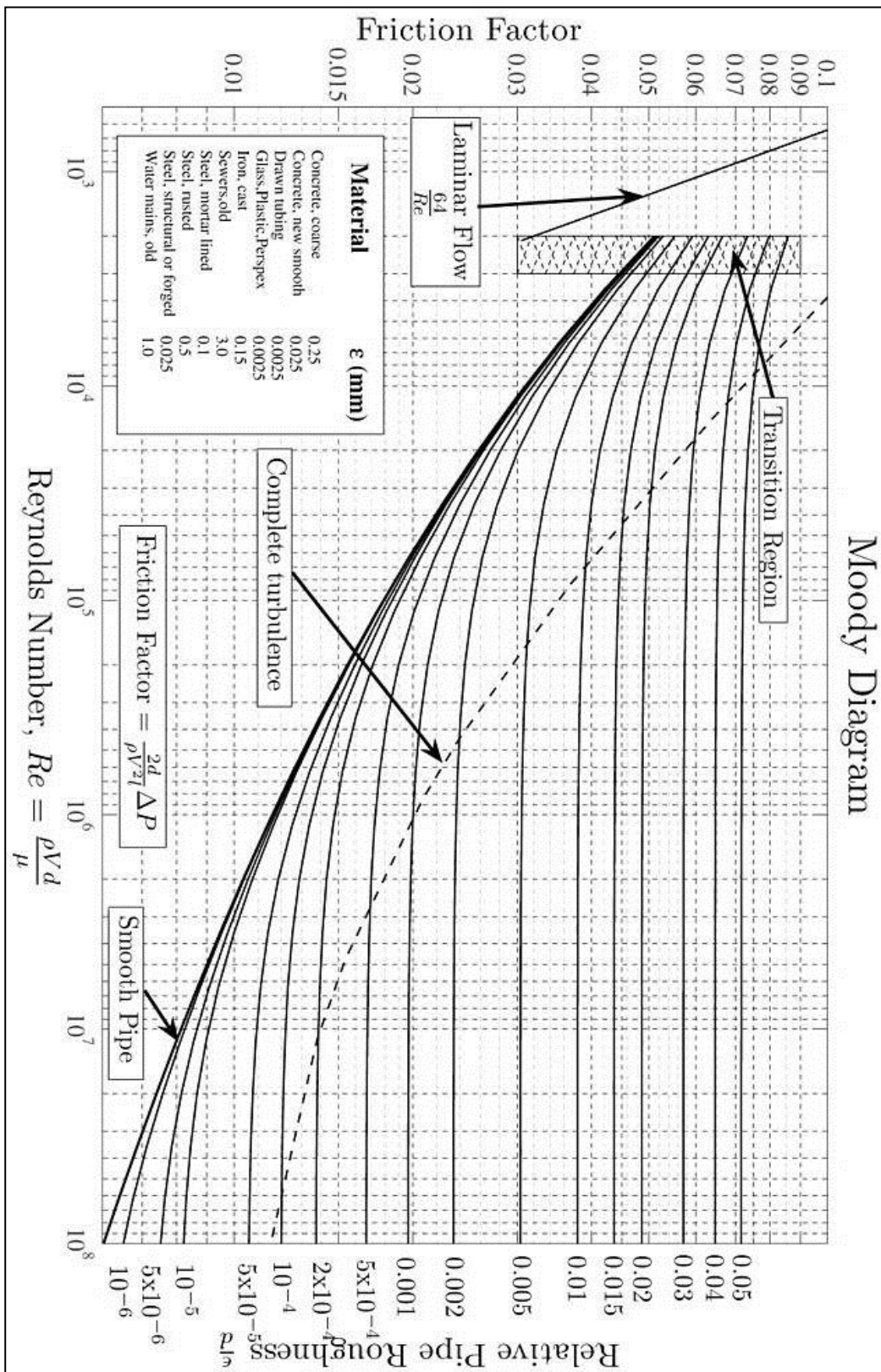


Figure 5-6: Moody diagram to relate friction factors and Reynolds numbers to relative roughness values for closed pipe flow

Using the input parameters in Table 5-2 to compute the necessary initial flow rate for expansion, friction factors obtained from Blasius, in Equation 5-28, are initially used, and the results can be seen in Table 5-3. The process to obtain these results is seen in the flow chart in Figure 5-7.

Table 5-2: Initial Values for critical flow calculation

	Initial Value	Units
k	2.32	W/mK
R	0.0048	m
T _f	0	°C
T _o	-10.0	°C
ρ_w	1000	kg/m ³

These initial properties of ice are the same as the coldest high flow rate experiment, and the results are used in comparison. This test can be seen initially in the high flow experiments (Section 4.9), and was run for a total of 10,000 seconds, or approximately 2.7 hours.

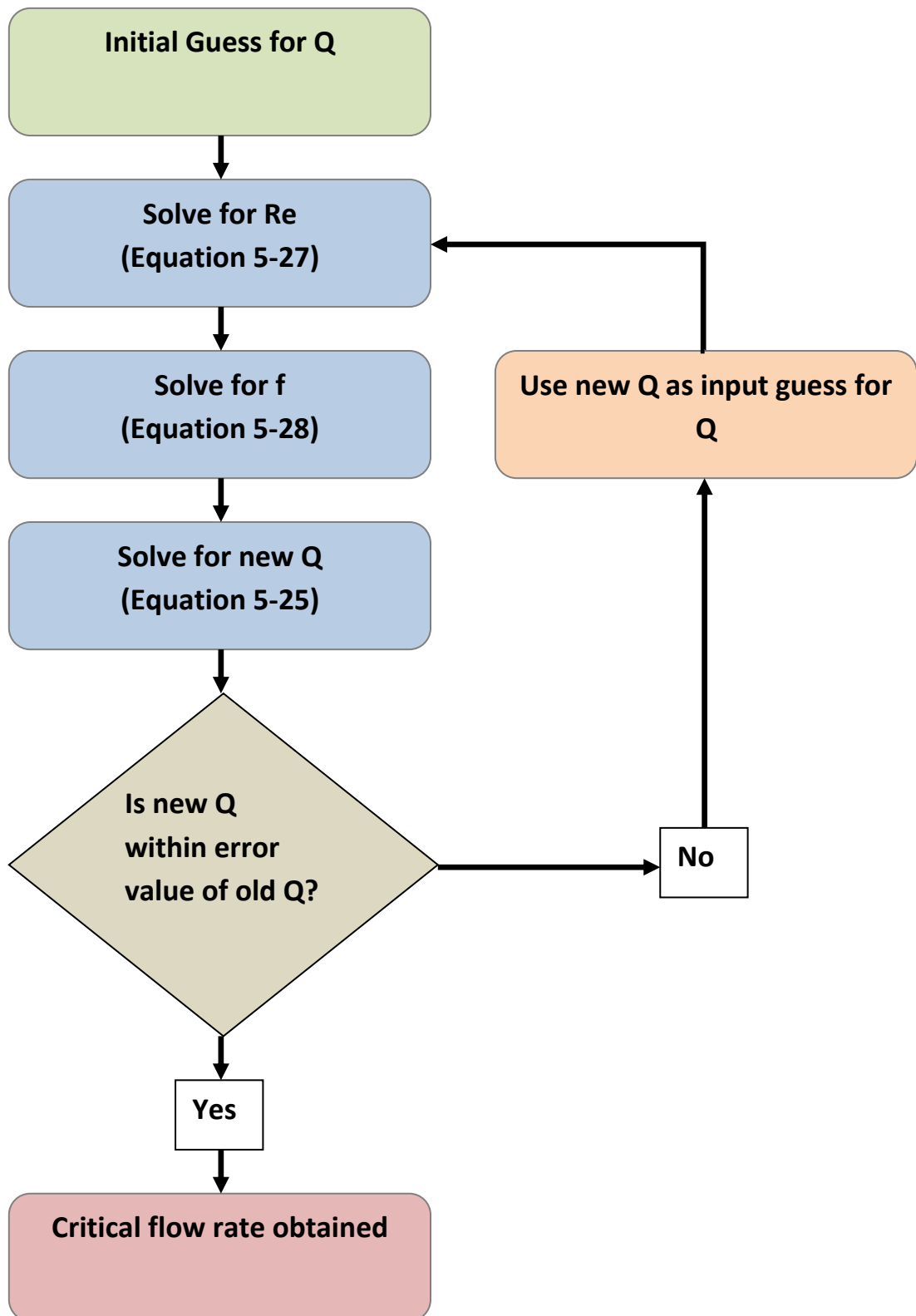


Figure 5-7: Iterative process to obtain critical flow rate using Blasius smooth pipe approximation used in the conduit refreezing regime.

Table 5-3: Critical flow rate values from the Blasius equation for parameters in Table 5-2, with varying constant a

Blasius Friction				
a	Re	f	Critical Flow	
0.1	23500	0.03	3.97E-04	m ³ /s
0.5	54400	0.02	7.57E-04	m ³ /s
1	70000	0.02	9.46E-04	m ³ /s

The Darcy friction factors shown above are well below the observed values, (Gulley, 2013), and the numbers generated for the critical flow rate are higher than the observed flow rates from the coldest high water flow test. This test, shown starting in the high flow experiments (Section 4.9), had a high flow rate of only 2.52×10^{-4} m³/s, which is below the calculated value using the Blasius resistance equation. It is therefore necessary to modify the approach to obtain the critical flow rate to match the physical experiments, using a method that no longer assumes a smooth interface.

As mentioned previously, upon conduit generation, the walls display a higher roughness to diameter ratio than observed in a smooth pipe, or even any pipe displayed on the Moody Diagram. The friction factors now used in the calculation of the critical flow rate are the same as those used in the numerical model, corroborating qualitative observations from the experiments, and assist in deciphering the value of the constant a needed to obtain the initial critical flow rate. No iterative process is needed, and all input values are used in Equation 5-25 to determine the critical flow. These results are shown in Table 5-4.

Table 5-4: Critical flow rate values using fixed friction values for parameters in Table 5-2, with varying constant a

Fixed Friction								
f=.2			f=.5			f=1		
a	Critical Flow		a	Critical Flow		a	Critical Flow	
0.1	2.02E-04	m ³ /s	0.1	1.45E-04	m ³ /s	0.1	1.20E-04	m ³ /s
0.5	3.41E-04	m ³ /s	0.5	2.52E-04	m ³ /s	0.5	2.02E-04	m ³ /s
1	4.29E-04	m ³ /s	1	3.15E-04	m ³ /s	1	2.52E-04	m ³ /s

The critical flow rate values from these fixed friction calculations, using Equation 5-25, match the experimental observational results much better than the assumption of a smooth pipe. The critical flow rate is always below the observed flow rate for growth when $a = .1$, and f could possibly be equal to 1 if the unitless constant a were as high as 1. It is within this range that the value should be used, although further testing and observations are necessary to determine the value of a friction factor f that should be used in further studies.

In the low flow rate experiments, although turbulent flow occurs even during refreezing, the closure geometry is assumed to be radial and symmetric. The eddies generated during this flow were assumed not to produce scalloping because there is refreezing rather than melting, and the Blasius equation was used in determining the critical flow rate for the Darcy-Weisbach friction factor.

Table 5-5: Comparison of theoretical critical flow rates to experimental flow rates of the low water flow experiments where $a=0.1$

Low Flow					
Initial Ice Temperature (°C)	Critical Flow Rate (m³/s)				
	Initial	Blasius	f=.2	f=.5	f=1
-14.0	1.29E-04	4.57E-04	2.23E-04	1.65E-04	1.31E-04
-14.3	1.18E-04	4.61E-04	2.25E-04	1.66E-04	1.31E-04
-14.9	1.29E-04	4.68E-04	2.28E-04	1.68E-04	1.33E-04
-19.3	1.18E-04	5.14E-04	2.49E-04	1.83E-04	1.45E-04
-19.9	1.31E-04	5.20E-04	2.51E-04	1.85E-04	1.47E-04
-20.1	1.94E-04	5.22E-04	2.52E-04	1.85E-04	1.47E-04
-20.6	1.62E-04	5.26E-04	2.54E-04	1.87E-04	1.48E-04

Table 5-5 shows a comparison of the critical flow rates generated from different friction factors used in Equation 5-25. Using a friction factor of 1, the critical flow rates are close enough to the actual flow rates to generate growth, so this large friction factor is ruled out as a possibility for the low flow trials.

Critical flow rate estimates from theory with $a=0.1$ are more consistent with the experimental results if a Blasius friction factor is used. In all low water flow cases, this factor ranged from 0.022-0.023. The closure times of the experiments are then compared with the closure times of the theoretical trials with differing friction factors, and the closure time using the Blasius equation matches the experimental closure time best. This can be seen in Table 5-6, where the closure time predicted using the Blasius equation does not exceed an error value of more than 2% from the actual closure time recorded.

This Blasius resistance law is used because the conduit is assumed to remain smooth during refreezing. For conduit growth, though, a higher friction factor is

justified because of scalloping. For the purposes of determining the critical flow rate, the higher friction factor is used, because it represents the frictional losses once conduit growth begins to occur.

For low flow rates (those below the critical flow rate level), refreezing occurs. Even though this behavior is dominated by the conductive heat flux, the energy supplied by the viscous/turbulent dissipation is not negligible and thus influences refreezing. Because the conduit walls remain smooth under these conditions, the Blasius resistance law is more appropriate.

Table 5-6: Comparison of closure times to experimental closure times of the low flow water experiments where $a=0.1$

Low Flow					
Initial Ice Temperature (°C)	Conduit Closure Time (s)				
	Experimental	Blasius	f=.2	f=.5	f=1
-14.0	250	252	276	298	321
-14.3	200	215	248	272	296
-14.9	260	265	271	285	302
-19.3	200	197	265	270	277
-19.9	200	196	199	206	215
-20.1	200	209	218	228	248
-20.6	170	167	176	185	195

It is this reasoning, along with the results presented in the low flow discussion (Section 4.8) that the Blasius equation for a smooth pipe is used to predict theoretical values within the ice for the refreezing regimes that begin with a smooth conduit.

The high flow experiments are then compared with their respective critical flow values in Table 5-7. The critical flow rate calculated with the Blasius equation over predicts the critical flow rate, and a much higher friction factor is needed to match the experimental results. All other friction factors evaluated in this thesis predict conduit growth, so additional observation is needed to determine the friction factor that most closely matches with the experimental data.

Table 5-7: Comparison of theoretical critical flow rates for the initial ice temperatures used in the high flow rate experiments where $a=0.1$

High Flow ($2.52E-04 \text{ m}^3/\text{s}$)				
Initial Ice Temperature (°C)	Critical Flow Rate (m^3/s)			
	Blasius	f=.2	f=.5	f=1
-1.66	2.11E-04	1.10E-04	8.08E-05	6.44E-05
-4.53	3.03E-04	1.53E-04	1.13E-04	8.96E-05
-4.60	3.05E-04	1.54E-04	1.14E-04	9.02E-05
-5.43	3.24E-04	1.63E-04	1.20E-04	9.53E-05
-5.51	3.26E-04	1.63E-04	1.21E-04	9.59E-05
-5.73	3.31E-04	1.66E-04	1.22E-04	9.72E-05
-6.03	3.37E-04	1.68E-04	1.24E-04	9.84E-05
-9.55	3.98E-04	1.97E-04	1.45E-04	1.15E-04
-10.74	4.15E-04	2.03E-04	1.50E-04	1.19E-04

Since no calculation of the radius, either while the test was running, or upon completion of the test, was feasible, only qualitative analysis can be used in the determination of a sufficient friction factor to be used for the conduit growth regime. Since the radius was observed, upon completion of the tests, to have roughly doubled in some areas throughout the conduit and remained somewhat

constant in others, as seen in the final conduit geometry of the high flow test (Figure 4-19), a friction factor of 0.2 is deemed the most accurate for the conduit expansion regime, although more in depth studies and field experiments are needed to provide sufficient evidence to support this.

6 Experimental and Numerical Comparison

6.1 Comparison (Stagnant water cases)

Using inputs of the initial ice temperatures, approximated as a homogenous medium with the same temperature initially throughout, the stagnant water tests are compared to the numerical model. Other approximations for initial variable ice temperatures using recorded thermocouple data did not match physical observations, as extrapolation from piecewise cubic harmonic functions and other polynomial equations predicted temperatures at the ice boundaries that far exceeded reality, so the generalized constant temperature was used.

Figure 6-1, shows ice temperature profiles through time for three different experiments, from the recorded temperature value closest to the conduit center to the farthest, compared to the theoretical values predicted by the model. Note these are the same temperature results presented in Section 4.5 and shown in Figure 4-22 to Figure 4-24.

The numerical code assumes a radial geometry for the problem being solved, yet the stagnant water tests were run in a slightly different setup, with square boundary conditions. This slight difference is neglected, which is justifiable for small radii and the thermocouples were in a line radially away from the conduit with the same distance to the exterior boundary as the model uses. The two and three-dimensional effects of the physical system were neglected, and the data matched below between the theoretical and experimental data.

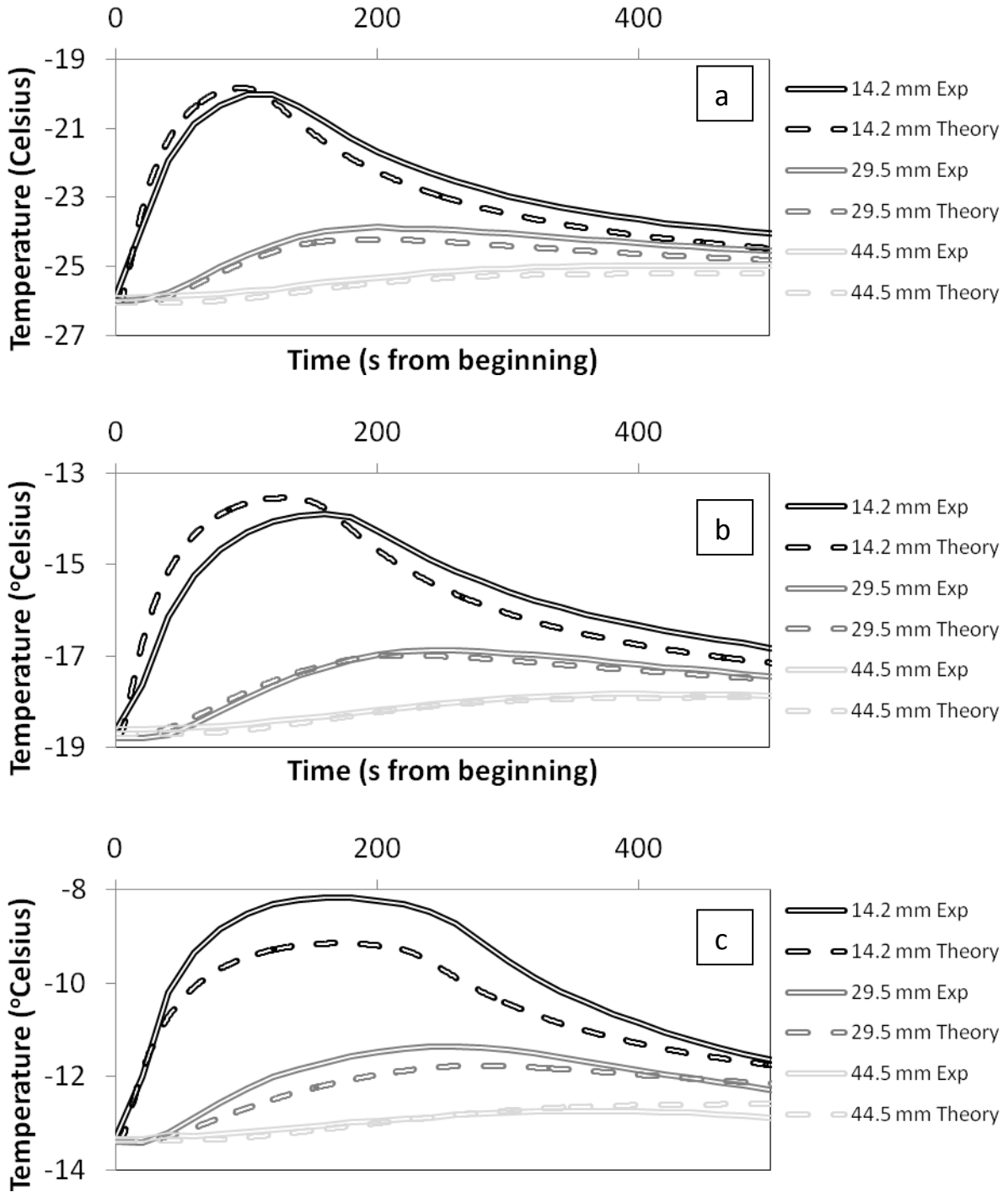


Figure 6-1: Stagnant test results showing a sample of individual thermocouple temperature recordings through time compared to their theoretical values for a) -26.0° Celsius b) -18.7° Celsius and c) -13.4° Celsius ice

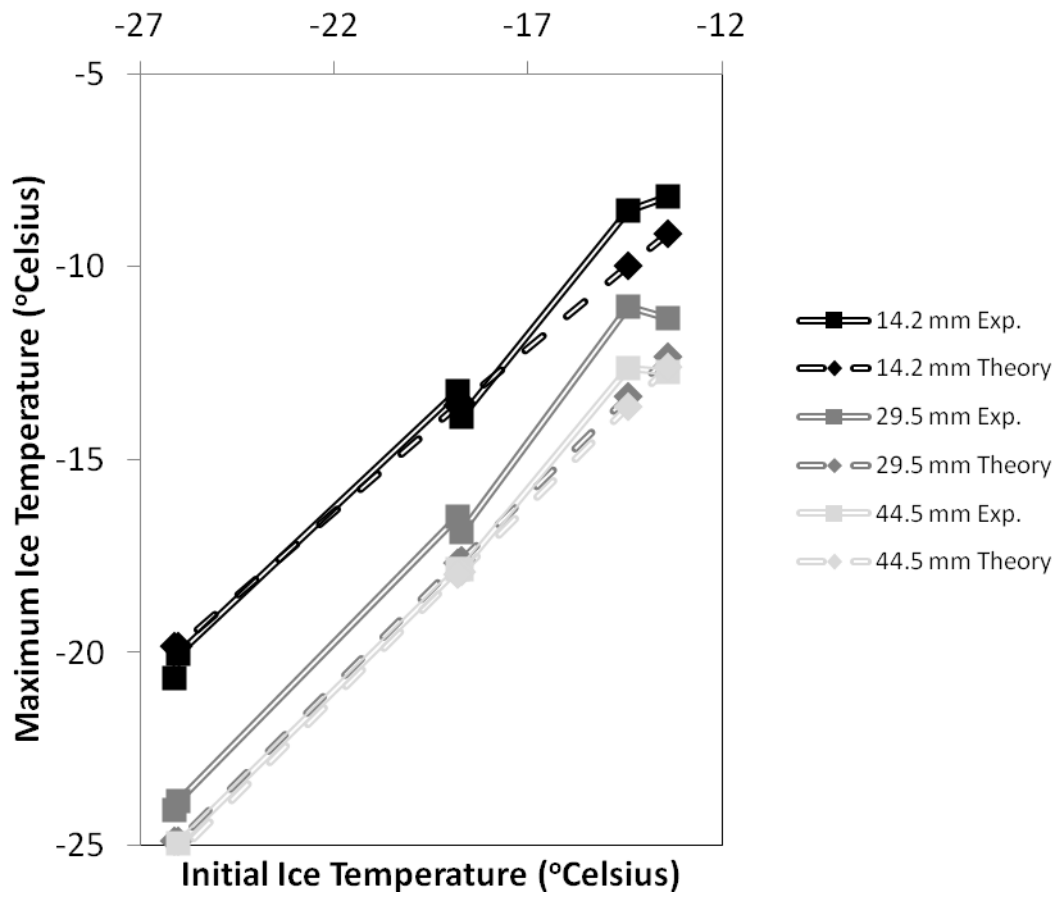


Figure 6-2: Stagnant test maximum temperatures compared between experimental and numerical values for all stagnant tests run

6.2 Discussion (Stagnant water comparison)

As a general trend from the experimental and theoretical comparison of the heat transfer from the stagnant water-filled conduit to its surrounding ice, the model matches the thermocouples placed farther away from the conduit center with more precision than the thermocouples located closest to the conduit center. The physical results differ by about a degree for most of the tests run, and these differences can be attributed to the multidimensionality of the physical experiment and the addition/loss of heat through the tubing connecting the water at the inlet and outlet of the experimental ice sample, as well as possible inhomogeneities within the sample.

Maximum temperatures experienced during the experiments are compared with the corresponding theoretical values in Figure 6-2. The experiment matches nicely with theory at both the closest and farthest thermocouple locations, yet the theoretical prediction is below the observed maximum temperature for the thermocouple located at 29.5mm away from the conduit center.

6.3 Comparison (Low water flow cases)

Again using inputs of the initial ice temperatures, approximated as a homogenous medium with the same temperature initially throughout, the numerical model was run to compare with the physical data recorded throughout the low flow water tests. The following figures, Figure 9-3 through Figure 9-5, show ice temperature profiles through time for three different experiments, from the recorded value closest to the conduit center, to the farthest, compared to the theoretical values predicted by the model. Note these are the same thermocouple results presented in Section 4.3 and shown in Figure 4-26 to Figure 4-28. Additional graphs of the theoretical radius through the experimental time are shown, in order to attempt to generate a more precise fit of the theoretical data to the experimental data.

Once again, the numerical code assumes a radial geometry for the problem being solved, yet the stagnant water tests were run in a slightly different setup, with square boundary conditions. This slight difference was neglected, and the thermocouples were in a line radially away from the conduit with the same distance to the exterior boundary as the model uses. The two and three-dimensional effects of the physical system were ignored, and the data is shown below.

Similar to the turbulent flow discussed in the high water flow section, the turbulent flow of water through the conduit generated an unknown geometry of freezing, though the model assumes it to be uniform throughout the conduit. Input values of the flow rate through time were also used, as shown in Figure 4-26

to Figure 4-28, and the additional viscous heating term is activated in the model, although the heat addition from this term at these low flow rates was small.

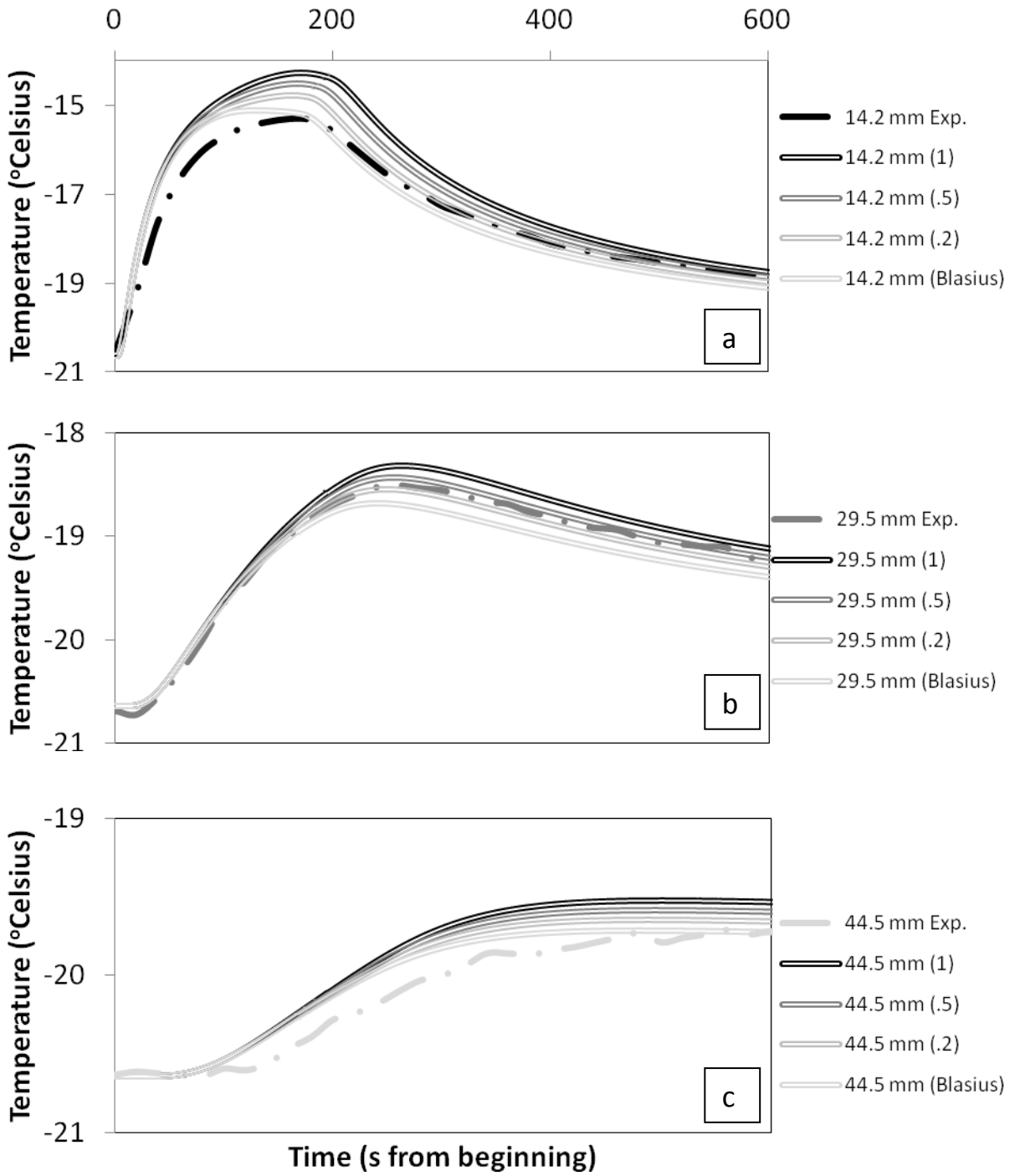


Figure 6-3: Low water flow comparison between theory and experiments from -20.6 Celsius at a) 14.2 mm from the conduit center b) 29.5 mm from the conduit center and c) 44.5 mm from the conduit center

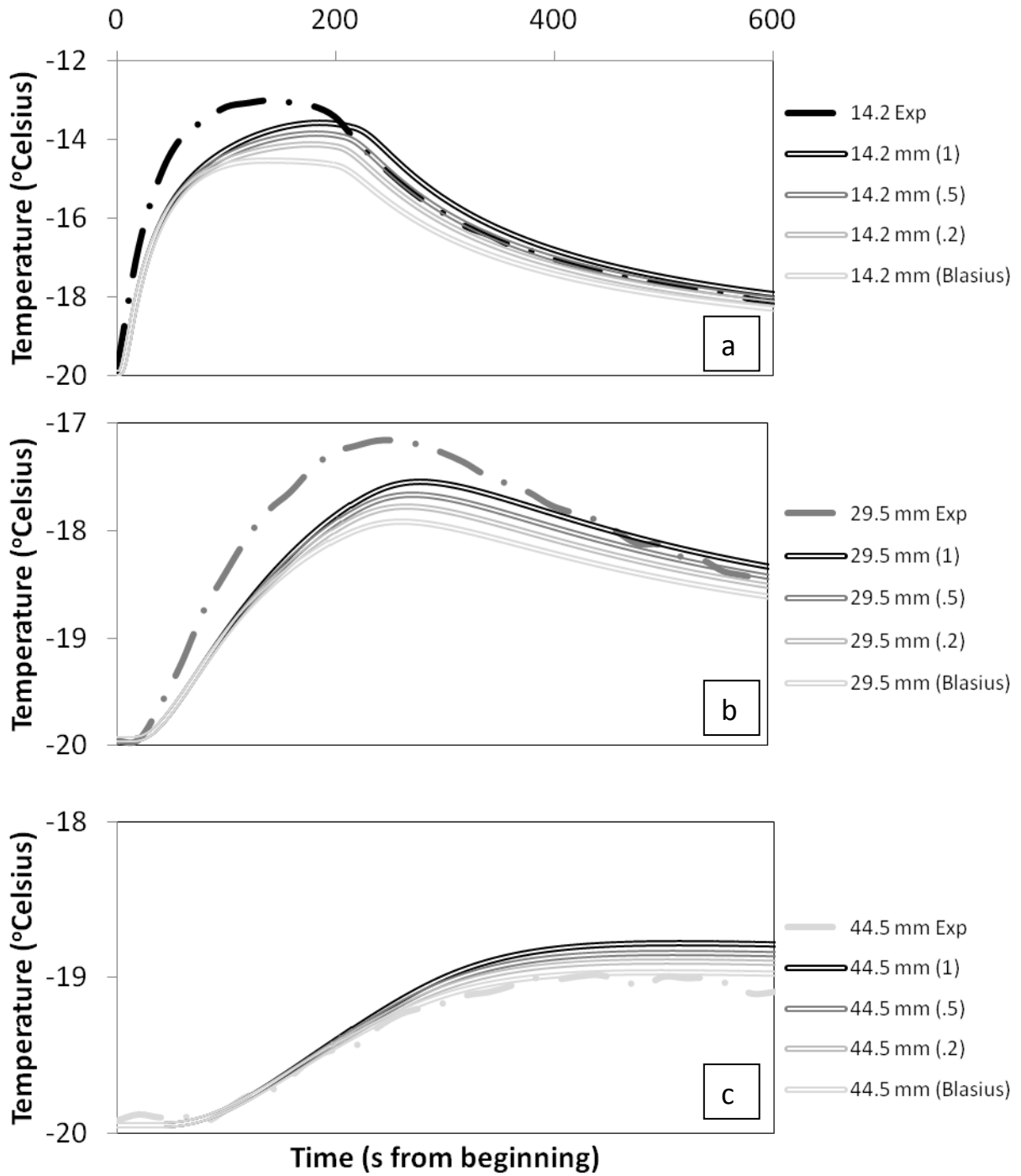


Figure 6-4: Low water flow comparison between theory and experiments from -19.9° Celsius at a) 14.2 mm from the conduit center b) 29.5 mm from the conduit center and c) 44.5 mm from the conduit center

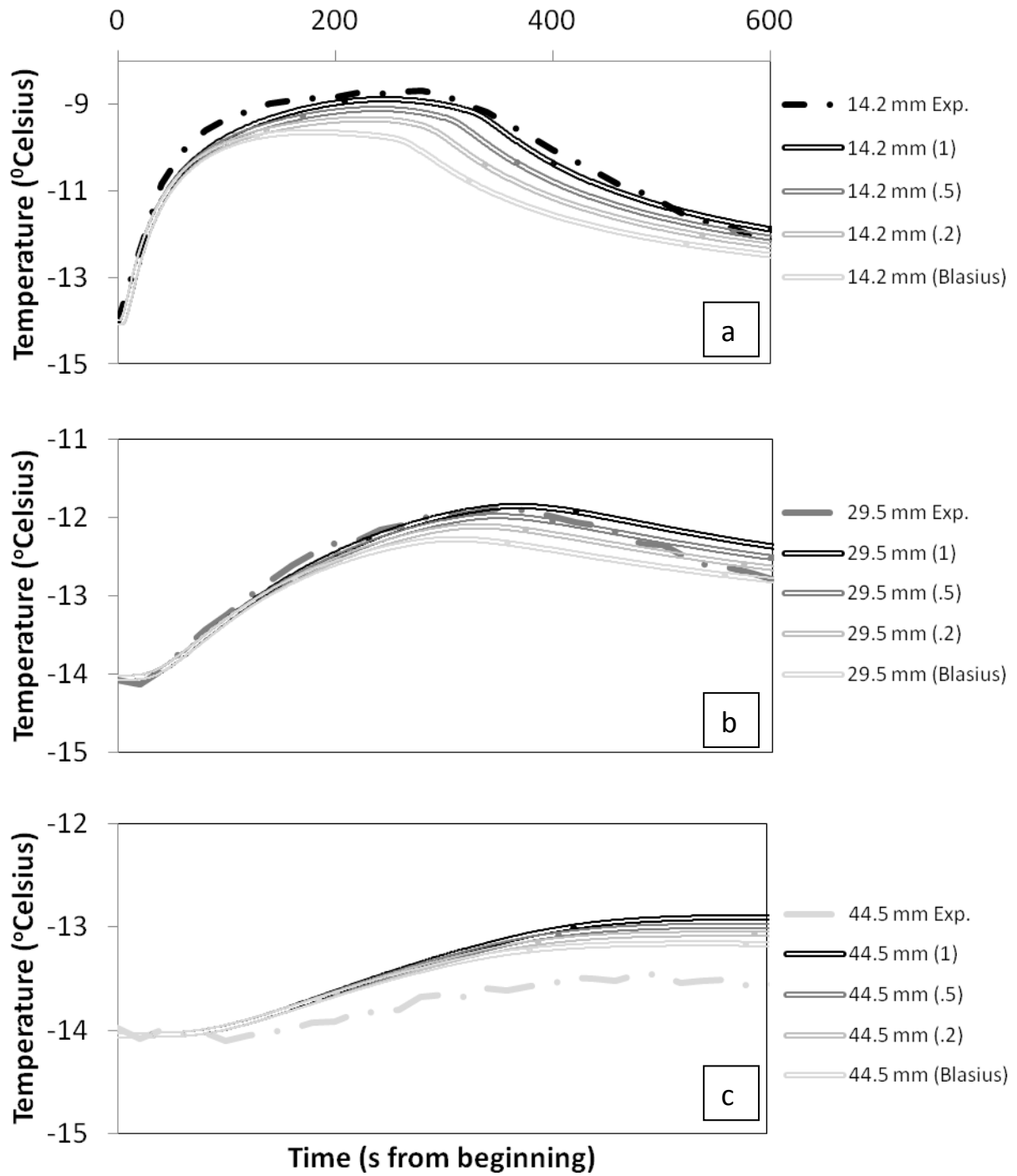


Figure 6-5: Low water flow comparison between theory and experiments from -14.0° Celsius at a) 14.2 mm from the conduit center b) 29.5 mm from the conduit center and c) 44.5 mm from the conduit center

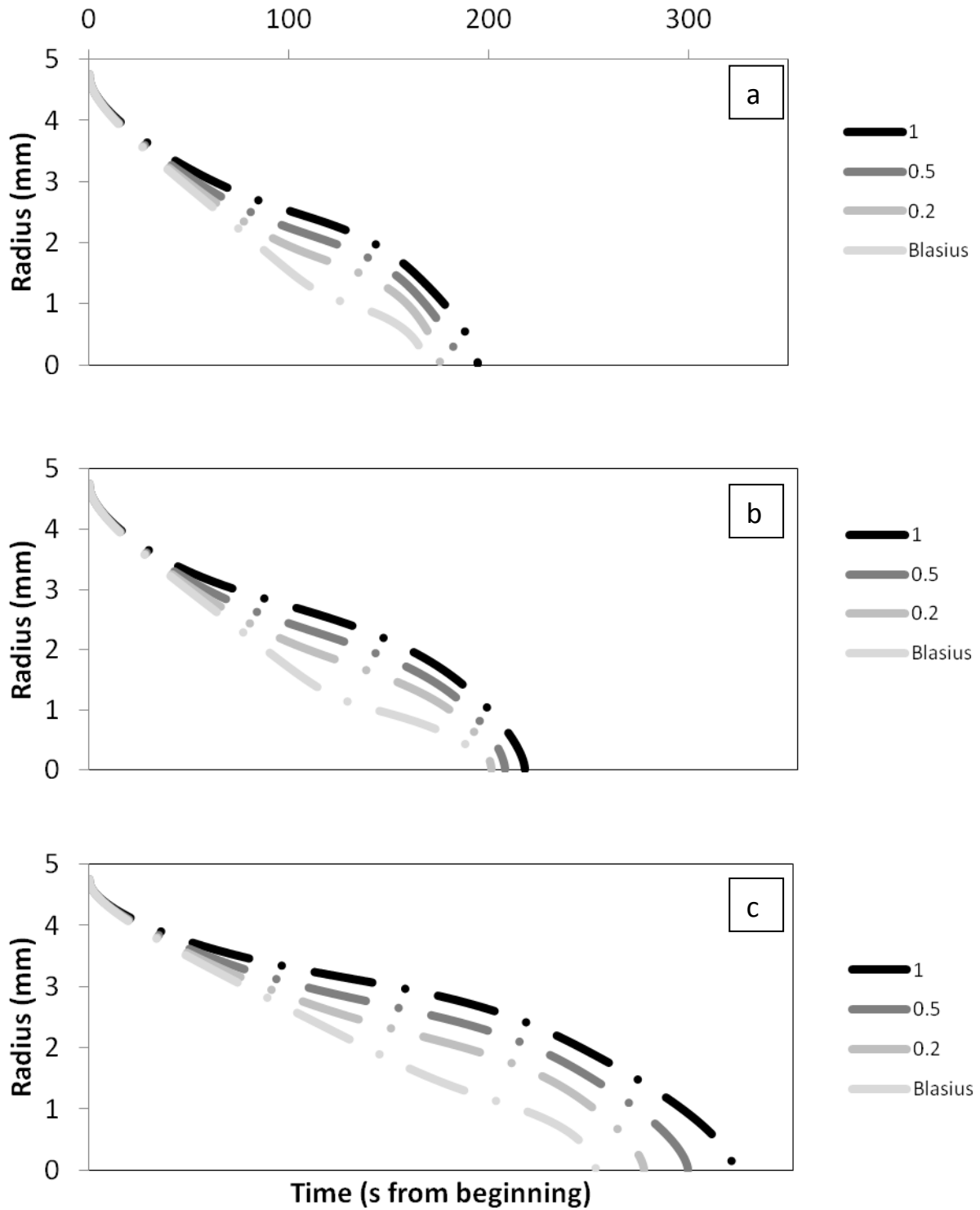


Figure 6-6: Theoretical radii of conduit through experimental time from a) -20.6° Celsius b) -19.9° Celsius and c) -14.0° Celsius ice at different Darcy-Weisbach friction factors

6.4 Discussion (Low water flow comparison)

When comparing the theoretical results from the low flow testing, the colder ice experiments, run initially at -20.6 and -20.1 Celsius, show temperature values throughout the ice which are below the model predicted temperatures. The experiments run after that at higher initial ice temperatures show values slightly higher than predicted by this numerical model consistently throughout the ice.

Differences between the model and experimental results can once again be attributed to the multidimensionality of the physical experiment, as well as possible unseen inhomogeneities within the ice. A sample of thermocouples and the maximum temperatures experienced during the experiments are compared with their theoretical values and presented in Figure 6-7. Like the stagnant experiments, the thermocouple located 44.5mm from the conduit center matches extremely well among all tests with its theoretical temperatures. Theoretical temperature predictions at 29.5mm now match experimental measurements quite well, and theoretical predictions at 14.2mm away from the conduit match experimental measurements better at colder temperatures.

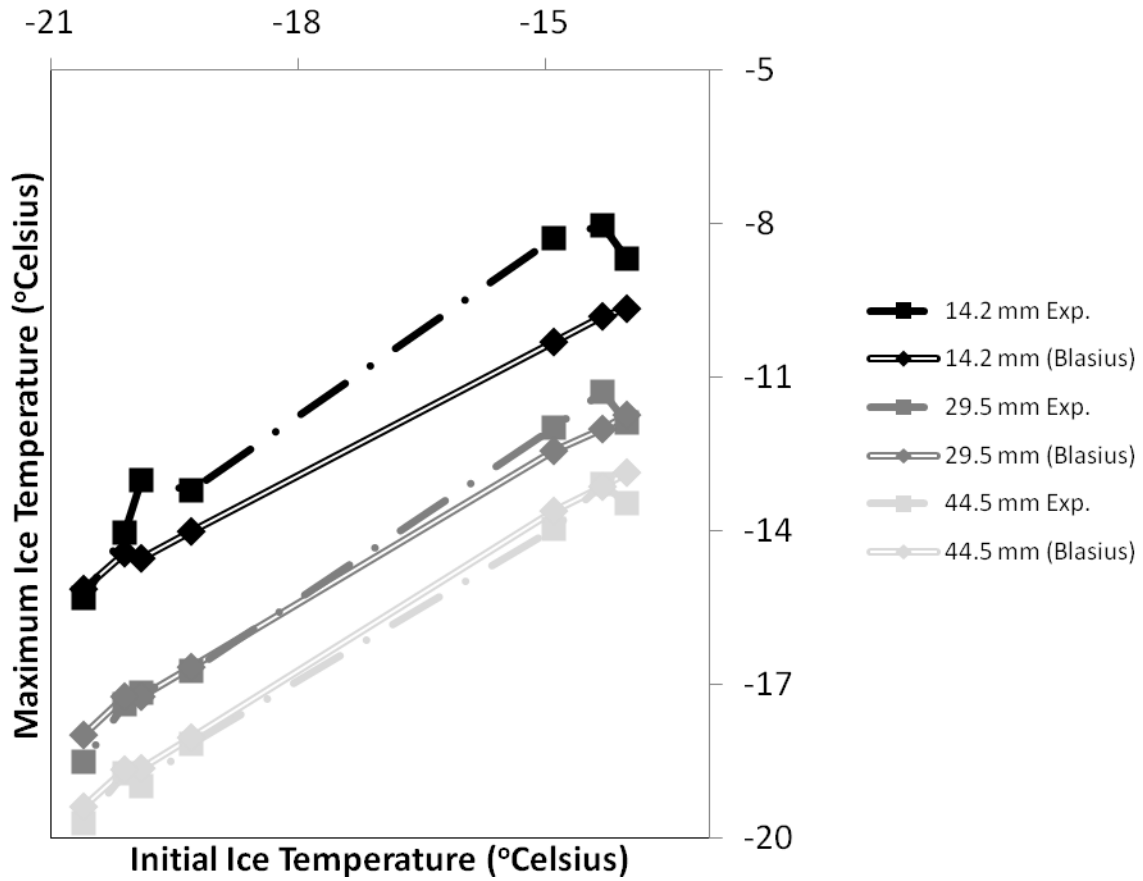


Figure 6-7: Maximum temperatures from the low water flow test compared between experimental and theoretical values at a friction factor of .02 (Blasius)

6.5 Comparison (High water flow cases)

Again inputs were used of the initial ice temperatures, approximated as a homogenous medium with the same temperature initially throughout the ice. The numerical model was run to compare with the physical data recorded during the high flow water tests. The following figures, Figure 6-8 through Figure 7-11, show ice temperature profiles through time for three different experiments, from the recorded value closest to the conduit center to the farthest, compared to the theoretical values predicted by the model. Note these are the same thermocouple results presented in the Results (High Flow) section and shown in Figure 4-31 to Figure 4-35. Additional graphs of the theoretical radius through experimental time are shown, in order to attempt to generate a more precise fit of the theoretical data to the experimental data, and match with experimental observations.

The assumption of a radial geometry in the numerical model fits precisely with the experiment in the high-flow rate experiments, as both have circular cross-sections, which was an improvement compared to the small box setup used in the stagnant and low flow trials.

As mentioned in Section 5.3, the turbulent flow of water through the conduit generated an unknown geometry of conduit expansion, though the model assumes it to be uniform throughout the conduit. The Darcy-Weisbach friction factor used in Equation 5-1 attempts to make up for this difference, and is modified slightly in order to match the numerical model to the physical experiments. Input values of the flow rate through time were also used, this time with a higher flow rate pumping a constant value through the system, and the additional viscous heating term is activated in the model.

Recent studies by J. D Gulley (2013) suggest that previously used friction factors values are well below observed friction factors in englacial conduits. Table 6-1 shows friction factors from previous studies, as well as his own, with friction factors as high as 326 times higher than prior estimated values. These factors are taken from conduits exiting the glacier with large boulders at the base, yet, due to scalloping effects from turbulent flow, can at least be partially used in this model.

Table 6-1: From (Gulley et al., 2013). Darcy-Weisbach friction factors used in previous case studies and numerical models

f	Source
0.01-0.02	(Colgan et al., 2011)
0.05	(Fowler, 2009)
0.25	(Spring and Hutter, 1981)
0.01-0.5	(Covington et al., 2009)
0.5	(Melvold et al., 2003)
0.008-0.6	(Boulton et al., 2007)
.97-75	(Gulley et al., 2012a, 2012b)

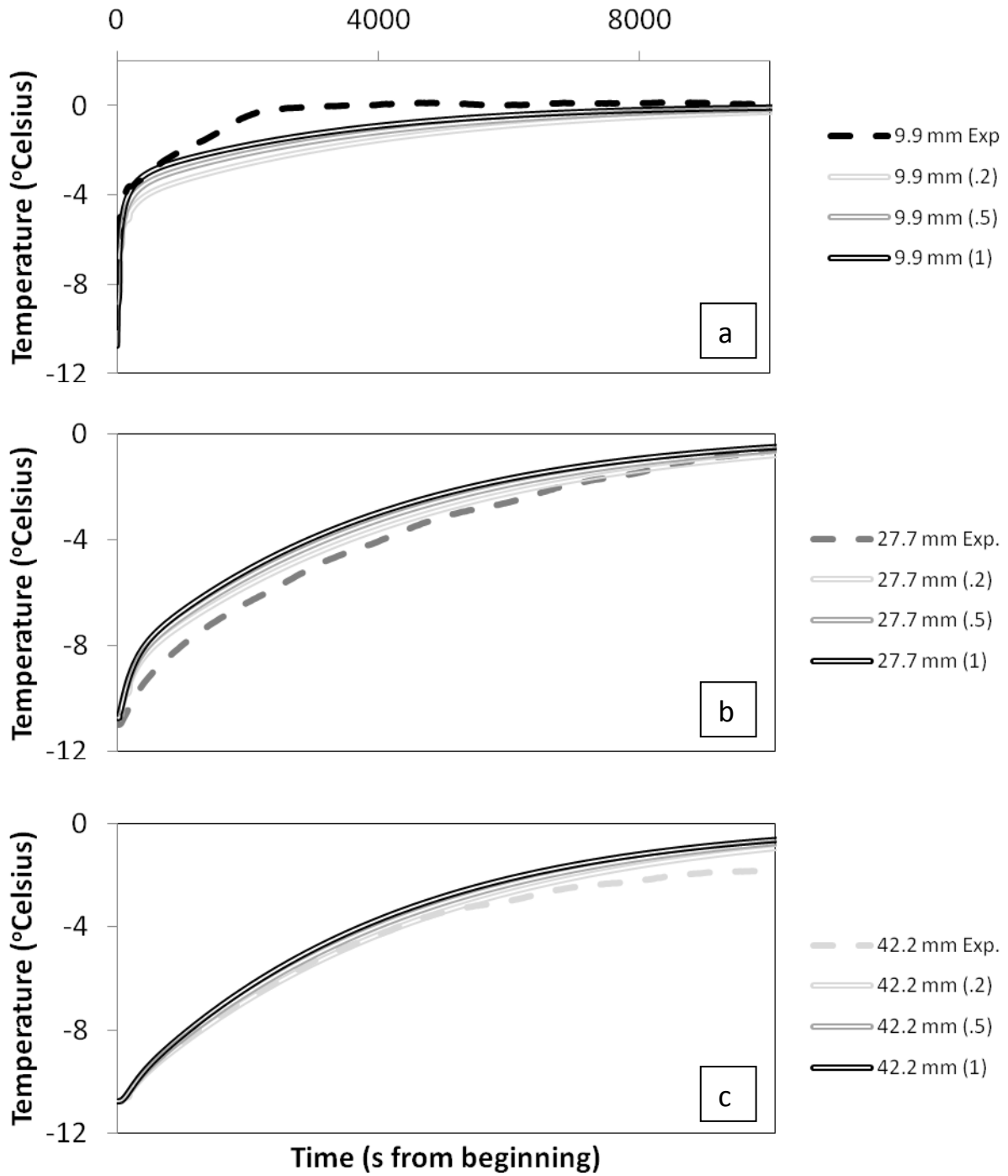


Figure 6-8: High water flow comparison between theory and experiments from -10.74° Celsius at a) 9.9 mm from the conduit center b) 27.7 mm from the conduit center and c) 42.2 mm from the conduit center

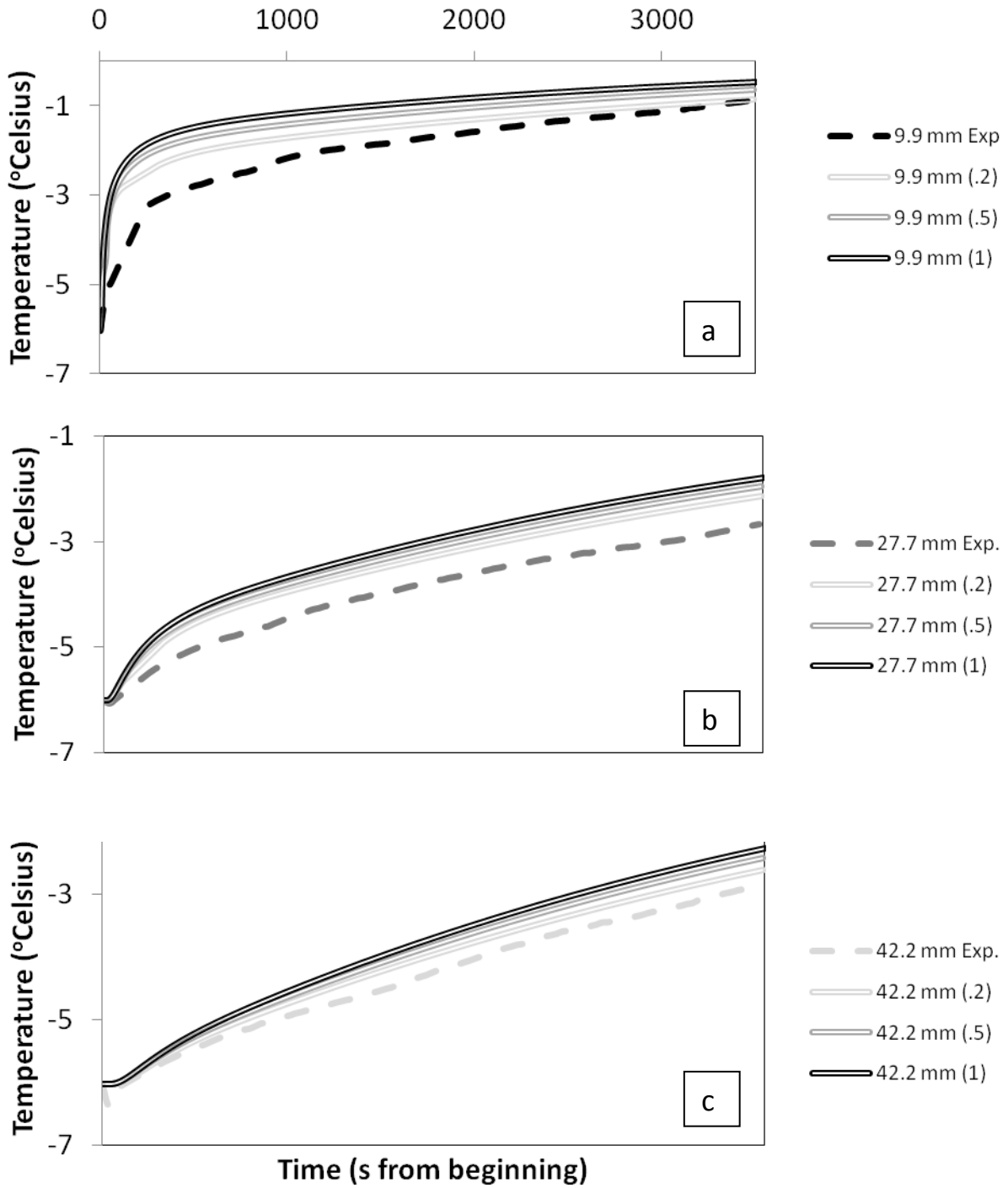


Figure 6-9: High water flow comparison between theory and experiments from -6.03° Celsius at a) 9.9 mm from the conduit center b) 27.7 mm from the conduit center and c) 42.2 mm from the conduit center

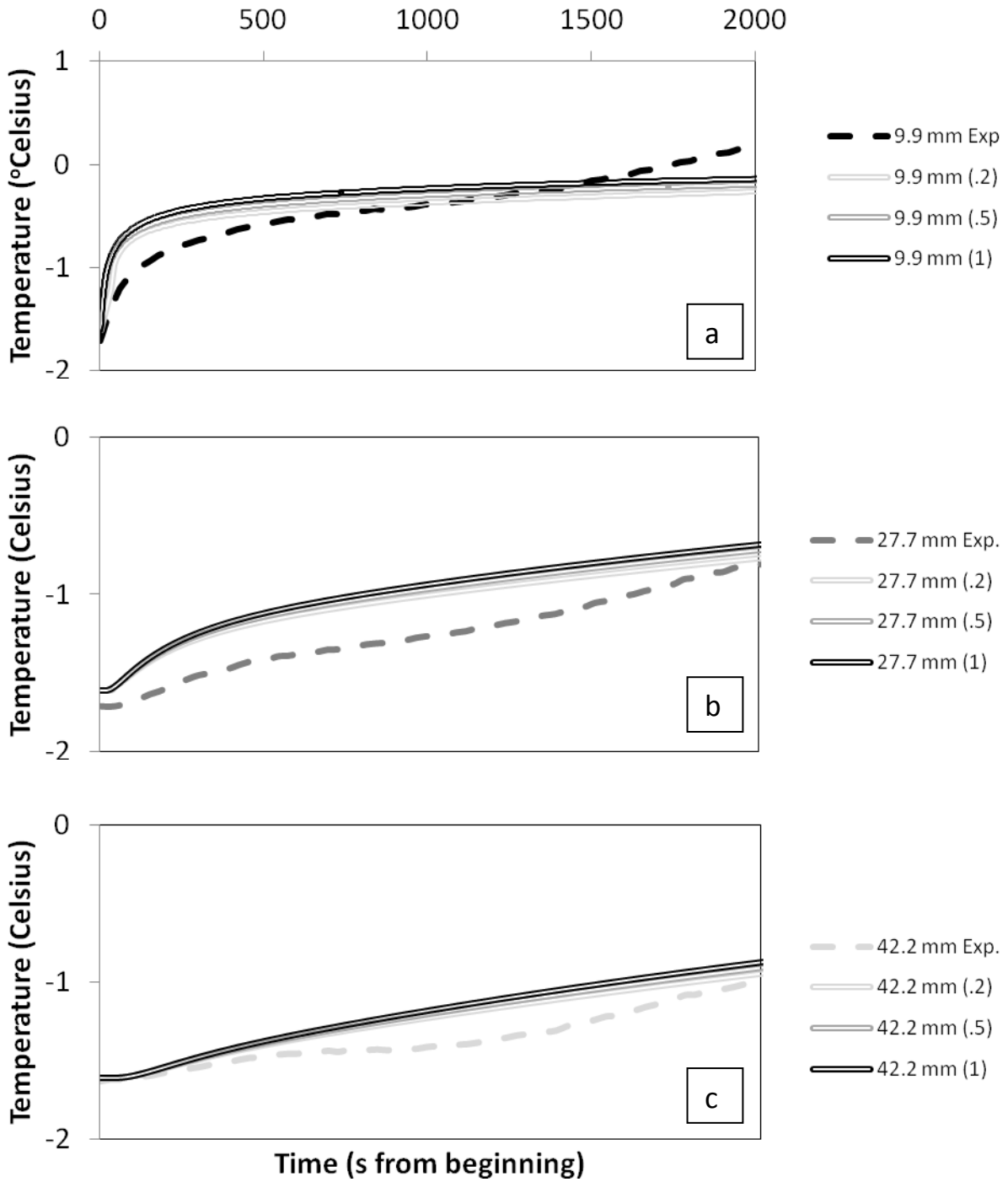


Figure 6-10: High water flow comparison between theory and experiments from -1.66° Celsius at a) 9.9 mm from the conduit center b) 27.7 mm from the conduit center and c) 42.2 mm from the conduit center

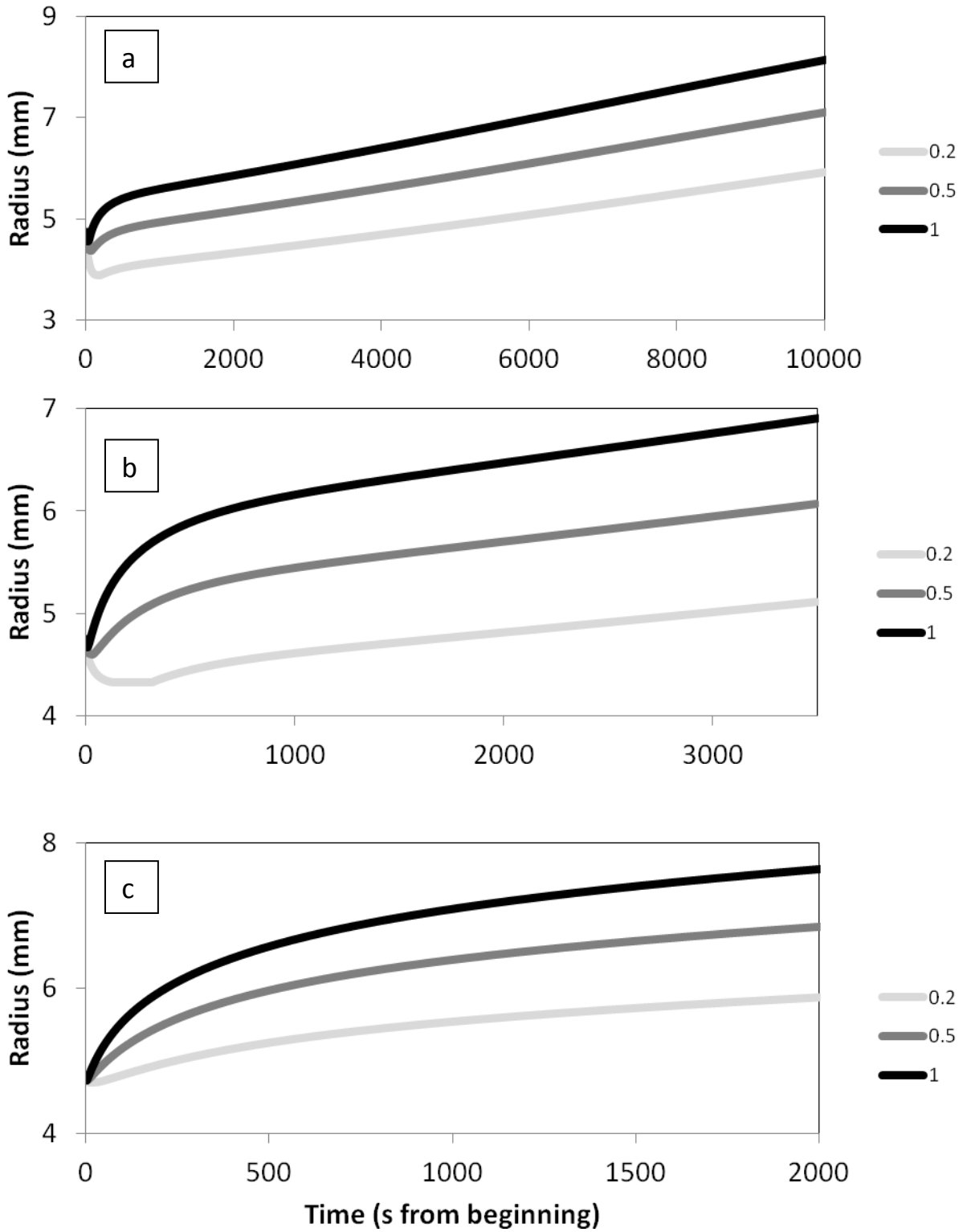


Figure 6-11: Theoretical radii of conduit from a) -10.74° Celsius b) -6.03° Celsius and c) -1.66° Celsius ice at different friction factors

6.6 Discussion (High water flow comparison)

In each test, significant conduit growth was observed to occur, leading to the determination of a higher friction factor for the numerical model, as shown by Gulley (Gulley et al., 2013). Although the model slightly overpredicts the temperature throughout the ice during the tests, a higher friction factor of 0.2 is assumed for the final conduit geometry observed in Figure 4-19. The exception to the overprediction of the model occurs at the closest thermocouple to the conduit center, presumably when that location is nearing the phase change into water. It is also hypothesized that the scallops formed from the turbulent flow lead to a non-symmetric non-circular conduit geometry and thus radius predictions assuming radial heat transfer are only approximate.

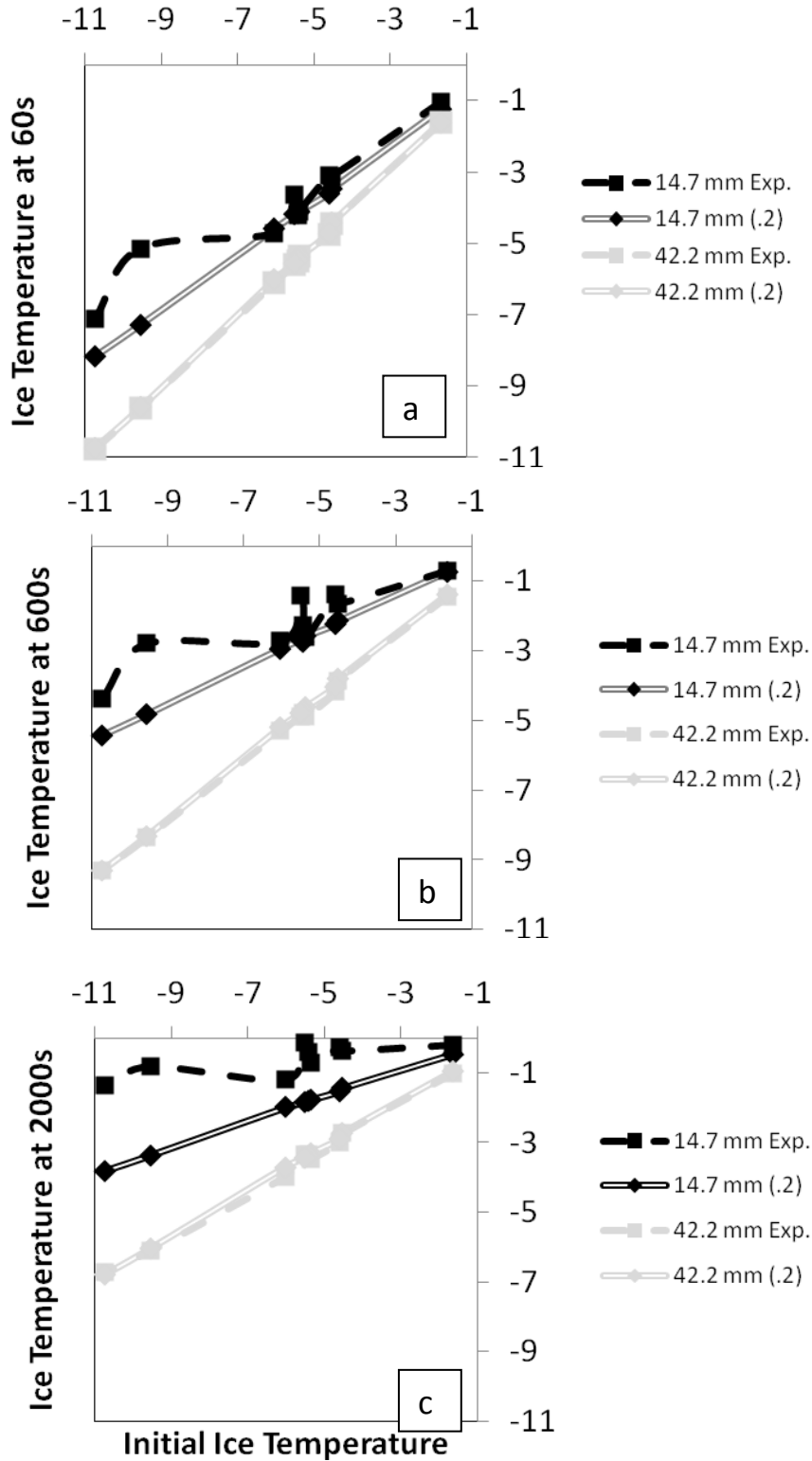


Figure 6-12: Ice temperature profile comparison between experimental and theoretical values at a)60 seconds b) 600 seconds and c) 2000 seconds into testing for all high flow tests

7 Conclusion

The experiments and calculations made here improve the understanding of the thermodynamic interactions between englacial ice and polythermal glaciers and ice sheets. The physics of heat exchange between water flowing through englacial conduits through both refreezing and growth regimes was studied and initial critical flow rates examined.

During stagnant and low flow water testing, theoretical models using existing processes predicted the temperatures of the surrounding ice well, and matched experimental values. For the low flow tests, the pipe is assumed to be smooth, as scalloping of conduit walls from closure, even with turbulent flow, is not thought to occur, because of refreezing.

Experiments at high flow rates, however, revealed that existing theoretical models predict observed behavior consistently only when high values of the friction factor are used. It may be noted that friction factors previously used in models even for conduit growth regimes are notably lower than those presented here. However, the recent field observations of Gulley (2013) corroborate the high values of friction factors used here. The ice temperatures surrounding the conduits are not extremely sensitive to the friction factor value, but the friction factor does play a large role in determining growth rates of englacial conduits, and will therefore influence the time that conduits can persist within the cold ice, especially when creep closure is also taken into account.

8 Appendix: The Bessel Function

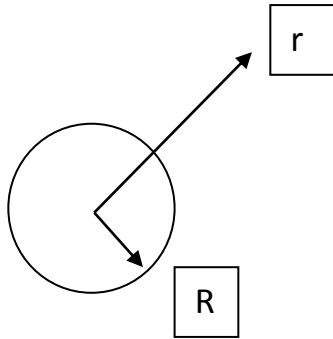


Figure 8-1: Two dimensional conduit schematic of the symbols used to characterize the conduit radius and the surrounding medium for the solution of the Bessel Equation

The Bessel function is defined, by (Carslaw, H. S., and J. C. Jaeger., 1959) as:

$$J_v(z) = \sum_{r=0}^{\infty} \frac{(-1)^r \left(\frac{1}{2}z\right)^{v+2r}}{r! \Gamma(v+r+1)}$$

Equation 8-1

Where

$$\Gamma(n) = (n-1)!$$

Equation 8-2

Equation 8-1 satisfies Bessel's equation of order v :

$$\frac{\partial^2 y}{\partial z^2} + \frac{1}{z} \frac{\partial y}{\partial z} + \left(1 - \frac{v^2}{z^2}\right) y = 0$$

Equation 8-3

The differential equation for the solution of the heat transfer problem in cylindrical coordinates is:

$$\frac{\partial \theta}{\partial t} - \frac{1}{r} \frac{\partial}{\partial r} \left(rk \frac{\partial \theta}{\partial r} \right) = 0$$

Equation 8-4

And after a separation of variables as a Bessel equation:

$$\frac{\partial^2 v}{\partial r^2} + \frac{1}{r} \frac{\partial v}{\partial r} - q^2 v = 0$$

Equation 8-5 (Carslaw, H. S., and J. C. Jaeger., 1959)

For outside of the conduit, where $r \geq R$ and $\theta(r, 0) = \theta_o$. And for the conduit edge through time, where $r \geq a$, $t > 0$, $\theta(a, t) = \theta_f$.

The analytical solution, from the Bessel function, for a surface when $r = a$ and at a constant temperature, is:

$$\theta(r, t) = \theta_f + \frac{2(\theta_f - \theta_o)}{\pi} \int_0^\infty e^{-ku^2 t} \frac{J_o(ur)Y_o(uR) - Y_o(ur)J_o(uR)}{J_o^2(uR) + Y_o^2(uR)} \frac{du}{u}$$

Equation 8-6

Where:

$$Y_\nu(z) = \frac{J_\nu(z) \cos \nu \pi - J_{-\nu}(z)}{\sin \nu \pi}$$

Equation 8-7

And:

$$J_n(z) = (-1)^n J_{-n}(z)$$

Equation 8-8

With:

$$\frac{\partial J_o(ur)}{\partial r} = -uJ_1(ur)$$

Equation 8-9

And:

$$\frac{\partial Y_o(ur)}{\partial r} = -uY_1(ur)$$

Equation 8-10

So the wall flux is:

$$\left. \frac{\partial \theta}{\partial r} \right|_{r=R} = -2\pi rk \frac{2(\theta_f - \theta_o)}{\pi} \int_0^\infty e^{-ku^2 t} \frac{Y_1(uR)J_o(uR) - J_1(ur)Y_o(uR)}{J_o^2(uR) + Y_o^2(uR)} du$$

Equation 8-11

At the initial time, where $t = 0$:

$$F_{wall} = -4kR(\theta_f - \theta_o) \int_0^\infty \frac{Y_1(uR)J_o(uR) - J_1(ur)Y_o(uR)}{J_o^2(uR) + Y_o^2(uR)} du$$

Equation 8-12

F_{wall} decreases rapidly at early time, so a dimensionless form of the integral is proposed where $v = uR$:

$$F_{wall} = -4k(\theta_f - \theta_o) \int_0^\infty e^{\frac{-kt}{R^2}v^2} \frac{Y_1(v)J_o(v) - J_1(v)Y_o(v)}{J_o^2(v) + Y_o^2(v)} dv$$

Equation 8-13

Unfortunately, as time goes to zero:

$$\lim_{t \rightarrow 0} -2\pi r k \left. \frac{\partial \tau}{\partial r} \right|_{r=R} = \infty$$

Equation 8-14

Leading to an infinite wall flux at time zero. This value, however, decreases rapidly as the time grows, and the integrated heat flux over any time interval is finite.

Noting that:

$$Y_1(v)J_0(v) - J_1(v)Y_0(v) = \frac{-2}{\pi v}$$

Equation 8-15

The flux can be expressed as:

$$F_{wall} = \frac{8k(T_f - T_o)}{\pi} \int_0^{\infty} e^{\frac{-kt}{R^2}v^2} \frac{dv}{v(J_0^2(v) + Y_0^2(v))}$$

Equation 8-16

Introducing:

$$\tau = \frac{\kappa t}{R^2}$$

Equation 8-17

So, for a small T value, the flux can be approximated by expanding all quantities in Taylor series as:

$$F_{wall} = \frac{k(T_f - T_o)}{a} \left\{ \frac{1}{\sqrt{\pi\tau}} + \frac{1}{2} - \frac{1}{4}\sqrt{\frac{\tau}{\pi}} + \frac{1}{8}\tau + \dots \right\}$$

Equation 8-18

9 Bibliography

- Alexander, L., Allen, S., Nathaniel L. Bindoff, François-Marie Bréon, John Church, Ulrich Cubasch, Seita Emori, Piers Forster, Pierre Friedlingstein, Nathan Gillett, Jonathan Gregory, Dennis Hartmann, Eystein Jansen, Ben Kirtman, Reto Knutti, Krishna Kumar Kanikicharla, Peter Lemke, Jochem Marotzke, Valérie Masson-Delmotte, Gerald Meehl, Igor Mokhov, Shilong Piao, Gian-Kasper Plattner, Qin Dahe, Venkatachalam Ramaswamy, David Randall, Monika Rhein, Maisa Rojas, Christopher Sabine, Drew Shindell, Thomas F. Stocker, Lynne Talley, David Vaughan, Shang-Ping Xie, 2013. Working Group I Contribution to the IPCC Fifth Assessment Report Climate Change 2013: The Physical Science Basis Summary for Policymakers.
- Alley, R.B., Dupont, T.K., Parizek, B.R., Anandakrishnan, S., 2005. Access of surface meltwater to beds of sub-freezing glaciers: preliminary insights. *Ann. Glaciol.* 40, 8–14.
- Alley, R.B., Joughin, I., 2012. Modeling Ice-Sheet Flow. *Science* 336, 551–552.
- Arendt, A., Bolch, T., J.G. Cogley, A. Gardner, J.-O. Hagen, R. Hock, G. Kaser, W.T. Pfeffer, G. Moholdt, F. Paul, V. Radić, L. Andreassen, S. Bajracharya, M. Beedle, E. Berthier, R. Bhambri, A. Bliss, I. Brown, E. Burgess, D. Burgess, F. Cawkwell, T. Chinn, L. Copland, B. Davies, H. De Angelis, E. Dolgova, K. Filbert, R. Forester, A. Fountain, H. Frey, B. Giffen, N. Glasser, S. Gurney, W. Hagg, D. Hall, U.K. Haritashya, G. Hartmann, C. Helm, S. Herreid, I. Howat, G. Kapustin, T. Khromova, C. Kienholz, M. Koenig, J. Kohler, D. Kriegel, S. Kutuzov, I. Lavrentiev, R. LeBris, J. Lund, W. Manley, C. Mayer, E. Miles, X. Li, B. Menounos, A. Mercer, N. Moelg, P. Mool, G. Nosenko, A. Negrete, C. Nuth, R. Pettersson, A. Racoviteanu, R. Ranzi, P. Rastner, F. Rau, B.H. Raup, J. Rich, H. Rott, C. Schneider, Y. Seliverstov, M. Sharp, O. Sigurðsson, C. Stokes, R. Wheate, S. Winsvold, G. Wolken, F. Wyatt, N. Zheltyhina, 2012. Randolph Glacier Inventory [v2.0]: A Dataset of Global Glacier Outlines, Global Land Ice Measurements from Space. Boulder Colorado, USA.
- Bamber, J.L., Griggs, J.A., Hurkmans, R.T.W.L., Dowdeswell, J.A., Gogineni, S.P., Howat, I., Mougnot, J., Paden, J., Palmer, S., Rignot, E., Steinhage, D., 2013. A new bed elevation dataset for Greenland. *The Cryosphere* 7, 499–510.

- Boon, S., Sharp, M., 2003. The role of hydrologically-driven ice fracture in drainage system evolution on an Arctic glacier. *Geophys. Res. Lett.* 30, n/a–n/a.
- Boulton, G.S., Lunn, R., Vidstrand, P., Zatsepin, S., 2007. Subglacial drainage by groundwater–channel coupling, and the origin of esker systems: part II— theory and simulation of a modern system. *Quat. Sci. Rev.* 26, 1091–1105.
- Carslaw, H. S., and J. C. Jaeger., 1959. *Conduction of Heat in Solids*. Clarendon Press, Oxford, England.
- Catania, G.A., Neumann, T.A., 2010. Persistent englacial drainage features in the Greenland Ice Sheet. *Geophys. Res. Lett.* 37, L02501.
- Chen, J.L., Wilson, C.R., Tapley, B.D., 2006. Satellite Gravity Measurements Confirm Accelerated Melting of Greenland Ice Sheet. *Science* 313, 1958–1960.
- Colgan, W., Rajaram, H., Anderson, R., Steffen, K., Phillips, T., Joughin, I., Zwally, H.J., Abdalati, W., 2011. The annual glaciohydrology cycle in the ablation zone of the Greenland ice sheet: Part 1. Hydrology model. *J. Glaciol.* 57, 697–709.
- Covington, M.D., Wicks, C.M., Saar, M.O., 2009. A dimensionless number describing the effects of recharge and geometry on discharge from simple karstic aquifers. *Water Resour. Res.* 45, n/a–n/a.
- Cuffey, K.M., Patterson, W.S.B., 2010. *The Physics of Glaciers*, Fourth. ed. Butterworth-Heinemann.
- Fountain, A.G., Walder, J.S., 1998. Water flow through temperate glaciers. *Rev. Geophys.* 36, 299–328.
- Fowler, A.C., 2009. Dynamics of subglacial floods. *Phys. Eng. Sci.* 1809–1828.
- Fretwell, P., Pritchard, H.D., Vaughan, D.G., Bamber, J.L., Barrand, N.E., et al., 2013. Bedmap2: improved ice bed, surface and thickness datasets for Antarctica. *The Cryosphere* 7, 375–393.

- Gulley, J.D., Grabiec, M., Martin, J.B., Jania, J., Catania, G., Glowacki, P., 2012a. The effect of discrete recharge by moulins and heterogeneity in flow-path efficiency at glacier beds on subglacial hydrology. *J. Glaciol.* 58, 926–940.
- Gulley, J.D., Spellman, P.D., Covington, M.D., Martin, J.B., Benn, D.I., Catania, G., 2013. Large values of hydraulic roughness in subglacial conduits during conduit enlargement: implications for modeling conduit evolution. *Earth Surf. Process. Landforms* n/a–n/a.
- Gulley, J.D., Walthard, P., Martin, J., Banwell, A.F., Benn, D.I., Catania, G., 2012b. Conduit roughness and dye-trace breakthrough curves: why slow velocity and high dispersivity may not reflect flow in distributed systems. *J. Glaciol.* 58, 915–925.
- Huff, R., 2006. Melt Anomalies on the Greenland Ice Sheet and Atmospheric Circulation. University of Colorado.
- Isenko, E., Naruse, R., Mavlyudov, B., 2005. Water temperature in englacial and supraglacial channels: Change along the flow and contribution to ice melting on the channel wall. *Cold Reg. Sci. Technol.* 42, 53–62.
- Johannessen, O.M., Khvorostovsky, K., Miles, M.W., Bobylev, L.P., 2005. Recent Ice-Sheet Growth in the Interior of Greenland. *Science* 310, 1013–1016.
- Krabill, Abdalati, Frederick, Manizade, Martin, Sonntag, Swift, Thomas, Wright, Yungel, 2000. Greenland Ice Sheet: High-Elevation Balance and Peripheral Thinning. *Science* 289, 428–430.
- Krabill, W., 2004. Greenland Ice Sheet: Increased coastal thinning. *Geophys. Res. Lett.* 31.
- Lamb, H.H., 2013. *Climate: Present, Past and Future*. Routledge Revivals.
- Latif, M., Böning, C., Willebrand, J., Biastoch, A., Dengg, J., Keenlyside, N., Schweckendiek, U., Madec, G., 2006. Is the Thermohaline Circulation Changing? *J. Clim.* 19, 4631–4637.
- Lemke, P., J. Ren, R.B. Alley, I. Allison, J. Carrasco, G. Flato, Y. Fujii, G. Kaser, P. Mote, R.H. Thomas and T. Zhang, 2007. Observations: Changes in Snow, Ice and Frozen Ground, in: *Climate Change 2007: The Physical Science Basis*.

Contribution of Working Group I to the Fourth Assessment Report of the Intergovernmental Panel on Climate Change [Solomon, S., D. Qin, M. Manning, Z. Chen, M. Marquis, K.B. Averyt, M. Tignor and H.L. Miller (eds.)]. Cambridge University Press, Cambridge, United Kingdom and New York, NY, USA.

Lunardini, V.J., 1981. Heat transfer in cold climates. Van Nostrand Reinhold Co., New York.

Luthcke, S.B., Zwally, H.J., Abdalati, W., Rowlands, D.D., Ray, R.D., Nerem, R.S., Lemoine, F.G., McCarthy, J.J., Chinn, D.S., 2006. Recent Greenland Ice Mass Loss by Drainage System from Satellite Gravity Observations. *Science* 314, 1286–1289.

Markus, T., Stroeve, J.C., Miller, J., 2009. Recent changes in Arctic sea ice melt onset, freezeup, and melt season length. *J. Geophys. Res. Oceans* 114, n/a–n/a.

Melvold, K., Schuler, T., Lappegard, G., 2003. Ground-water intrusions in a mine beneath Høgenesbreen, Svalbard: assessing the possibility of evacuating water subglacially. *Ann. Glaciol.* 37, 269–274.

National Snow and Ice Data Center, 2013. All About Glaciers. What Types Glaciers Are There.

Nye, J.F., 1953. The Flow Law of Ice from Measurements in Glacier Tunnels, Laboratory Experiments and the Jungfraufirn Borehole Experiment. *Proc. R. Soc. Lond. Ser. Math. Phys. Sci.* 219, 477–489.

Phillips, T., Rajaram, H., Colgan, W., Steffen, K., Abdalati, W., 2013. Evaluation of cryo-hydrologic warming as an explanation for increased ice velocities in the wet snow zone, Sermeq Avannarleq, West Greenland. *J. Geophys. Res. Earth Surf.* n/a–n/a.

Phillips, T.P., 2010. The characterization of the cryo-hydrologic system of the Sermeq Avannarleq Glacier in Greenland and its influence on ice temperature.

- Ramillien, G., Lombard, A., Cazenave, A., Ivins, E.R., Llubes, M., Remy, F., Biancale, R., 2006. Interannual variations of the mass balance of the Antarctica and Greenland ice sheets from GRACE. *Glob. Planet. Change* 53, 198–208.
- Rignot, E., Kanagaratnam, P., 2006. Changes in the Velocity Structure of the Greenland Ice Sheet. *Science* 311, 986–990.
- Rignot, E., Velicogna, I., van den Broeke, M.R., Monaghan, A., Lenaerts, J.T.M., 2011. Acceleration of the contribution of the Greenland and Antarctic ice sheets to sea level rise. *Geophys. Res. Lett.* 38, n/a–n/a.
- Roethlisberger, H., 1972. Water pressure in intra- and subglacial channels. *J. Glaciol.* 11, 177–203.
- Shreve, R.L., 1972. Movement of Water in Glaciers *Journal of Glaciology*, 205–214.
- Spring, U., Hutter, K., 1981. Numerical studies of Jökulhlaups. *Cold Reg. Sci. Technol.* 4, 227–244.
- Steitz, D.E., 2002. GRACE Launch Press Kit. National Aeronautics and Space Administration.
- Thomas, R., Davis, C., Frederick, E., Krabill, W., Li, Y., Manizade, S., Martin, C., 2008. A comparison of Greenland ice-sheet volume changes derived from altimetry measurements. *J. Glaciol.* 54, 203–212.
- Thomas, R., Frederick, E., Krabill, W., Manizade, S., Martin, C., 2006. Progressive increase in ice loss from Greenland. *Geophys. Res. Lett.* 33, L10503.
- Thomas, R., Frederick, E., Li, J., Krabill, W., Manizade, S., Paden, J., Sonntag, J., Swift, R., Yungel, J., 2011. Accelerating ice loss from the fastest Greenland and Antarctic glaciers. *Geophys. Res. Lett.* 38, n/a–n/a.
- Velicogna, I., Wahr, J., 2006. Acceleration of Greenland ice mass loss in spring 2004. *Nature* 443, 329–331.
- Wanner, H., Bronnimann, S., Casty, C., Gyalistras, D., Luterbacher, J., Schmutz, C., Stephenson, D.B., Xoplaki, E., 2001. North Atlantic Oscillation - Concepts and studies. *Surv. Geophys.* 22, 321–382.
- WeatherSpark, 2013. WeatherSpark. Beautiful Weather Graphs Maps.

Zwally, H.J., Abdalati, W., Herring, T., Larson, K., Saba, J., Steffen, K., 2002. Surface Melt-Induced Acceleration of Greenland Ice-Sheet Flow. *Science* 297, 218–222.

Zwally, H.J., Giovinetto, M.B., Li, J., Cornejo, H.G., Beckley, M.A., Brenner, A.C., Saba, J.L., Yi, D., 2005. Mass changes of the Greenland and Antarctic ice sheets and shelves and contributions to sea-level rise: 1992–2002. *J. Glaciol.* 51, 509–527.